Forensic Electrochemistry: Time Since Deposition (TSD) Estimation of Degrading Bloodstains using Differential Pulse Voltammetry

by

Mitchell Tiessen

A thesis submitted to the
School of Graduate and Postdoctoral Studies in partial
fulfillment of the requirements for the degree of

Master of Science in Applied Bioscience

Faculty of Science

University of Ontario Institute of Technology (Ontario Tech University)

Oshawa, Ontario, Canada

December, 2021

THESIS EXAMINATION INFORMATION

Submitted by: **Mitchell Tiessen**

Master of Science in **Applied Bioscience**

Thesis title: Forensic Electrochemistry: Time Since Deposition (TSD) Estimation of Degrading Bloodstains using Differential Pulse Voltammetry

An oral defense of this thesis took place on November 30, 2021 in front of the following examining committee:

Examining Committee:

Chair of Examining Committee	Dr. Janice Strap
Research Supervisor	Dr. Theresa Stotesbury
Examining Committee Member	Dr. Bradley E. Easton
Thesis Examiner	Dr. Olena Zenkina, Ontario Tech University

The above committee determined that the thesis is acceptable in form and content and that a satisfactory knowledge of the field covered by the thesis was demonstrated by the candidate during an oral examination. A signed copy of the Certificate of Approval is available from the School of Graduate and Postdoctoral Studies.

ABSTRACT

Methods for bloodstain time since deposition (TSD) estimation are still in development. Hemoglobin (Hb) oxidative changes remain one of the primary means of bloodstain aging. This research explores the use of differential pulse voltammetry as a technique to analyze degrading bloodstains. The optimized conditions were determined to be 1µL of whole blood analyzed in a pH 7.0 phosphate buffer. This protocol was used to measure changes in electrochemical response in a two-week time series experiment using 9 biological replicates across 5 environmental conditions. Linear mixed models suggested that the peak height and area ratios for the Hb redox reactions were significantly correlated with time ($p < 0.033$). Absolute dating and principal component analysis demonstrate significant changes ($p < 0.043$) at the 96-hour time point and present opportunities for forensic TSD predictions. Overall, the changes in Hb redox peaks over time offers insight into oxidative changes and cellular degradation in bloodstains.

Keywords: Forensic chemistry; Red blood cells; Hemoglobin; Heme redox activity; Trans-membrane electron transfer

AUTHOR'S DECLARATION

I hereby declare that this thesis consists of original work of which I have authored. This is a true copy of the thesis, including any required final revisions, as accepted by my examiners.

I authorize the University of Ontario Institute of Technology (Ontario Tech University) to lend this thesis to other institutions or individuals for the purpose of scholarly research. I further authorize University of Ontario Institute of Technology (Ontario Tech University) to reproduce this thesis by photocopying or by other means, in total or in part, at the request of other institutions or individuals for the purpose of scholarly research. I understand that my thesis will be made electronically available to the public.

Mitchell Tiessen

STATEMENT OF CONTRIBUTIONS

I hereby certify that I am the sole author of this thesis and that no part of this thesis has been published or submitted for publication. I have used standard referencing practices to acknowledge ideas, research techniques, or other materials that belong to others. Furthermore, I hereby certify that I am the sole source of the creative works and/or inventive knowledge described in this thesis.

ACKNOWLEDGEMENTS

Firstly, I would like to thank my amazing supervisor, Dr. Theresa Stotesbury. I am very grateful to have been given the this opportunity to be a part of the start of the Forensic Chemistry and Materials Lab at Ontario Tech University. Throughout the past research projects at Trent University and during this Masters project, Dr. Stotesbury has offered invaluable supervision and support. I would like to express my gratitude for her guidance and her role in shaping my career goals.

I would like to extent my thanks to Dr. E. Bradley Easton for allowing me to use the instrumentation in his lab to complete this project. His expertise and contributions to the experimental methods and result interpretations are treasured. I would also like to thank and the members of the Electrochemical Materials Lab, especially Holly Fruehwald and Dr. Reza Alipour for their assistance in all electrochemical research questions, from training to troubleshooting.

I would like to thank my fellow lab mates at Ontario Tech University and Trent University for the cherished time spent together in the lab and in social settings, especially Amanda Orr and Colin Elliott. Your practical suggestions, helpful advice, and encouragement throughout the stages of the research is greatly appreciated.

Lastly, I would like to thank my friends and family for their support all through my studies. The last few years was not how I expected my Masters to go but I am very grateful for their valued impact they made to my life beyond the scope of my studies.

TABLE OF CONTENTS

LIST OF TABLES

Chapter 3:

Chapter 4:

LIST OF FIGURES

Chapter 1:

Chapter 2:

Chapter 3:

Chapter 4:

LIST OF ABBREVIATIONS AND SYMBOLS

ACD-A	Acid Citrate Dextrose Anticoagulant
BAC	Blood Alcohol Content
BrAC	Breath Alcohol Content
BPA	Bloodstain Pattern Analysis
deoxyHb	Deoxygenated Hemoglobin
DPV	Differential Pulse Voltammetry
GC	Glassy Carbon
HC	Hemichrome
Hb	Hemoglobin
LOD	Limit of Detection
LSV	Linear Scan Voltammetry
metHb	Methemoglobin
Naf	Nafion
N_2	Nitrogen Gas
O_2	Oxygen Gas
ORR	Oxygen Reduction Reaction
oxyHb	Oxygenated Hemoglobin
PCV%	Packed Cell Volume Percent
PRISMA	Preferred Reporting Items for Systematic Reviews and Meta-Analyses
PCA	Principal Component Analysis
PC	Principal Component
RBCs	Red Blood Cells
RH%	Percent Relative Humidity
RSD	Relative Standard Deviation
RHE	Reversible Hydrogen Electrode
RDE	Rotating Disk Electrode
RPM	Rotations per Minute

SEM	Scanning Electron Microscopy
TSD	Time Since Deposition
VOCs	Volatile Organic Compounds
WBCs	White Blood Cells

Chapter 1: Introduction

1.1 Blood and bloodstained evidence in forensic science

Blood samples and bloodstained evidence remain among the most frequently collected substances by forensic professionals [1,2]. Blood is a complex and multi-component fluid whose primary purpose is facilitating the transportation of gases and essential nutrients throughout the body [3]. Blood also plays an important role in maintaining homeostasis within the body [3]. Whole blood largely contains cells (red blood cells (RBCs), white blood cells (WBCs), and platelets) suspended in a liquid plasma that contains proteins, ions, nutrients, metabolites and other biomolecules [4–8]. In forensic science, bloodstains encountered at crime scenes and blood samples obtained for investigative purposes hold high evidentiary value for investigators because of its distinctive physical, chemical and biological properties [9–13]. Blood serves as a matrix for several biomolecules of interest to forensic and medical professionals including DNA and RNA, hemoglobin (Hb), drugs and their metabolites. For example, forensic investigators collect blood evidence for source attribution through DNA profiling and interpretations of the events involving bloodshed can be made using the principles of Bloodstain Pattern Analysis (BPA) [13–16]. Forensic toxicologists routinely analyze blood samples for the presence of illicit or impairing drugs, poisons, and prescribed medications [1,17–19]. Both forensic and medical toxicologists analyze a number of biological fluids and tissues, with blood being a widely collected sample type given its ubiquity, ease of collection, storability, and versatility for assessing a large number of analytes [1]. In forensic science blood is a driving force of investigations and holds a wealth of data on an individual and crime scene.

1.2 Bloodstain formation and degradation

For this thesis the terms ‘bloodstain’ (forensic context) and ‘blood film’ (materials characterization) are used interchangeably, both referring to the film created as a result of a blood droplet being deposited across a surface. When a blood film is formed on a given surface, the rheological properties drive the film formation process [20,21]. Once a bloodstain has formed, a cascade of physicochemical processes begins [22]. The moment a bloodstain forms is defined as the initial equilibrium state [23]. The process of

drying begins as soon as blood is deposited on a surface. Desiccation begins almost immediately. This is largely influenced by the plasma which contains roughly 92% water by volume [12,23]. As water evaporation and volatile organic compound (VOC) emission occurs the solid components of the film are participating in self-assembling interactions. During this phase, the cellular components and biomolecules such as proteins migrate towards the periphery of the film [8,23]. As continuous evaporation occurs the WBCs and platelets migrate towards the center region of the bloodstain; and the RBCs stack and assemble themselves in a ring-like structure at the edge of the stain. Additionally, the smaller solid components such as proteins settle on the outermost edges of the dried stain, a phenomenon and feature described in BPA as serum separation [21]. The compression of RBCs occurs as the cells settle in the ring of the film and eventual cracking is expected as dehydration continues and cellular components begin to degrade. Research focused on developing a deeper understanding of the phase transitions of drying blood stains has been ongoing for several decades. Methodologies using optical microscopy [8,22,23], scanning electron microscopy (SEM) [23–25] and Raman spectroscopy [16,26] have been used to characterize these events for forensic and diagnostic purposes. Many of these research areas are focused on the morphology of drying blood stains based on physical changes, most with applications in aging estimation [16,26,27].

Additionally, many forensic researchers are interested in the chemical changes that occur when blood is exposed to the environment. On the molecular level, the degradation of blood components happens continuously as the blood leaves the body. As previously mentioned, the evaporation of water and VOCs begins immediately and leads to the drying of the stain; leaving the solid components in a thin film on the surface [20,28,29]. These solid components are primarily comprised of RBCs, where the Hb within these cells makes up about 90% of their dry weight. This has led to Hb as one of the most widely studied biomolecules in forensic science and why the changes of this protein one of the primary means of bloodstains aging studies [15].

1.2.1 Hemoglobin

Globins are a superfamily of heme-containing proteins that are responsible for binding and transporting of oxygen (O_2) in blood. Four types of globins have been found in humans: myoglobin (Mb), neuroglobin (Ngb), cytoglobin (Cygb), and Hb [30]. Each

of these proteins have different structures, functions and relative distributions in the body. For example, Hb is a tetrameric protein located in RBCs and is responsible for the transport of O_2 through the circulatory system. Figure 1.1 shows the structure of the Hb, highlighting the heme groups and their position within the protein. Hb was first isolated in 1840 by Hünefeld but its structure remained unknown until 1959, when it was determined by Perutz [15,30]. Hb is a metalloprotein and has a molecular weight of 64.5 kDa. It consists of four polypeptide chains, two identical α and β subunits, with 141 and 146 amino acid residues respectively [15]. Each of these chains contains one heme molecule. The heme molecule's role is to facilitate O_2 binding and transport which is key for aerobic respiration and energy conversions in the body. The heme structure is an organic protoporphyrin ring with a central iron atom [31]. The iron directly participates in ligand binding and is integral to the chromophoric properties of RBCs. To understand how Hb changes outside of the body (*ex vivo*), it helps to understand the states that it exists within the body (*in vivo*) and the natural changes it undergoes.

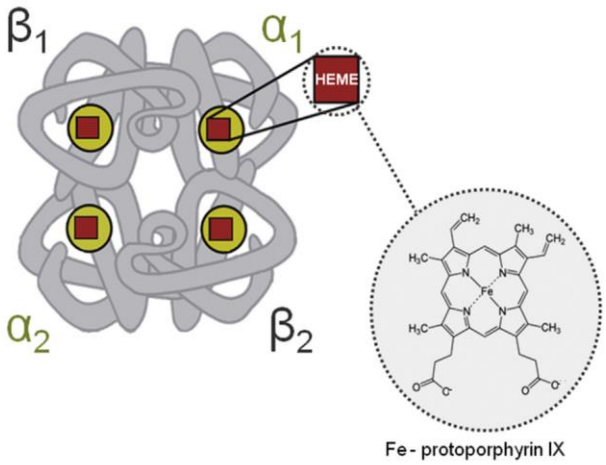

Figure 1.1: *Structure of a hemoglobin molecule, from Zadora and Menżyk 2018 [15]. Permission to reproduce obtained through publisher (found in Appendix A).*

1.3 Hemoglobin degradation

In a healthy individual, Hb exists in 3 states: oxygenated Hb (oxyHb), deoxygenated Hb (deoxyHb), and methemoglobin (metHb). OxyHb refers to when the primary ligand, oxygen, is reversibly bound to the central iron atom located in the protoporphyrin ring. There is debate whether iron is in its ferrous (Fe^{2+}) or ferric (Fe^{3+}) oxidation state during this configuration with the majority of the research claiming the

ferrous definition [15,32,33]. Upon oxygen binding, the central iron atom is brought into plane with the protoporphyrin ring, adopting a low spin state. The absence of oxygen in the Hb-protein complex refers to deoxyHb. In this state, the central iron atom is in a ferrous state and sits 0.4 Å outside the protoporphyrin ring to protect itself from oxidative damages [15]. These two states form the majority of Hb in a healthy individual. However, despite the stability of oxyHb, roughly 3% is oxidized daily to metHb [15,34]. During this process, the bound O_2 is reduced to water, coupled with the oxidation of Hb from its Fe^{2+} to Fe^{3+} form. In its Fe^{3+} form, water is the primary ligand and the Hb protein is unable to carry O_2. In a healthy individual the concentrations of metHb are maintained through internal reduction mechanisms such as glutathione peroxidase, cytochrome b_5 oxidoreductase, and methemoglobin reductase [15,35,36]. These mechanisms effectively recycle metHb to deoxyHb where they can carry O_2 again. Issues with these internal reduction systems are the primary causes for blood related conditions such as anemia and thalassemia [15,30,31,37]. In a bloodstain, similar oxidative changes to Hb occur over time with additional degradation processes to cellular components.

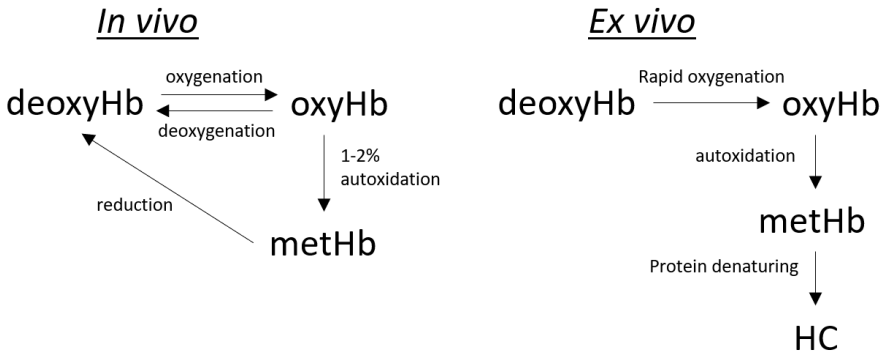

Figure 1.2: *Comparison of in vivo (left) and ex vivo (right) hemoglobin degradation pathways, adapted from Bremmer, 2012* [32].

In *ex vivo* conditions, the available deoxyHb is immediately saturated with atmospheric oxygen and is converted to oxyHb. The high affinity for an O_2 molecule by free heme is responsible for this immediate reaction [31]. From here, the oxyHb begins its gradual oxidation to metHb. The enzymes responsible for converting metHb back to deoxyHb are no longer available due to denaturation [15]. Following this, the degradation continues with both reversible and irreversible changes to the protein structure resulting in the formation of hemi- and hemochrome (HC). These species are named from the

oxidation state of the iron, either in its ferric (hemichrome-Fe^{3+}) or ferrous (hemochrome-Fe^{2+}) states [15]. These changes to Hb *in vivo* and *ex vivo* are summarized in Figure 1.2 with a detailed *ex vivo* pathway shown in Figure 1.3 reproduced from Zadora, 2018. Over time further degradation of the bloodstain is driven by environmental stresses leading to cellular damage and hemolysis.

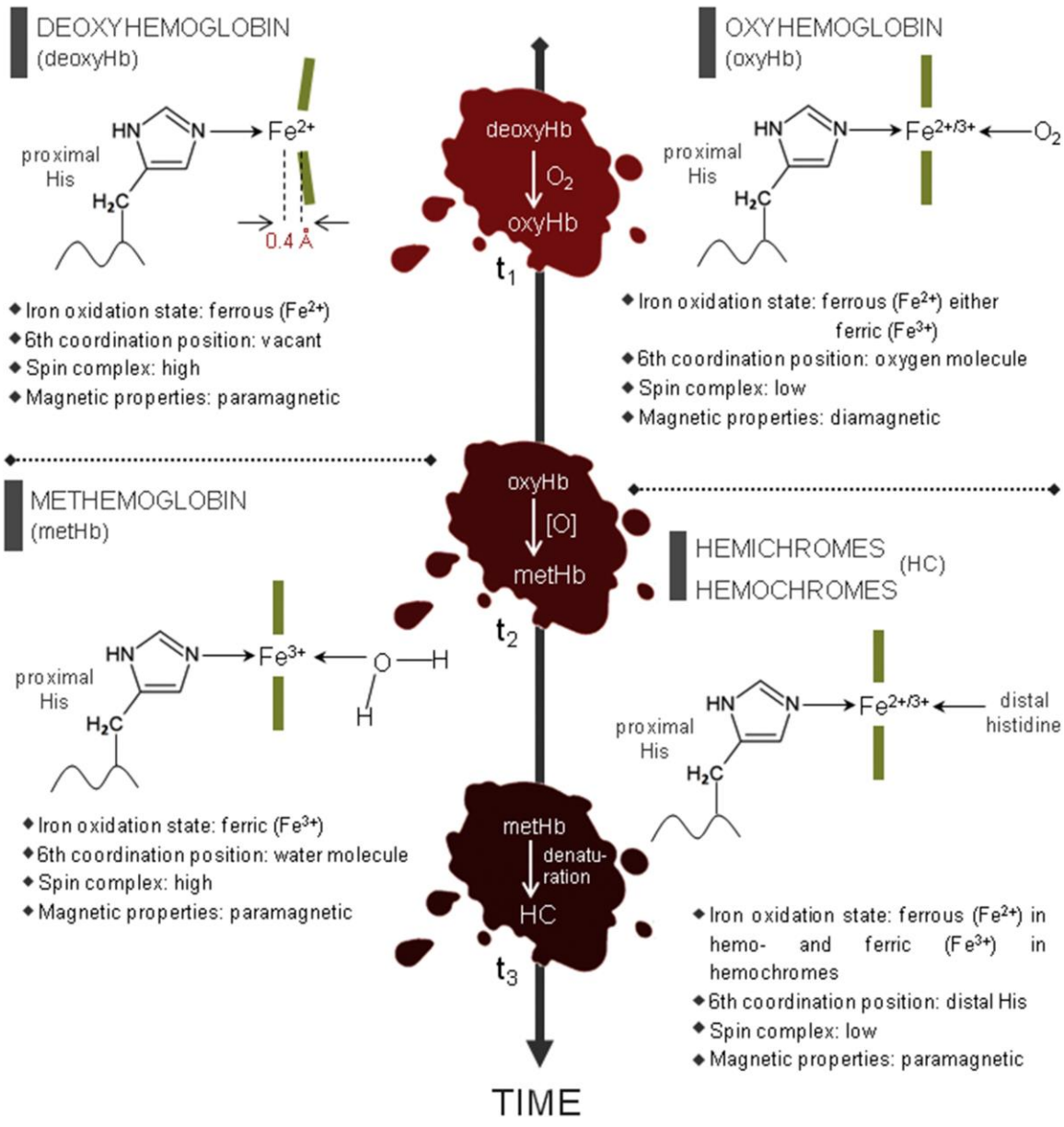

Figure 1.3: *Pathway of ex vivo Hb degradation from Zadora and Menżyk 2018 [15]. Permission to reproduce obtained through publisher (found in Appendix A).*

The *ex vivo* Hb degradation pathway is of interest to forensic researchers as it offers insight in temporal information regarding blood shedding events. Forensic questions regarding time since deposition (TSD) remain at the core of criminal investigations and has been a focal point of forensic research for roughly 20 years [15]. A number of forensically relevant samples that have been studied for TSD applications include: paints/inks [38,39], fingerprints [40], and various biological evidence including blood [3,15,41,42]. The TSD bloodstain literature has studied multiple blood-related analytes with respect to aging bloodstains. The two largest groups including those studying Hb and cellular components through spectrographic techniques [3,16,33,43–45] and those characterizing the changes in DNA and/or RNA [42,46–51]. Across the TSD literature, the unity of place and time is a primary objective in evidence analysis. Linking an individual or material to a location within a particular time frame offers a more detailed explanation to the sequence of events. This is valuable information for law enforcement and courtroom testimony. However, there is currently no generally accept method for determining the TSD of a bloodstain, and previously proposed methods have fallen short due to poor time resolution and weak age correlation [45,52,53]. Additionally, the environmental effects such as temperature, humidity, and sunlight are all key questions when estimating a bloodstains age and are important considerations when establishing TSD [15,43,54]. Many studies, regardless of method, demonstrate that increasing the storage temperature of bloodstains changes the kinetics of degradation and often increases the rate of change [43,45,55–57]. This highlights the need to include environmental parameters when conducting these studies before they are applied to real-world scenarios. Many researchers consider environmental parameters and have begun to study bloodstain degradation in various conditions. However, the complexity of blood as a sample matrix and variability between replicates still presents challenges for many analytical techniques. Forensic researchers have yet to develop standalone methods with acceptable accuracy and precision to answer questions surrounding the TSD of a bloodstain, and alternative analytical techniques may help answer these questions and pair with existing methods.

Electrochemistry is a proposed tool to study bloodstain degradation in this thesis. The sensitivity and specificity of electrochemistry as a characterization technique offers

an unexplored research avenue for bloodstain TSD research. Forensic electrochemistry is an emerging discipline in forensics and these analytical techniques have been used to detect and quantify various forensically relevant samples including: explosives [58], gunshot residue [59], and illicit drugs [60,61]. Within the medical electrochemistry field, there has been biomedical research into Hb changes for diagnosing blood related diseases [62,63]. These same principles based on the oxidation of oxyHb to metHb in the body could be applied to forensic blood analysis in relation to bloodstain degradation. Similar autoxidative and cell damaging events that can be detected in the body can be detected by electrochemical methods and translated to the natural degradation of Hb in the environment. From a forensic context, bloodstain aging through Hb oxidation is well discussed in the literature and electrochemical methods complement the currently used techniques [15,33,43,44,51]. Research design and proof-of-concept methodologies using electrochemical methods are the first steps toward applying electrochemical methods to TSD estimates in criminal investigations.

A systematic review on the use of electrochemistry for whole blood analysis was conducted and the following sections summarize the key findings. The methods and summary of all the evaluated articles can be found in Appendix A.

1.4 Systematic review on whole blood electrochemistry

Presented here is a summary of the systematic review conducted using the Preferred Reporting Items for Systematic Reviews and Meta-Analyses (PRIMSA) guidelines for reporting articles in systematic reviews and meta-analyses [64]. The databases PubMed, Scopus, and Web of Science were used to complete 20 literature searches involving the words: ‘electrochemistry’, ‘potentiometry’, ‘differential pulse voltammetry, ‘cyclic voltammetry’, ‘blood’, ‘whole blood’, ‘hemoglobin’, ‘arterial blood’, and ‘forensic’. From the literature search 1461 article were collected and screened (PubMed = 428, Scopus = 726, and Wed of Science = 305, independent library = 7). After article exclusion and the removal of duplicates, 68 papers were reviewed and included in the summary of the current trends in the electrochemical analysis of whole blood. Studies where minimal sample pretreatment was performed were included. Recent research has demonstrated that the use of whole blood samples for electrochemical analysis is possible and with forensic practices in mind, minimal sample deconstruction

and manipulation is desirable for analysis purposes. The goal of this review was to highlight the novel technologies involving whole blood analysis using electrochemical methods, evaluate and interpret the clinical research with forensic applications in mind, and, to offer future research directions. This summary highlights the major finding and previous research related to the Hb electrochemical research, other analytes including glucose and prescribed drugs are included in the full review. The article screening and selection methods along with the comprehensive results can be found in Appendix A. In the summary table the electrochemical methods used to analyze blood, the common electrode modifications, blood pretreatment methods for different analyses, and a summary of the objectives across the electrochemistry research are presented.

1.4.1 Electrochemistry and forensic science

Electrochemical methods have been used to analyze a variety of forensic samples. For example, drugs in biological and non-biological samples have been studied including: ethanol (blood alcohol) [65,66], xylazine [67], mephedrone [68], THC [69,70], heroin [61], MDMA [60], synthetic cathinone derivatives [71], fentanyl [72], and benzodiazepines such as Flunitrazepam [73,74].

Within recent years several researchers have developed electrochemical methods to detect, identify, and quantify ethanol [75–77]. Electrochemical sensors are commonly employed breath alcohol detectors in practical settings. These systems employ a two-electrode fuel cell configuration to detect the oxidation of ethanol in breath samples [78]. These technologies use breath alcohol content (BrAC) to correlate with blood alcohol content (BAC). Recent electrochemical technologies have developed ethanol sensors for blood samples. From the literature search two articles were found that involve the electrochemical detection and quantification of ethanol in whole blood for roadside testing applications. The detection of blood ethanol level using electrochemical sensors has the advantage of being low cost, fast, and portable [66]. These qualities make it desirable for *in situ* analysis, whether that be roadside or in a clinical setting. [65]. These articles present accessible, simple, and fast analysis methods that demonstrate high linearity with ethanol concentration in the applicable range [65,66]. One study focusses on developing a smartphone-based potentiostat for whole blood ethanol determination, highlighting the developed method has an accurate linear response between 0-0.125 g/L

of ethanol [66]. The other article develops an amperometric disposable serum-based alcohol biosensor and reports a limit of detection (LOD) of 1.6×10^{-6} mol/L. The manufacturing and stability of the electrode surfaces are significant considerations for ethanol electrochemical sensors, especially when legal questions are presented. Additionally, the two articles highlight the elimination of laborious sample preparation steps, allowing direct whole blood electrochemical analysis.

For the majority of the forensic electrochemistry literature involving drug identification and quantification, many of these substances are validated in buffer solutions using voltammetric methods. Few studies have taken this one step further to apply these methods to sample matrices such as urine or whole blood. The often-low dosage, and high biotransformation of many drugs has been problematic to diagnose after ingestion and the application of electrochemical sensors allows a quick, cost-effective, and sensitive analysis in practical settings [73,74]. Beyond the scope of drug samples electrochemical methods have also been applied to the forensic analysis of explosive compounds [58,79], gunshot residues [59,80,81], and fingerprint residues [82,83]. The 'at-the-scene' testing capabilities of these sensors offers time advantages to investigators and highlights the central focus of developing field-deployable analytical instruments with future research into testing the LOD, specificity, and optimization of these technologies [58,60,61,70,72]. Forensic researchers are adopting electrochemical methods for a number of sample types given their advantages. Expansion of analytes and sample matrices is encouraged as it relates to forensic evidence.

1.4.2 Electrochemistry and whole blood

Articles kept for inclusion in the full review were split into 4 categories based on analyte, including: cells and Hb (n = 35), biomolecules (n = 16), drugs (n = 5), and metals (n = 12). Across all of the articles the research goals remained consistent, with objectives in identification and quantification of a desired analyte in blood. Many of the articles use whole blood but a small number had simple dilution steps. The study of biological samples using electrochemistry has presented challenges in the past due to the complexity of these samples in their natural forms. Issues with electron transfer and sample biofouling have been the primary challenges [30,85,86]. In recent years, advances in electrochemical methods have achieved a high degree of sensitivity, being able to detect

electron transfer reactions at the electrode surface of biological samples [87]. Researchers continue to improve on the sensitivity and specificity of electrochemical sensors through studying reaction kinetics and electroactive material interactions. The diversity of electrochemical techniques and their ability to monitor small-scale reactions make them widely studied methods for various analytes and matrices, with voltammetric methods being amongst the most popularly used.

1.4.3 Electrochemical cells and Hb analysis in whole blood

The largest category was the studies involving Hb electron transfer reactions or Hb catalyzed oxygen reduction reactions (ORR) in RBCs. The applications and objectives of these studies ranged from medical analysis of Hb related diseases [62,88,89], to using Hb as an electrocatalysis for biofuels [90]. The central focus of many studies is centered around the further understanding the oxygen-iron bonding in RBCs as is relates to the ORR [85,91,92]. The principles of O_2 binding and reduction catalyzed by Hb directly relate to these studies objectives in medical and material characterization disciplines.

Within this category, the samples used in the analysis varied, and the pretreatment steps ranged. The common sample types included: whole blood [34,62,93], purified RBCs [94–97], and purified Hb [84,98–101]. One article by Matsuoka *et al.* (1995) used oxygen electrodes to study the fractional values of oxyHb and metHb as it related to TSD of bloodstains [57]. This study tested various bloodstain storage temperature conditions before the stains were dissolved for analysis. This is the only article in this category that used electrochemical methods to study bloodstain age. No further work has been published on the use of electrochemical methods for bloodstain TSD estimates. The authors found that increasing the temperature during bloodstain storage accelerated the degradation process; however, further studies to improve reliability were recommended [57]. The promising results of this study highlights application of electrochemical methods for bloodstain analysis in forensic science research.

The vast majority of articles in this category focussed on Hb detection and quantification for medical purposes. Normal levels of Hb in whole blood for adults are roughly 14–18 g dL^{-1} for males, and 12–16 g dL^{-1} for females [62]. Irregularities in these

concentrations relates to certain medical conditions including anemia (Hb deficiency), thalassemia (irregular/fragile function), and sickle cell anemia (faulty cell shape) [34,62]. These conditions are often tested in clinical settings using spectrographic techniques, although electrochemical methods offer faster results and require minimal sample pretreatment at most [62,63,88]. Research involving the direct immobilization of blood on electrodes demonstrates differences in voltammetric signals that are attributed to transmembrane electron transfers related to physiological changes in erythrocytes [62,88]. The research surrounding differentiation of healthy and abnormal Hb species demonstrates the applicability to bloodstain analysis. Similar Hb oxidation states are present between physiological Hb species and the natural oxidation pathway of Hb *ex vivo* (i.e. oxyHb to metHb).

Analysis of purified Hb samples compared to RBCs or whole blood shows electron transfer reactions are slowed by the cellular components and the coupled iron/oxygen reduction in many cases is not a completely reversible process in whole blood samples [84,102]. However, other articles demonstrate the opposite, that under certain conditions the redox reaction can show reversibility [101–104]. Across articles several electrode modifications have demonstrated high linearity, good reproducibility, and sensitivity to Hb contained within RBCs [6,34,62,93,102,105].

1.4.4 Forensic application to electrochemical blood analysis

Advancements in electrochemical sensitivity and electrode design have overcome many early challenges in electrochemical blood analysis, with current research demonstrating the ability to study blood-related electron transfers with very little to no sample pretreatment. The direct immobilization of blood on electrodes has demonstrated electron transfers involving Hb imbedded in RBCs – a process that was once considered to be difficult to monitor due to the cell membrane barrier. Many researchers highlight the efficacy of these sensors and show that they demonstrate a high degree of accuracy and precision even when whole blood is the sample matrix [89,91,94,106]. The glassy carbon (GC) electrode has been shown to offer superior performance compared to other electrodes; particularly when immobilizing the whole blood/RBCs using the common binder Nafion® (Naf) [107].

Many of the Hb related electrochemical biosensors demonstrate high linearity, good reproducibility, and sensitivity to Hb contained within RBCs [6,34,62,93,102,105]. On GC electrodes, Hb concentration in whole blood samples has demonstrated linear response between 8-16 g dL^{-1} [62]. The comparable accuracy of these methods to other analytical techniques used in forensic chemistry highlights the value of electrochemistry. The methods described possess many desirable characteristics for forensic researchers and practitioners. The simplicity and quick analysis times offers several advantages to forensic investigators both in the field and in the laboratory for identification and quantification purposes. The use of electrochemical systems for Hb monitoring in bloodstains is proposed as the next research venture for forensic scientists when posed with TSD questions. Understanding how environmental conditions influence blood degradation and Hb oxidative changes could be answered with electrochemical methods.

1.5 Research objectives

The goal of this research was to assess the use of electrochemical techniques to monitor Hb and whole blood degradation. Researchers have demonstrated that electrochemical methods are sensitive for the study of whole blood with clinical applications. These techniques have not yet been tested and interpreted using a forensic perspective and could offer new opportunities for forensic analysis. These objectives were reached through answering a series of research questions:

1. Are electrochemical techniques applicable for forensic samples, particularly bovine blood?
2. Can these methods be applied to TSD estimates of bloodstains?
3. How does temperature influence TSD estimates?

It was predicted that, whole blood collected from a crime scene, or is this case a simulated crime scene, has the potential to be used in electrochemical analysis. Forensic researchers have validated mammalian blood sources for research purposes [10,108,109]. Similar rheological and hematological properties exist between the mammalian and human blood; researchers recommend bovine blood for forensic purposes when used within 50 hours of collection [108]. Small volumes and no sample pretreatment make electrochemical methods desirable for blood analysis and allow for evidence

preservation. Given the biomedical research into Hb oxidation for diagnosing blood related diseases [62,63], these principles could be applied to forensic blood analysis. The phenomenon of oxidative and cell damaging events that can be detected in medical blood samples can be carried over to the natural degradation of Hb in the environment. The electrochemical monitoring of coupled Hb and O_2 reduction in a bloodstain can give insight into concentrations of oxyHb and metHb in a bloodstain.

As a bloodstain ages, the concentration of O_2 decreases as oxidative processes occur naturally. Fresh stains are expected to have higher oxyHb levels compared to metHb, where older stains are dominated by metHb and HC species. Comparable differences are seen when using electrochemical methods to study healthy and anemic blood [62]. These differences are predicted to be comparable to the differences in fresh and old bloodstains and their rates of change are influenced by temperature. Using voltammetric methods, the reduction signal of O_2 is expected to decrease over time and degradation of the blood film is expected to effect electrochemical signals. The influence of temperature has been shown to effect Hb degradation rates with warmer temperature increasing the kinetics of Hb oxidation [15,43]. Research in colder temperatures is studied less often and it is hypothesized that cooler temperatures decrease the kinetics of Hb oxidation. This research contributes to the bloodstain TSD literature in standard and various temperature conditions using electrochemical techniques. Warmer temperatures were tested and compared to complementary TSD methods and the novelty of testing colder temperature is presented.

1.6 Thesis outline

The following chapters outline the experimental work from this research. Chapter 2 comprises the general methods of the experimental sections. This includes the procedures and methods that are consistent across experiments: blood collection, blood characterization, and electrode preparation steps are detailed here. Specific experimental descriptions are found in their respective chapters. Chapter 3 details the blood film characterization experiments. This section focusses on the redox reactions occurring on the electrode surface and the film structure corresponding to the deposited blood. This section also includes voltammetric optimization experiments involving different experimental conditions and electrode imaging experiments using scanning electron

microscopy and photography. Chapter 4 builds on the characterization study to determine the effects of analysis when blood is aged on electrodes under various temperature conditions. This includes the results and data interpretation of 9 two-week time-series, five replicated in standard conditions and 4 under different single replicate temperature-controlled variations. Lastly, Chapter 5 comprises on the discussion, future directions and conclusions of this project. The summary of the systematic review which focusses on the electrochemical techniques used for whole blood analysis beyond the scope of this thesis can be found in Appendix A.

Chapter 2: General Materials and Methods

This Chapter details the methods across all electrochemical experiments. Discussed here are the blood property measurements, electrode preparation steps, electrochemical analysis and data analysis. Any methods differing from this general set are detailed in subsequent Chapters.

2.1 Blood source and blood property measurements

Whole bovine blood with 12.5% v/v acid citrate dextrose anticoagulant (ACD-A) was obtained from Windcrest Meat Packers in Port Perry, Ontario. Bovine blood is a recognized blood substitute for forensic research, and was used across all analsyes [108]. The blood was always used for electrochemical preparation and fluid property measurements within 2 hours of blood collection. The blood was stored in a sealed and opaque amber bottle in the refrigerator (4°C) when not in use. The packed cell volume percentage (PCV%) and density the blood was measured on all days of electrode preparations. For the characterization experiment, presented in Chapter 3, electrochemical measurements were taken across five consecutive days. Fluid property measurements were recorded each day the blood was used and was visually inspected for clots. During the time-series experiment, property measurements were recorded the day of collection/electrode preparation.

Density was measured using a 1 mL Hamilton glass syringe and FA/JA series electronic balance. Dry weight of the syringe and with 1 mL of blood was used to determine density in replicates of 5 each day. Density measurements of Millipore water were obtained to report relative density measurements for the blood. The PCV% measurements were obtained by centrifuging whole blood-filled capillary tubes at 12,000 rpm for 2 minutes using the Haematokrit 200 (Hettich Zentrifugen) in replicates of 8. After centrifugation the packed RBC layer height was measured and divided by the total column height to obtain PCV%. using the was measured using the Density and PCV% were measured at room temperature (22°C and 40 RH%) for both property measurements, the same conditions as electrode preparation conditions.

2.2. Electrode preparation

GC electrodes were polished with 0.05 µm alumina slurry on a microcloth pad prior to film preparation and after each analysis. Following polishing, any residual polishing solution was washed off using DI water and air-dried using a compressor within a fume hood. Before surface preparation each electrode was visually inspected to ensure the surface was clean. A digital multimeter was used to confirm each electrode was working properly before analysis and blank electrode measurements were recorded for each electrode before blood deposition and measurement.

Electrodes were fixed up vertically using a retort stand for surface coating. The final film deposited on the electrode is represented by: Naf/Blood/Naf, and is illustrated in Figure 2.1. Using a Hamilton #75, 5 µL glass syringe, 1 µL of a 5 wt% Naf 117 solution was dispensed on the electrode surface followed by a select volume (0.5, 1, or 2 µL) of bovine blood and then with an additional 1 µL layer of the Naf solution. Five minutes for drying was allotted between each layering stage. Uniform layers were approved through manual inspection.

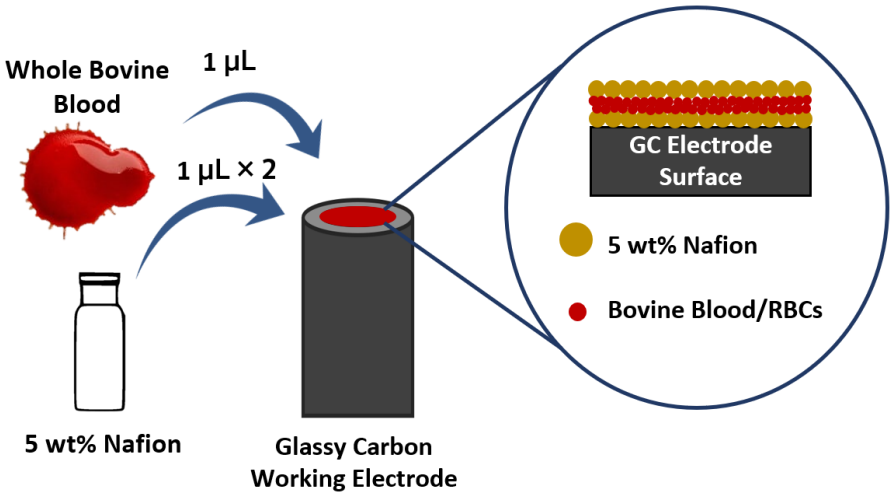

Figure 2.1: *Schematic of blood deposited films on GC electrode surface, Naf/Blood/Naf.*

2.3. Electrochemical experimentation

Following electrode preparation steps the electrode to be analyzed was placed in an electrochemical cell was filled with 0.05 M disodium phosphate buffer solution (Na_2HPO_4). The pH of this solution was adjusted using 85 wt% phosphoric acid to 3.0 or

7.0, and was measured prior to electrochemical measurements using a Mettler Toledo™ FiveEasy Plus™ FEP20 pH meter. All reagents were purchased from Sigma-Aldrich (Oakville, ON). The electrochemical cells were then purged with high purity N_2 (99.998%) for 15 minutes to allow deoxygenation of the solution to occur. Immediately after purging, differential pulse voltammetry (DPV) was used to analyze the electrode.

Electrochemical measurements were obtained using a Pine Instruments model AFPC2 and Pine WaveDriver 20 potentiostat connected in a three-electrode system contained in an all-glass one-compartment electrochemical cell with a Teflon cap. The three electrodes include: a platinum wire counter electrode, a Hg/Hg_2SO_4 reference electrode saturated in K_2SO_4, and a working GC electrode with deposited Naf/Blood/Naf film. All electrodes were obtained from CH Instruments (Austin, USA). The GC working electrodes (CHI 104) had a 3.0 mm carbon diameter (0.0707 cm^2 surface area), 6.35 mm total diameter including the inert K-shell. The same Hg/Hg_2SO_4 reference electrode (CHI 151) was used for all analysis and the reported electrochemical potentials are adjusted to the reversible hydrogen electrode (RHE).

Cyclic DPVs were collected between 300 mV to -1000 mV (vs Hg/Hg_2SO_4) with a 10 mVs^{-1} scan rate. The initial potential was 300 mV and once the potential was reached -1000 mV the potential was reversed to go back to 300 mV. The pulse parameters used for analysis were: height of 50 mV, width of 250 milliseconds, and period of 2 seconds. All electrochemical analyses were performed at room temperature (22-25°C). Voltammograms were collected using AfterMath version 1.5.9807 software.

Following electrochemical data collection, the electrodes were cleaned, polished and reused for subsequent analysis. When not in use the electrodes were stored in capped plastic vials in a cupboard free of moisture and light exposure.

2.4. DPV analysis

Raw data from the DPVs were extracted from Aftermath and were processed through blank subtraction using Microsoft Excel. Additionally, all potential values were corrected to the RHE. The reduction and oxidation sweeps were separated for further analyses in OriginPro 2019b. The blank subtracted voltammograms were then imported into OriginPro 2019b graphing and analysis software. DPVs were first smoothed with the

Savitzky-Golay method with 5 points of window and 2nd polynomial order. The smoothed current was then plotted against the potential for peak analysis. The peak analyzer function in OrginPro was used to integrate resolved peaks in both the reduction and oxidation sweep. In these cases, a defined baseline was first established. Ten points were manually selected for each voltammogram to establish a baseline. The 'snap to spectrum' and 'auto subtract baseline' parameters were applied. Following this the number of peaks of interest was inputted and the automatic peak finder integrates the peaks of the highest maxima. The peak area, height, and maxima were recorded in an Excel table for further statistical analysis, described in Chapters 3 and 4.

Unresolved peaks were processed using a manual baseline and peak deconvolution. Using the 'multiple peak fit' function in OrginPro a Gaussian (Gauss) distribution was selected and the overlapping peaks were chosen. Prompting the software to complete the deconvolution by selecting 'fit until converged' in the processing window outlines the deconvolution trace. If the accepted Chi-square tolerance value is reached the deconvolution is satisfactory and publishes the data in the workbook window. The peak area, height, and maxima was recorded for each of the unresolved peaks. This multi-peak fit methodology was required for the oxidation peaks across all experimental conditions and for some of the reduction peaks in the acidic pH groups.

Chapter 3: Electrochemical Characterization of Blood Films on Glassy Carbon Electrodes

3.1 Overview

The characterization study is divided into three main sections: i) factorial design experiment, ii) Rotating disk electrode (RDE) experiment, and iii) electrode imaging. Together they focus on understanding the redox reactions associated with the bovine blood film and determining the optimal experimental conditions to study these reactions for forensic science purposes. The first experiment conducted was a factorial design experiment, focusing on how select experimental conditions affect the electrochemical measurements. During this experiment the effects of buffer pH, the volume of blood deposited on the electrode, and the concentration of blood were assessed.

Following the characterization study, the optimized experimental condition along with 0.1 M H_2SO_4 and KOH buffers were used to determine the reactions involved in the Hb mediated ORR on the electrode using a RDE. The objectives of this experiment were to understand the pathway of electron transfers in the bovine blood film, particularly the products of O_2 reduction. The optimal experimental condition provides insight into reactions occurring during characterization and the time series experiments. The varying pH conditions provide results that were compared to other electrochemical systems involving the ORR.

Insight into how the bovine blood was drying on the electrode surface was obtained through digital photography and SEM. These images provide insight in how the blood is drying on the electrode surface, the associated morphology, and relate to the observed variability.

3.2 Factorial design experiment for blood film characterization

3.2.1 Methodology

Electrodes were prepared (according to Chapter 2) in sets of five for the electrochemical analysis of each experimental condition in the characterization study. The three factors assessed include: pH of the phosphate buffer, the volume of blood immobilized on the electrode, and the concentration of blood used. Two buffer pH

solutions were tested: 3.0 and 7.0. The blood volumes placed on the electrode were of 0.5, 1, and 2 µL. Lastly, the blood concentrations of whole blood (denoted as 1) and 50:50 blood:DI water mixture (v:v, denoted as 0.5) were evaluated. Each set of factors were analyzed in replicates of 5, for a total of 60 measurements. DPV were processed according to the methods in Chapter 2.

3.2.2 Data analysis

As previously described, Origin 2019b software was used to gather peak potentials (V), heights (µA) and areas (µW) for each observed peak. Ratios between the reduction and oxidations peak heights and areas were calculated. The Grubbs Test was applied to determine outliers with experimental conditions and if the data point met the definition of an outlier they were manually removed from the dataset. ANOVA analysis was performed using RStudio version 3.6.2 (2019), and p-values were reported to determine whether influencing and/or interaction effects are present between the three independent variables. Data for each response variable was plotted in a boxplot to visualize the observed variation between and within experimental conditions. Method optimization was determined as a combination of visual analysis of the voltammograms, boxplots, and statistical analysis.

3.2.3 Blood Properties

The same blood source was used for all experimental conditions and replicates across 5 days. Density and PCV% data were collected each day to monitor changes in the blood. Table 3.1 presents the PCV% and density measurements for the 5 days of the factorial design experiment, including the relative standard deviations (RSD) within each day. Using a one-way ANOVA, the p-values for the PCV% and density were 0.995 and 0.792 respectively. Both values are not significant, demonstrating that there is no change in these properties over a 5-day period when the blood was stored in the fridge. The stability of these properties, most heavily linked to film deposition mechanics and Hb concentrations; across days of analysis suggests that changes in electrochemical measurements are therefore attributed to experimental condition changes and not RBC or Hb damages.

Table 3.1: *Average PCV% (n = 8) and density (n = 5) measurements for each day of analysis during the factorial design experiment, for a total of 5 days. RSD = Relative Standard Deviation*

Day of Analysis	PCV% (RSD)	Density (g/mL) (RSD)
1	46.85 ± 0.01 (2.65 %)	1.0481 ± 0.0093 (0.88 %)
2	46.79 ± 0.01 (1.47 %)	1.0492 ± 0.0031 (0.30 %)
3	49.81 ± 0.01 (1.91 %)	1.0429 ± 0.0046 (0.45 %)
4	47.44 ± 0.01 (2.28 %)	1.0462 ± 0.0064 (0.61 %)
5	46.54 ± 0.01 (1.57 %)	1.0483 ± 0.0031 (0.29 %)

3.3 DPV characterization

The data collected from the factorial design experiment were used to characterize the electrochemical peaks in the DPVs. Upon initial analysis it was clear that pH had the greatest effect on peak presence and shape. Several peaks are consistent between pH conditions; however, pH 3.0 presented additional peaks than pH 7.0. Figure 3.1 shows DPVs from the acidic (A, left) and neutral (B, right) pH conditions and Table 3.2 summarizes the presence and average peak potential of the observed peaks in pH groups. Peaks were named based on the order they appeared in the pH 7.0 voltammograms with 'Red' (reduction) or 'Ox' (oxidation) attributed to cathodic and anodic sweeps respectively.

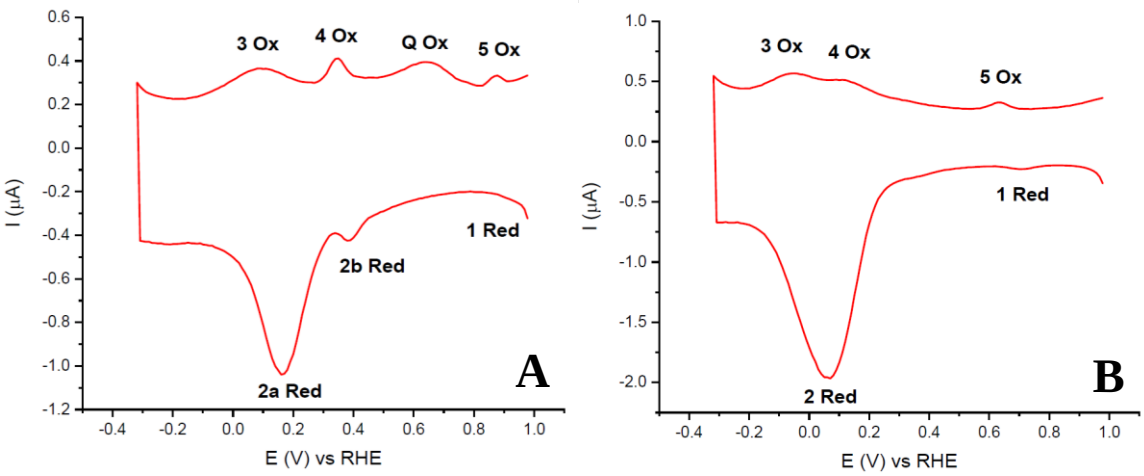

Figure 3.1: *Cyclic DPVs of 1 μL whole bovine blood deposited on GC electrodes (Naf/Blood/Naf) in pH 3.0 (A) and pH 7.0 (B). 10 mV/sec scan rate and purged with N_2.*

Table 3.2: *Summary of specific peak presence and potential in DPVs of whole bovine blood deposited on GC electrodes (Naf/Blood/Naf). The table is split into sections with reduction peaks (above) and oxidation peaks (below).*

Observed Reduction Peak	Presence in pH 3	Average peak potential vs RHE	Presence in pH 7	Average peak potential vs RHE
1 Red	Yes *	0.8157 V ± 0.2773	Yes	0.7062 V ± 0.0175
2/2a Red	Yes	0.1658 V ± 0.0385	Yes	0.0465 V ± 0.0386
2b Red	Yes *	0.2493 V ± 0.1794	No	N/A

*Not present in all replicates

Observed Oxidation Peak	Presence in pH 3	Average peak potential vs RHE	Presence in pH 7	Average peak potential vs RHE
3 Ox	Yes	0.0864 V ± 0.0321	Yes	-0.0751 V ± 0.0168
4 Ox	Yes	0.3342 V ± 0.0062	Yes	0.0799 V ± 0.0268
Q Ox	Yes	0.6488 V ± 0.0192	No	N/A
5 Ox	Yes	0.8696 V ± 0.0056	Yes	0.6339V ± 0.0120

The peaks 1 Red and 5 Ox are attributed to the reduction of quinone and hydroquinone species on the GC electrode surface. These peaks are seen in varying magnitudes in both pH groups with a more positive peak potential in the acidic group. In the neutral pH the 5 Ox peak is at a lower potential compared to the 1 Red peak; and opposite for the acidic pH: supporting the hypothesis that these are attributed to different quinone redox reactions. The Q Ox peak, in Figure 3.1, is only seen in the pH 3.0 group and is likely attributed to an additional quinone species oxidation. The identity of this peak was first questioned to belong to quinone or hydrogen peroxide oxidation. To answer this question, the Naf/Blood/Naf film was analyzed with the vertex potential set before the 2b Red peak (0.48 V vs RHE). This figure is shown in Appendix B and the Q Ox peak is still present. If this peak belonged to hydrogen peroxide oxidation, then no peak would be present since no hydrogen peroxide would be produced in the cathodic sweep. The peak potential of roughly 0.6 V vs RHE in the Q Ox peak correlates with

other research focused on quinone species reduction on GC electrodes [110–112]. Research surrounding GC electrode corrosion and studying various quinone redox potentials demonstrate that these reactions are pH dependent [110,113,114]. Reaction mechanisms from these studies support a 2-electron and 2-electron/2-proton redox reaction for quinone species and is shown in Equation 1 [110,113]. In the research presented here none of these peaks were removed from blank electrode voltammogram subtractions. The explanation for this belongs to the Naf/Blood/Naf film created on the electrodes. Naf is a perfluorosulfonate linear polymer commonly used as an immobilization matrix due to its film forming properties and good proton-conductivity [115]. Naf acts as a proton donor in these reactions which was not observed in bare electrode analyses.

$$Quinone + 2e^- + 2H^+ \rightarrow Hydroquinone \qquad (1)$$

The largest peak in the voltammograms is the 2 Red peak. This peak is present in both pH groups but in several cases, a smaller unresolved peak was present in the pH 3.0 group ($E^{\circ}_{obs} = 0.2493$ V ± 0.1794). For this DPV, the 2 Red peak is labelled 2a Red ($E^{\circ}_{obs} = 0.1658$ V ± 0.0385) and 2b Red, with 2a Red being the larger of the two in every case. The separation of peaks in the acidic pH is attributed to variations in film structure where the acidic pH was lysing cells providing differences in electron transfers. Additionally, this onset peak could be indicative of hydrogen peroxide formation by Hb [93]. The 2b Red peak was not present in all replicates.

In both pH conditions this/these peak corresponds to Hb catalyzed oxygen reduction and reduction of ferric Hb ($HbFe^{3+}$). With Hb's main role in the body to carry and transport O_2, the heme molecules have a high affinity for O_2 compared to other ligands. In addition to the transport of O_2 through the body, Hb facilitates the ORR at the same potential of $HbFe^{3+}$ reduction [31,116].

When blood is exposed to the environment, atmospheric O_2 is able to enter the plasma membrane and rapidly reacts with the ferrous Hb ($HbFe^{2+}$) to give the physiologically important $HbFe^{2+}$-O_2 [31,116–118]. This process is shown in Equation 2. *In vivo* the vast majority of Hb in a healthy individual is maintained in this form as either

oxyHb or deoxyHb. Upon oxygen binding, the central iron atom is brought into plane with the porphyrin ring and is converted to a low spin state [15,31]. These structural changes of Hb protect against oxidative damages *in vivo,* specifically through the protection of the heme molecules in the hydrophobic pockets of the protein [15]. Maintaining iron in its Fe^{2+} state upon O_2 binding and during the ORR is critical for aerobic respiration and is accomplished through the Hb protein structure.

$$HbFe^{2+} + O_2 \rightarrow HbFe^{2+}\text{–}O_2 \qquad (2)$$

The ORR is one of the most widely studied electrochemical reactions. This reaction is fundamental to aerobic life and involves the transport of O_2 and conversion of energy. Hb has high catalytic activity and electrochemical stability to carry out this reaction. In aqueous solutions the ORR is propagated through two pathways: a direct 4-electron/4-proton pathway forming water, and a 2-electron/2-proton transfer pathway forming hydrogen peroxide. The pH of solution influences which pathway is present, which will be discussed further in this Chapter when investigating ORR pathways using RDE. The two ORR pathways catalyzed by Hb are shown below in Equations 3 and 4.

$HbFe^{2+}\text{–}O_2 + 4e^- + 4H^+ \rightarrow HbFe^{2+} + 2H_2O$ (3), $E^{\circ}_{obs\ (pH=7)} = 0.0465\ V \pm 0.0386$

$HbFe^{2+}\text{–}O_2 + 2e^- + 2H^+ \rightarrow HbFe^{2+} + H_2O_2$ (4), $E^{\circ}_{obs\ (pH=7)} = 0.0465\ V \pm 0.0386$

$HbFe^{2+}$ is able to catalyze the reduction of oxygen at the potential of $HbFe^{3+}$ reduction, shown in Equation 5, while preserving its ability to bind oxygen. In other words, during the process of oxygen reduction, $HbFe^{2+}$ is able to stay in its healthy form without being oxidized to its physiologically damaging $HbFe^{3+}$ form. The oxidation of $HbFe^{2+}$ to $HbFe^{3+}$ does occur and has the potential of initiating an oxidative cascade that leads to heme loss and cellular damages [31]. This reaction is shown in reaction 6. The active site geometry of Hb makes the pathway in Equation 2 highly favoured over the oxidative pathway in Equation 6. [31,119]. *In vivo* the concentrations of $HbFe^{3+}$ are kept to a minimum by reductive enzymes, but *ex vivo* this oxidation remains permanent.

$HbFe^{3+} + e^- \rightarrow HbFe^{2+}$ (5), $E^{\circ}_{obs(pH=7)} = 0.0465\ V \pm 0.0386$

$$HbFe^{2+} + O_2 \rightarrow HbFe^{3+} + O_2^{\cdot -} \qquad (6)$$

In summary, the 2 Red peak corresponds to the Hb catalyzed ORR and the reduction of $HbFe^{3+}$, shown in Equations 3, 4, and 5. Within the neutral pH buffer, the peak potential for these reactions is, $E^{\circ}_{obs} = 0.0465$ V ± 0.0386, and in the acidic buffer $E^{\circ}_{obs} = 0.1658$ V ± 0.0385. Shift in reduction potentials are attributed to proton availability in the buffers and the structural changes pH has on the blood film, influencing electron transfer kinetics. Within the 2 Red Peak, the $HbFe^{2+}$-O_2 species are able to undergo electrochemical reduction at the potential of $HbFe^{3+}$ reduction to produce $HbFe^{2+}$ again [34,116,119]. This reduction process of bound O_2 while maintaining Hb in its physiological important oxidation state is critical to life and relates to the reusability of Hb. Given the high affinity $HbFe^{2+}$ has for O_2, any dissolved O_2 in the buffer solution would bind and undergo reduction, increasing the magnitude of this peak. For this reason, the electrochemical cell was purged with N_2 prior to analysis to remove any dissolved O_2. The catalytic activity of Hb is important from a biomedical or clinical perspective but this research focusses on the electrochemical responses within the bloodstains so any dissolved O_2 would cause an over estimation of the 2 Red peak. Literature concerned with this electrochemical process for biomedical purposes have demonstrated that high O_2 saturation levels correspond to higher reduction peak magnitudes [91,117]. From a forensic science perspective, only the bound O_2 within the bloodstain is of interest. As mentioned previously, at the potential of O_2 reduction, $HbFe^{3+}$ reduction is occurring. This reaction is shown in Equation 5. In an aged bloodstain the concentration of naturally oxidized Hb increases, and this has been demonstrated using spectroscopy [32,44,57]. The combination of these reactions making up the 2 Red peak leads to the hypothesis that the properties of this peak are correlated with time since the O_2 concentration within the stain decreases as the bloodstain ages.

Coupled to the O_2 and $HbFe^{3+}$ reduction are peaks 3 Ox and 4 Ox in the anodic sweep, shown closer in Figure 3.2. Within the neutral pH buffer, the peak potential for the 3 Ox and 4 Ox reactions are, $E^{\circ}_{obs} = -0.0751$ V ± 0.0168, and $E^{\circ}_{obs} = 0.0799$ V ± 0.0268 respectively. These peaks are not fully resolved with slightly better separation seen in the acidic pH group. These peaks are predicted to be the Hb contained iron oxidation, on the basis that these regions are roughly at the same potential of the oxygen and $HbFe^{3+}$ reduction. Heme containing iron oxidation is shown below in Equation 7.

$$HbFe^{2+} \rightarrow HbFe^{3+} + e^{-} \quad (7),$$

$E^{\circ}_{obs\ (pH=7)}$ = -0.0751 V ± 0.0168 and $E^{\circ}_{obs\ (pH=7)}$ = 0.0799 V ± 0.0268

The two regions of these peaks are seen across replicates and it is proposed that these regions are related to the structural integrity of the RBCs. Similar peak characteristics were observed in the anodic sweep of research published by Doménech-Carbó *et al.* (2016) when studying hemolysis using square wave voltammetry [88]. Both peaks relate to the electron transfer involving $HbFe^{2+}$/$HbFe^{3+}$ but peak potentials are shifted based on varying cell membrane properties that favour/resist electron transfer processes. Peak 3 Ox is proposed as corresponding to "healthy" or undamaged cells which contain $HbFe^{2+}$. Electron transfers from the electrode surface are able to migrate through the cell membrane to the protected $HbFe^{2+}$ contained within the cell's microenvironment. Peak 4 Ox is proposed as the electron transfer process of lysed, or structurally faulty, cells [88]. Drying conditions and exposure to the environment leads to the degradation of cell structures. As cellular components break down, damages to the cell membrane expose the Hb to environmental stresses that can change protein structures. This along with the layering of cells leads to increased resistance in electron transfers to the electrode surface.

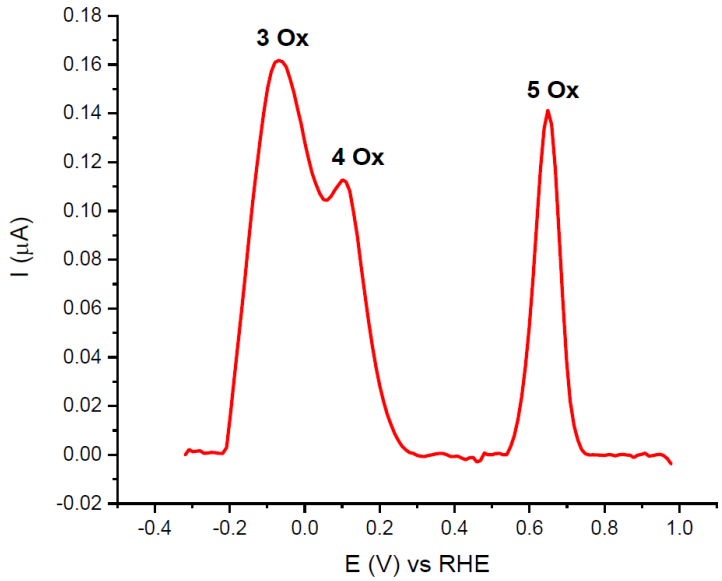

Figure 3.2: *Blank subtracted anodic sweep of cyclic DPV of 1 μL whole bovine blood deposited on GC electrodes (Naf/Blood/Naf) in pH 7.0, 10 mV/sec scan rate and purged with N_2. 10 mV/sec scan rate and purged with N_2.*

The differentiation of these peaks, 3 Ox and 4 Ox, may provide insight into forensic TSD through cell lyses processes. Research that has reported this observation before and have applied it to biomedical diagnosis of blood-related conditions and to the better understanding of blood storage practices for clinical applications [88,116]. Similar processes occur in bloodstains and can be interpreted through a forensic lens. As a bloodstain ages healthy cells begin to lyse from environmental factors such as temperature, humidity, and sunlight. Older bloodstains are predicted to have a smaller ratio of unlysed:lysed cells. If this is true and electrochemical methods are sensitive enough to distinguish the differences, then older bloodstains should have a greater magnitude in the 4 Ox peak compared to the 3 Ox peak due to sample degradation over time. The opposite would be true for the fresher bloodstains, where most of the cells are expected to be intact with few lysing quickly. A greater magnitude in the 3 Ox peak is expected.

3.4 Method optimization for forensic TSD

The factorial design experiment consisted of 12 experimental conditions each analyzed in replicates of 5 for a total of 60 analyses. The effects of pH, blood volume, and blood concentration were assessed to determine an optimal experimental condition.

Peak potentials (V), heights (μA) and areas (μW) were measured for all the observed peaks in the DPV. For optimization purposes the reproducibility of the Hb related peaks were the primary focus as they directly relate to the blood film. This includes the 2 Red, 3 Ox, 4 Ox peaks as well as their respective peak ratios.

The effects of blood volume, blood concentration and pH of the buffer are all observed to have an effect on electrochemical analysis. A three-factor ANOVA was used for statistical analysis to provide a more detailed understanding of which independent or combined factors have the greatest influence on the electrochemical response. Table 3.3 lists the influencing effects for each of the measured response variables, along with the p-value for each significantly correlated effect. Only the statistically significant individual and/or combined effects on electrochemical measurements are included in the table. Additionally, distribution boxplots are presented here to demonstrate the variation seen within each experimental condition; for all boxplots refer to Appendix B.

Table 3.3: *Statistical analysis of Hb related redox peaks in Naf/Blood/Naf film created on GC electrodes, analyzed using cyclic DPV. The dependent variable column refers to measured response associated for each peak or the respective ratio between identified peaks. Influencing effects refers to the individual, two-way or combined effects influencing the corresponding dependent variable. (Significance is denoted by: 0.001***, 0.01**, 0.05*)*

Peak Identification	Dependent Variable	Influencing Effects	Pr(>F)
2a Red	Potential (V)	Buffer	< 2e-16 ***
		Concentration	0.000256 ***
		Volume	0.001484 **
		Buffer:Concentration	0.000153 ***
		Buffer:Volume	0.027287 *
		Concentration:Volume	9.82e-6 ***
	Height (µA)	Volume	0.03188 *
		Concentration:Volume	0.00589 **
	Area (µW)	Buffer	0.023784 *
		Concentration	0.000493 ***
		Volume	0.021344 *
		Concentration:Volume	0.005343 **
2b Red	Height (µA)	Buffer	3.47e-13 ***
		Concentration	0.02273 *
		Volume	0.00783 **
		Buffer:Concentration	0.02014 *
		Buffer:Volume	0.00767 **
		Concentration:Volume	9.94e-5 ***
		Buffer:Concentration:Volume	5.46e-5 ***
	Area (µW)	Buffer	2.53e-13 ***
		Concentration	0.00251 **
		Volume	0.03554 *
		Buffer:Concentration	0.00196 **
		Buffer:Volume	0.03105 *
		Concentration:Volume	2.83e-6 ***
		Buffer:Concentration:Volume	2.05e-6 ***
3 Ox	Potential (V)	Buffer	<2.16e-16 ***
		Volume	0.00319 **
		Buffer:Volume	9.50e-10 *
		Buffer:Concentration	0.01140 *
		Buffer:Concentration:Volume	3.88e-11 ***
	Height (µA)	Buffer:Concentration	0.010123 *
		Buffer:Volume	0.000153 ***
		Concentration:Volume	0.000146 ***
	Area (µW)	Buffer	1.06e-8 ***
		Buffer:Volume	0.000165 ***
		Concentration:Volume	0.000197 ***
		Buffer:Concentration:Volume	0.024474 *
4 Ox	Potential (V)	Buffer	< 2e-16 ***

		Concentration	5.23e-6 ***
		Volume	0.01031 *
		Buffer:Concentration	0.00197 **
		Buffer:Volume	2.97e-5 ***
		Concentration:Volume	1.11e-6 ***
		Buffer:Concentration:Volume	3.39e-5 ***
	Height (µA)	Concentration	0.002913 **
		Buffer:Concentration	0.018189 *
		Buffer:Volume	2.83e-10 ***
		Concentration:Volume	0.000718 ***
		Buffer:Concentration:Volume	5.04e-7 ***
	Area (µW)	Buffer	1.17e-14 ***
		Concentration	3.27e-6 ***
		Volume	1.21e-7 ***
		Buffer:Concentration	5.38e-7 ***
		Buffer:Volume	4.03e-13 ***
		Concentration:Volume	1.84e-8 ***
		Buffer:Concentration:Volume	1.20e-10 ***
2a Red/3 Ox	Height	Buffer	0.000282 ***
		Buffer:Concentration	6.29e-5 ***
		Buffer:Volume	0.005683 **
	Area	Buffer	4.17e-11 ***
		Buffer:Concentration	0.00736 **
		Buffer:Volume	0.01778 *
		Buffer:Concentration:Volume	0.01683 *
2a Red/4 Ox	Height	Volume	0.00187 **
		Buffer:Volume	1.15e-5 ***
		Buffer:Concentration:Volume	0.00920 **
	Area	Buffer	0.0145 *
		Volume	0.0124 *
		Buffer:Volume	1.6e-5 ***
		Concentration:Volume	0.0299 *
2b Red/4 Ox	Height	Buffer	5.77e-12 ***
		Concentration:Volume	0.000127 ***
		Buffer:Concentration:Volume	0.000182 ***
	Area	Buffer	1.27e-11 ***
		Concentration	0.0224 *
		Buffer:Concentration	0.0194 *
		Concentration:Volume	4.69e-5 ***
		Buffer:Concentration:Volume	6.653-5 ***
2a Red + 2b Red/ 3 Ox + 4 Ox	Height	Buffer:Concentration	0.00197 **
	Area	Buffer	4.25e-9 ***
		Concentration	1.72e-5 ***
		Volume	1.47e-6 ***
		Buffer:Volume	0.00807 **
		Buffer:Concentrtion:Volume	0.03511 *

3.4.1 Effect of pH

The effect of buffer pH was significant in electrochemical response, as demonstrated in the electrochemical characterization section. As seen in Table 3.3 the electrolyte pH, labeled 'Buffer', had a significant effect for most of the peak variables. Between pH conditions, similar peak shapes and distributions were noticed with shifts to more positive potentials in the acidic pH due to increased proton availability. The neutral pH group provided greater reproducibility for many of the Hb associated electrochemical peaks. The reduction peak height of the 2 Red peak in Figure 3.3 demonstrates this, particularly in the high blood volume conditions. Within the neutral pH the average peak height of the 2 Red peak was found to be 1.2516 ± 0.2866 µA (22.89% RSD), and in the acidic pH it was 1.2268 ± 0.6284 µA (51.22% RSD). Similar average peak currents (i.e. heights) were measured between pH groups but a larger variation is observed in the acidic pH replicates. It is important to note that Hb related redox peaks are able to be studied in lower pH's with no noticeable effects on electrode biofouling or deposited material leaching into solution. The layers of Naf between the blood was effective in immobilizing the blood onto the electrodes. Additionally, within the acidic pH, the 2 Red peak was found to have two distinct regions in some cases (labelled 2a and 2b Red), but was not observed in all replicates. The neutral pH provided consistent peak shapes in all replicates, regardless of blood volume and concentration.

Comparing the 3 Ox and 4 Ox peaks; in many cases the acidic pH did provide a better peak separation and comparable variation observed between pH groups. The peak heights for the 3 Ox peak in the pH 3.0 and 7.0 samples were measured to be 0.1788 ± 0.0670 µA (37.49% RSD) and 0.1581 ± 0.0537 µA (33.97% RSD) respectively. Similarly, the peak heights for the 4 Ox peak in the pH 3.0 and 7.0 samples were measured to be 0.1073 ± 0.0458 µA (42.68% RSD) and 0.1131 ± 0.0677 µA (59.91% RSD) respectively. Larger variations were seen in the Hb oxidation peaks compared to the 2 Red Hb reduction peak. However, within pH groups the 3 and 4 Ox peaks have similar RSD. It is important to state that these values do not consider blood volume or concentration, which are contributing to the electrochemical responses. The 3 Ox and 4 Ox peaks were not fully separated in the neutral pH however peak deconvolution was achievable using a Gaussian function.

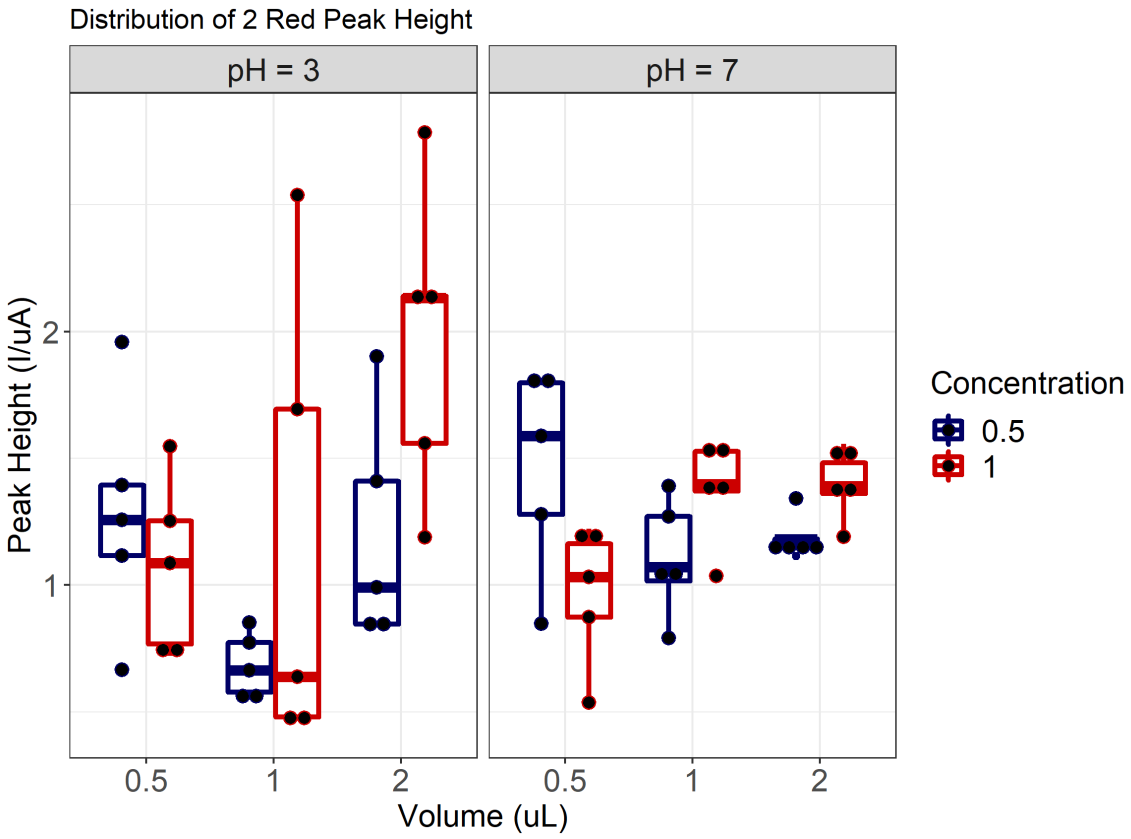

Figure 3.3: *Distribution boxplot of 2 Red peak height (2a Red in pH 3.0 group) in Naf/Blood/Naf film created on GC electrodes, analyzed using cyclic DPV. The boxes group the pH of the phosphate buffer of 3.0 and 7.0 respectively, volume (µL) of blood deposited on the electrode is represented on the independent axis, and concentration is shown for each corresponding volume where blue (left) corresponds to diluted blood (0.5) and red (right) corresponds to whole blood (1).*

The effect of buffer pH has an important role in the redox reaction of Hb. The ORR is an electron/proton coupled reaction. The accessibility of protons to the heme molecules influences the electron transfer [120]. The ORR involves protons in the reaction and reduction pathways vary based on proton availability [121–123]. The appropriate concentration of protons has been shown to facilitate the redox reaction of Hb, and suggests that increased concentrations can change the polypeptide structure of Hb [124,125]. This experiment found that a pH of 7.0 was optimal for the analysis; and is consistent with previous research that has used pH 6-8 to characterize purified Hb samples [34,62,88,120,126]. Lower pH values have also demonstrated electro-inactive behaviour and irreversible redox electron exchange in Hb and blood samples, which was not observed here [62,84,102]. A buffer pH of 7.0 suggests that the Hb remans accessible

to electron transfers and ORR catalytic activity. This pH is also close to the physiologically maintained pH of blood which is around 7.3-7.4 [127].

3.4.2 Effect of blood volume

The volume of blood deposited on the electrode was an influential factor in electrochemical response. The greater the volume the more RBCs and Hb is present for potential electron transfer sites. The mass loadings of each of the blood volumes used, given the average density of 1.04694 g/mL and surface area of the electrodes, was calculated to be: 7404 μg/cm^2 for 0.5 μL, 14808 μg/cm^2 for 1 μL, and 29616 μg/cm^2 for the 2 μL volume.

Firstly, the deposition and drying time was noticeably different for each volume. The smallest and largest volumes, 0.5 μL and 2 μL, were difficult to spread across the surface of the electrode evenly. Both volumes created visually non-uniform films on the electrode surfaces. The volume of blood is hypothesized to influence drying patterns and effect reproducibility [20,21,128,129]. The 1 μL observed an even and reproducible distribution of blood across replicates. Additionally, with each larger increment of volume the drying time increased, where the largest volume took much longer to dry compared to the lesser volumes. The drying of the blood on the electrode likely has an effect on electrochemical analysis. As the film dries the RBCs stack and layer each other in the film. An uneven distribution of cells influences the ability of electrons to access the active sites within the heme molecules. Cells further from the electrode surface or ones that are in complex drying structures create resistance for electron transfers to occur. The number of RBCs is directly proportional to the volume of blood immobilized on the electrode surface. Higher volumes impose restrictions on material distribution on the electrode surface. The ability for the RBCs to assemble in a reliable and reproducible drying pattern is critical in the analysis and the blood volume plays an important role in this feature.

The complexity of blood drying morphology effects the quantity of Hb that can participate in redox reactions. In cases where the blood film was unevenly distributed or where RBC drying arrangements effect the number of reaction sites. It was noticed across pH groups that larger 2 Red currents are associated with larger currents in the 3 Ox and 4

Ox peaks. This is explained through the Hb molecules that are able to participate in these reactions. When the $HbFe^{2+}$-O_2 or $HbFe^{3+}$ molecules are reduced during the cathodic sweep, those same specific molecules are able participate in oxidation in the anodic sweep. Furthermore, the Hb molecules unable to participate in redox reactions are not contributing to the reduction or oxidation peaks. This is supported by Figure 3.4 where the ratio of reduction:oxidation peak areas in plotted across experimental conditions. Within each experimental condition relatively reproducible results were obtained, with slightly higher ratios in the neutral pH. The influence of blood volume is significant across many measured response variables. The volume directly relates to the drying of blood on the electrode surface which in turn affects which Hb or RBCs are able to participate redox reactions.

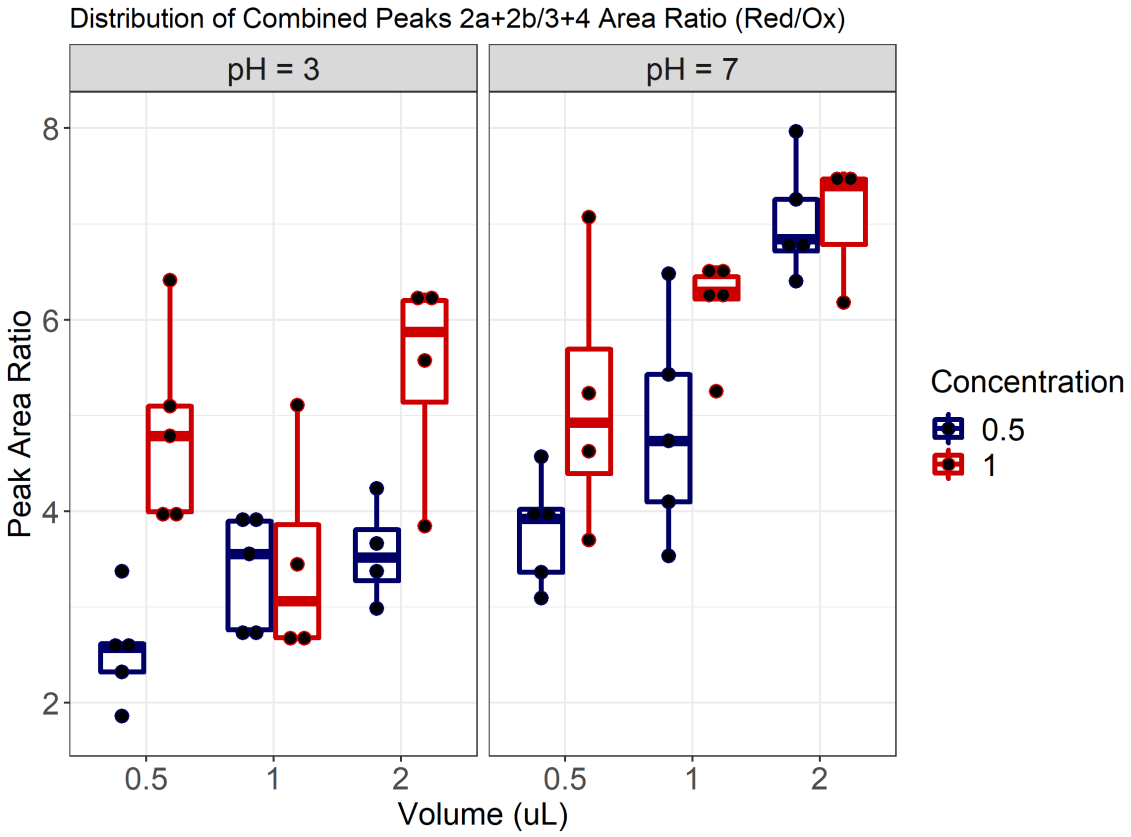

Figure 3.4: *Distribution boxplot of the combined Hb related peak area ratio (2a Red + 2b Red/ 3 Ox +4 Ox) in Naf/Blood/Naf film created on GC electrodes, analyzed using cyclic DPV. The boxes group the pH of the phosphate buffer of 3.0 and 7.0 respectively, volume (µL) of blood deposited on the electrode is represented on the independent axis, and concentration is shown for each corresponding volume where blue (left) corresponds to diluted blood (0.5) and red (right) corresponds to whole blood (1).*

This research is consistent with the literature immobilizing blood on electrode surfaces. With 1 µL being reported as the deposited blood volume given an electrode surface area of 0.0707 cm^2 [34,107,126]. This volume was the most effective for electrode preparation but also electrochemical peak reproducibility. Peak heights and areas are proportional to concentration; therefore the 2 Red, 3 Ox, and 4 Ox peaks are related to the concentration of Hb within the blood film. Larger volumes correlate to more Hb molecules deposited on the electrodes and greater electrochemical responses are expected. Figures 3.3 and 3.4 demonstrate this, specifically in the pH 7.0 group within the 1 and 2 µL volumes. Within these volumes the 1 µL volume had the greatest reproducibility across replicates, specifically within the neutral pH group.

3.4.3 Effect of blood concentration

This parameter was introduced into the study to determine if whole blood concentration affects the reproducibility of analysis. Lowering the concentration of RBCs was hypothesized to affect the assembly of cells during the drying process. It was thought that this would allow electrons to access the RBCs/Hb more efficiently since the cells would be closer to the electrode surface and less layered. Statistical analysis demonstrated that concentration had an effect on many of the recorded dependent variables. However, variation of replicates was greater for the diluted samples compared to the whole samples within similar experimental conditions. When looking 2 Red peak height, Figure 3.3, this is observed in the neutral pH condition. Within the 1 µL, neutral pH group the average peak height and standard deviation for the whole and diluted samples were 1.3734 ± 0.2027 µA (14.75% RSD) and 1.1086 ± 0.2328 µA (21.00% RSD) respectively. The diluted blood did not necessarily lead to reduced peak heights or areas and in many cases, the results between diluted and whole blood of the same volume were comparable. Whole blood was chosen as an optimized method, since it had the lowest variation within replicates and is a more realistic sample encountered by forensic professionals.

3.4.4 Optimal experimental method summary

From this study the optimized analysis Hb in blood using electrochemistry was determined to be 1 µL of whole blood in a neutral pH phosphate buffer. These conditions promote reproducible and redox specific response in the DPVs. The optimal determined conditions are consistent with the pH values and volumes used in the literature. This study used bovine blood for DPV analysis which is recognised as a blood substitute for forensic research [108] and has been used for electrochemical analysis before [130].

The means of preparing electrodes proved to be a crucial step when ensuring the analysis is reproducible. The layering of the cells as the blood dries is an important factor that is influenced by the volume and concentration of blood deposited. This experiment demonstrates that electron transfer reaction associated with Hb and the ORR can be studied in each experimental group and that the electrolyte pH, blood volume and blood concentrations are necessary considerations when studying blood using electrochemical

methods. Developing a reliable method that was practical in regards to forensic blood evidence was kept in mind.

3.5 RDE results

The ORR is among the most important reactions, from biological processes such as cellular respiration to the energy conversions in fuel cells. The use of RDE techniques have become fundamental electrochemical methods for studying the electrocatalytic properties of materials for O_2 reduction at the electrode surface [131–133]. Evaluating catalysts and understanding the ORR mechanisms necessary crucial for the characterize of these materials. Within the body, Hb and Mb are the two proteins responsible for catalyzing the reduction of oxygen and energy conversion [31].

The most efficient pathway is the four-electron pathway for the ORR is where oxygen combines with 4-protons and 4-electrons to form water [116,134,135]. This reaction is shown in Equation 8. The less efficient pathway involves two steps, in which oxygen is first reduced to a hydrogen peroxide intermediate followed by a reduction to water. These reactions are shown in Equations 9a and 9b. The reaction 9b may not always occur and the ORR is referred to as a 2-electron pathway, forming hydrogen peroxide only.

$$O_2 + 4e^- + 4H^+ \rightarrow 2H_2O \quad (8)$$

$$O_2 + 2e^- + 2H^+ \rightarrow H_2O_2 \quad (9a)$$

$$H_2O_2 + 2e^- + 2H^+ \rightarrow H_2O \quad (9b)$$

Using RDE to study Hb catalytic activity involves the understanding of mass transport of oxygen to the electrode and the fundamental mechanics of oxygen reduction [132,136]. A rotating electrode drives the various mass transport mechanisms of dissolved O_2 to the electrode surface where an ORR catalyst performs its function. Increasing the rotation rate effectively increases the rate of O_2 supply to the catalyst until a diffusion limited current is reached, which in turn will yield kinetic information. These processes work on principles of convection and diffusion [131]. The rotation of the electrode generates convection currents that would otherwise be stagnant in the electrolyte solution at a steady state. During the rotation, in this case, O_2 is brought to the

electrode surface. At this point diffusion forces become more important. As the dissolved oxygen must diffuse through the film to be catalyzed. Following the ORR, the products radiate outward away from the electrode.

A Koutecky-Levich Study is a common experiment to study the ORR reaction, where a range of rotation rates are chosen to study a material's catalytic activity at the limiting current. At higher rotation rates, the magnitude of the half reaction should increase when only governed by mass transport effects [131]. Reaching limiting currents is ideal, where the magnitude of current plateaus at respective rotation rates, referred to as the diffusion limited current. These data from this experiment was used to create Koutecky-Levich plots for the blood deposited rotating electrode. In this form, the reciprocal limiting current is plotted against the reciprocal square root of the angular rotation rate. If limiting currents are used the plot should have a linear fit and the intercept of the line should intersect at zero on the dependent axis. The slope can be used to find the number of electrons involved in the reaction by substituting known values and constants into the Koutecky-Levich equation (Equation 10). Where i_L is the limiting current (A), i_K is the kinetic current (A), F is Faradays constant (96485 C/mol), A is the area of the electrode (cm^2), D is the O_2 diffusion coefficient (cm^2/sec), v is the kinematic viscosity of the buffer (cm^2/sec), C is the concentration of dissolved O_2 (mol/cm^3), and ω is the angular rotation rate (rad/sec).

$$\frac{1}{i_L} = \frac{1}{i_K} + \left(\frac{1}{0.620nFAD^{2/3}v^{-1/6}C}\right)\omega^{-1/2} \quad or, \quad \frac{1}{i_L} = \frac{1}{i_K} + \left(\frac{1}{B}\right)\omega^{-1/2} \qquad (10)$$

From this experimental design the number of electrons involved in the ORR and the reaction kinetics can be determined. The reciprocal of the Levich constant (B) multiplied by the slope of the Koutecky-Levich plot is used to determine the number of electrons involved in the reaction. Sluggish redox reactions require larger overpotentials to overcome resisted redox kinetics and reach higher limiting currents. The goal of this study in relation to Hb catalytic activity was to understand the redox reactions Hb is facilitating on the electrode surface in conditions similar to the characterization study. Additionally, basic and acidic pH conditions were tested to compare to other iron-based ORR catalysts.

3.5.1 RDE methodology

Using a Pine research E6R1 ChangeDisk Series rotating ring-disk glassy carbon working electrode (5.0 mm diameter, 0.1963 cm^2 surface area) linear scan voltammograms (LSV) were obtained between 300 mV and -1300 mV (vs Hg/Hg_2SO_4). Consistent electrode preparation steps were maintained for creating the Naf/Blood/Naf film on this electrode. To keep the same mass loading of blood used on the 3.00 mm electrode, 2.75 µL of 5% wt Naf and whole bovine blood were deposited on the rotating ring-disk electrode. The same electrode preparation steps were applied with blood sandwiched between two equal layers of Naf.

Voltammograms were obtained through AfterMath version 1.5.9807 software. The electrode was held in a large voltammetric glass cell (approximately 250 mL) by a Pine research modulated speed rotator. Within the cell a Hg/Hg_2SO_4 reference electrode and platinum wire counter electrode was used.

Three electrolyte solutions were tested. The first being 0.05 M disodium phosphate buffer solution (Na_2HPO_4) with a pH of 7.0, which was adjusted using 85 wt% phosphoric acid. The other electrolyte solutions include 0.1 M H_2SO_4 (pH = 1.25) and 0.1 M KOH (pH = 13.0). The same reference electrode was used for each electrolyte solution and was calibrated so the voltammograms could be plotted in the same potential range of 0.96 V to -0.64 V vs RHE.

After filling up the cell and securing the Naf/Blood/Naf rotating electrode the cell was purged with nitrogen gas for 20 minutes. Next, a blank LSV was obtained, and then the cell was then purged with oxygen for 20 minutes. The rotator was then turned on and the oxygen was set to a slow continuous purge. Voltammograms were collected at the following RPM: 1000, 800, 600, 400, and 200 (additionally 50 RPM was collected in the neutral pH).

Measurements were completed with two separate bovine blood collections. The first involved the pH 7, 0.05 M PBS. Five replicates of fresh bovine blood were analyzed on the day of collection and two weeks after. The blood was stored in an opaque container in the refrigerator over the two weeks. Additionally, blood was deposited on the electrode after the first day of analysis without the top Naf layer. This electrode was aged

for three days in the ESPEC SH-262 environmental chamber at 22°C and 40% RH (percent relative humidity). After the aging period the top Naf layer was deposited, and the single analysis was conducted. The LSV analysis in the acidic and basic electrolytes were completed using the same bovine blood source and were both analyzed in replicates of five using fresh blood only.

Following the data collection, the data was organized in Microsoft Excel (version 1808) and OriginPro 2019b was used to build Koutecky-Levich plots and visual voltammograms.

3.5.2 Experimental results from blood film RDE

Results from the RDE experiments are presented in Tables 3.4-3.6. The first two tables are from the results for the neutral pH RDE analysis of the fresh and aged blood, Tables 3.4 and 3.5 respectively. The LSV curves were consistent across the replicates of the fresh blood replicates and the general distributions were maintained in the aged blood samples. Figure 3.5 shows the LSV of the fresh Naf/Blood/Naf film in the neutral pH buffer for 50-1000 RPM. The Koutecky-Levich equation was used to solve for electron number involved in the reaction. For the fresh blood in the neutral pH the average was close to three (2.86 ± 0.17). This implies that both the 4-electron and 2-electron processes are occurring. Stated another way, Hb is catalyzing the ORR to form water and hydrogen peroxide. This is consistent with results found in the literature with reports of hydrogen peroxide and water being formed as products with whole blood samples in neutral pH buffers [62,93,116]. In the context of this research, bovine blood has similar hematological properties has human blood, with similar RBC size, and Hb concentrations [137]. The onset peak at approximately -0.2 V vs the RHE supports the claim that at least some peroxide formation is occurring. This has been observed in similar RDE blood analyses and is related to the formation of hydrogen peroxide before water [93]. The onset peak also supports the observation that both ORR pathways are present (Equations 8, 9a and 9b). Alternatively, the blood could be catalyzing the ORR through hydrogen peroxide formation followed by subsequent water formation.

In the neutral pH, the 2-week aged blood stored in the refrigerator saw an average electron number closer to two (2.28 ± 0.13). Therefore, as the blood ages its ability to

directly reduce O_2 to water decreases and is dominated by a 2-electron reduction process forming hydrogen peroxide. This offers interesting results to forensic and biomedical fields when storing blood over longer periods. Hydrogen peroxide can lead to destructive oxidative pathways for Hb and other proteins found in blood [31]. The blood aged three days on the electrode provided an electron number of 2.75. This relates to a 3-electorn process, the same as the fresh blood. This demonstrates that the Hb within the blood aged on the electrode is maintaining its catalytic activity to form water after 3 days. A limitation to this finding is that no replicates were obtained for the group; additional analysis would be required to confirm with certainty that Hb activity is maintained.

The analysis of aged blood samples was not found in the literature and has applications to forensic and clinical blood studies in storability and insight into how Hb catalytic activity changes as blood ages in *ex vivo*. Additional analysis with older blood samples is recommended as it relates to both forensic and medical fields. Across all the analyses in the neutral pH, high correlation coefficients were observed in the Koutecky-Levich plots although limiting currents were not reached in this potential window. In other words, the catalyst (i.e. Hb) is still in a diffusion-controlled region at this potential and the movement of O_2 within the film is the limiting factor. The LSV curves show the beginning of the plateau and the plotting of near limiting currents show that this reaction is sluggish given the intercept greater than zero. In other words, the blood film and Hb accessibility remains the limiting factor here and is not governed by mass transport.

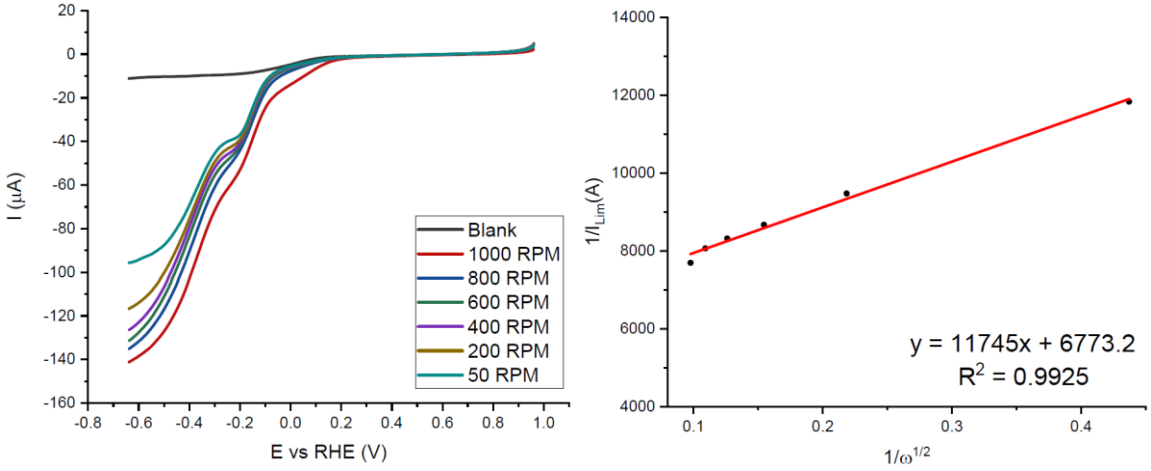

Figure 3.5: *LSV scans of fresh Naf/Blood/Naf film on GC-RDE in 0.05 M disodium phosphate buffer (pH = 7.0) with different RPM (50-1000), purging gas O_2 (right). Koutecky-Levich plot for currents at -0.6384 V vs RHE (left).*

Table 3.4: *Koutecky-Levich analysis summary of fresh blood films in disodium phosphate buffer at -0.6384 V vs RHE.*

Fresh blood (Day of collection, Buffer = 0.05 M Na_2HPO_4)				
Replicate	**Number of electrons**	**KL plot correlation coefficient**	**Kinetic current (mA/cm^2)**	**Onset Potential (V vs. RHE)**
1a	3.1114	0.9925	0.7521	0.1768
2a	2.825	0.9617	0.7126	0.1869
3a	2.924	0.9812	0.6036	0.1718
4a	2.7443	0.9818	0.6583	0.1819
5a	2.6843	0.9793	0.7253	0.1718
Average	**2.8578**	**0.9793**	**0.6904**	**0.177840**
St Dev	**0.1679**	**0.0111**	**0.0593**	**0.006569**

Table 3.5: *Koutecky-Levich analysis summary of aged blood films in disodium phosphate buffer at -0.6384 V vs RHE.*

Aged blood (2 weeks in fridge, Buffer = 0.05 M Na_2HPO_4)				
Replicate	**Number of electrons**	**KL plot correlation coefficient**	**Kinetic current (mA/cm^2)**	**Onset Potential (V vs. RHE)**
1b	2.2253	0.9657	0.7166	0.2071
2b	2.2103	0.9816	0.7495	0.1819
3b	2.5182	0.9886	0.6738	0.1819
4b	2.2152	0.9688	0.62883	0.1618
5b	2.2294	0.8765	0.697	0.1869
Average	**2.2800**	**0.9562**	**0.6931**	**0.183920**
St Dev	**0.1336**	**0.0455**	**0.0454**	**0.016153**
Aged blood (three days on the electrode**,** Buffer = 0.05 M Na_2HPO_4)				
1c	2.7478	0.9842	0.6753	0.1416

Within the additional pH conditions, the acidic replicates did not reach limiting currents or the beginning of a plateau. The LSV for the acidic pH condition can be found in Appendix B. For this reason, Koutecky-Levich analysis was not completed since, regardless of RPM, currents remained the same. This was expected as the ORR is a coupled electron/proton process and with unlimited mass transport of O_2 to the electrode surface and constant supply of protons from the buffer, Hb is able to catalyze the ORR continuously. The self-protective nature of Hb to catalyze the ORR without oxidizing its central iron to its Fe^{3+} oxidative state makes it an excellent O_2 catalyst.

The basic pH samples did reach limiting currents and also had the similar onset peak to the neutral pH samples. Figure 3.6 shows the LSV curves and the Koutecky-Levich plot at 0.2263 V vs RHE. Table 3.6 summarizes the data between replicates in this pH group. High linear correlation coefficients were found at this potential and the average electron number involved in the reaction was close to two (1.72 ± 0.10). Alkaline buffers are commonly used to study the ORR. The lower pH provide a less corrosive environment to catalysts and the ORR kinetics are more rapid compared to acidic media [121]. This is related to why higher magnitude currents are observed in this pH compared to the neutral pH samples. Within alkaline buffers the 4 and 2 electron pathways are

different. The 4-electron pathway is shown in Equation 11. The 2-electorn pathway involves the reduction of oxygen to a hydrogen superoxide (Equation 12a) followed by the possible reduction to hydroxide (Equation 12b) [121,138]. These results suggest that the 2-electron pathway outlined in Equation 12a is occurring.

$$O_2 + 2H_2O + 4e^- \rightarrow 4OH^- \qquad (11)$$

$$O_2 + H_2O + 2e^- \rightarrow HO_2^- + OH^- \qquad (12a)$$

$$HO_2^- + H_2O + 2e^- \rightarrow 3OH^- \qquad (12b)$$

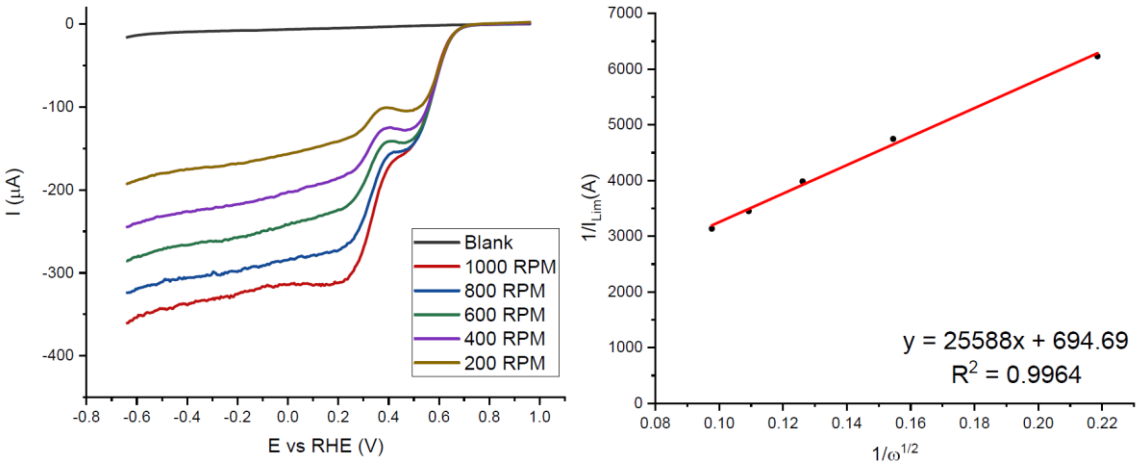

Figure 3.6: *LSV scans of Naf/Blood/Naf film on GC-RDE in 0.1 M potassium hydroxide buffer (pH = 13) with different RPM (200-1000), purging gas O_2 (right). Koutecky-Levich plot for currents at 0.2263 V vs RHE (left).*

Table 3.6: *Koutecky-Levich analysis summary of blood films in 0.1 M potassium hydroxide (pH = 13.0) electrolyte at 0.2263 V vs RHE.*

Fresh Blood (Day of collection, Buffer = 0.1 M KOH)				
Replicate	**Number of electrons**	**KL plot correlation coefficient**	**Kinetic current (mA/cm^2)**	**Onset Potential (V vs. RHE)**
1d	1.8439	0.9951	78.912	0.6593
2d	1.7808	0.9877	10.6267	0.6492
3d	1.7039	0.9964	7.3331	0.6442
4d	1.6055	0.992	44.6276	0.6392
5d	1.6537	0.9945	8.9107	0.6442
Average	**1.71756**	**0.99314**	**30.08202**	**0.647220**
St Dev	**0.095895**	**0.003436**	**31.38546**	**0.007622**

The results from the RDE analysis in the basic pH offer insight into the catalytic activity of Hb in whole blood for biofuel cell technologies [139]. Several studies have focussed on the ORR activity of Hb in neutral pH solutions given their native function in blood which has a pH of 7.3-7.4 [127]. This research studies these reaction in whole blood, which is something that has been done by few [85,93]. The results from the neutral pH RDE experiment offer applications to blood storage and stability. In the context of this research the ORR activity over time was of particular interest as it relates to blood films exposed to the environment. As a bloodstain ages a decrease in the water formation pathway was observed, with a shift to the hydrogen peroxide formation pathway. This offers insight into the Hb oxidative changes in an aged bloodstain and the lost of Hb's native function to directly catalyze O_2 to water overtime. Understanding these reactions and the shift in electrochemical pathways is fundamental to correlating Hb oxidative changes with time.

3.6 Blood drying morphology on GC electrodes

3.6.1 Electrode imaging methodology

The surface morphology of the dried blood is important when considering electron transfer kinetics. Digital photography and SEM were used to characterize the blood films deposited on GC electrodes. An electrode was prepared in the previously described manner without the top layer of Naf. A Canon EOS Rebel T6i camera with a macro lens was used to image the electrode surface. The image specifications were: ¼ shutter speed, 100 ISO and 3.2 F-stop. A photography of the 1 µL blood deposited electrode is in Figure 3.6.

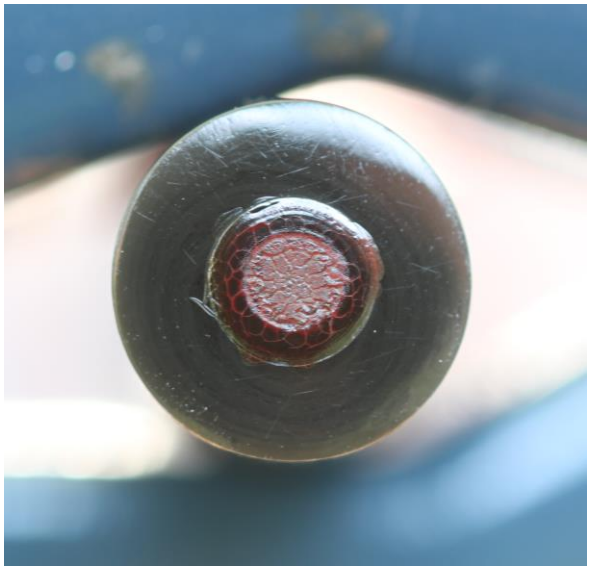

Figure 3.7: *Photograph of 1 µL blood deposited GC electrode using a Canon EOS Rebel T6i camera.*

The SEM was used to obtain detailed surface images on a blood deposited electrode in a vacuum. A 3.00 mm diameter GC electrode (CHI 104) was previously cut to fit into the SEM. Fresh whole bovine blood and 5% wt Naf 117 were deposited in the same manner previously described. Issues with imaging fresh blood on the day of collection presented problems where the fluid was moving after the blood film had supposedly dried. For movement made SEM images suboptimal. Using the fresh blood, the SEM electrode was prepared on a Friday and the analysis was completed the following Monday with successful results. During this brief aging period the electrode was stored in an environmental chamber at 22°C and 40% RH. The top layer of Naf was not put on the surface of the blood film so to not interfere with the conductive current between the blood and electrode stub. Several images were collected from across the electrode surface and under various magnifications. A FlexSEM 1000 was used to the analysis. The SEM working conditions were: 15.0 kV accelerating voltage, 3.57 cm working distance, and an emission current of 108000 nA.

3.6.2 Digital image of blood deposited GC electrode

The 1 µL deposition volume of blood was found to be the easiest to distribute across the electrode surface. The ability to reproduce a blood film proved most effective with this volume compared to the other volumes tested.

The blood on the electrode surface immobilized above Naf base layer and did not flake off the surface. The morphology of the film shows that the blood did not recede from the deposited area and dried in place across the entire electrode surface. These blood films created on electrodes are different from the morphology observed in blood droplets formed on other non-porous surfaces [140]. In blood droplets that have been left to dry, the RBCs assemble themselves in a ring-like structure around the outside of the center of the stain. The reasons for this are due to the convective currents present during drying and the self-pinning and agglomeration of RBCs to each other and the substrate [22,141,142]. In these photographs, this structure is not visible upon inspection. The absence of ring-like structure is likely because the blood was spread across the electrode surface compared to being dropped in many BPA drying studies [22,141]. Photographs of blood deposited electrodes show an overall consistent distribution with possible clustering of cells in the center of the film. With the small volume used, evaporation of water and the self-assemble of RBCs begins rapidly. The hydrophobic nature of GC influences drying of blood films and the cracking patterns over time [140]. These conditions likely have a major effect on the drying characteristics of the blood film.

In relation to electrochemical analysis, even distribution of blood across the electrode surface is desirable. The goal of the electrode imaging was to understand how the blood films are drying on the electrode, specifically if uniform morphology was being achieved. With the characterization experiments 1 µL proved to be most effective in electrode preparation consistency and initial photographs confirm this. An uneven distribution or clumping of RBCs after drying impedes redox reactions, leading to higher variation in electrochemical signal. After photographic inspection of the electrode surface, SEM images were obtained to look closer at film morphology.

3.6.3 SEM images of blood deposited GC electrode

Using SEM, the blood film morphology was examined at the center and on the edges of the film. These areas were of primary interest from previous imaging analysis given the insight that the RBCs could be clustering in the center of the film. Figure 3.7 shows the SEM images of the blood film on the GC electrode stub.

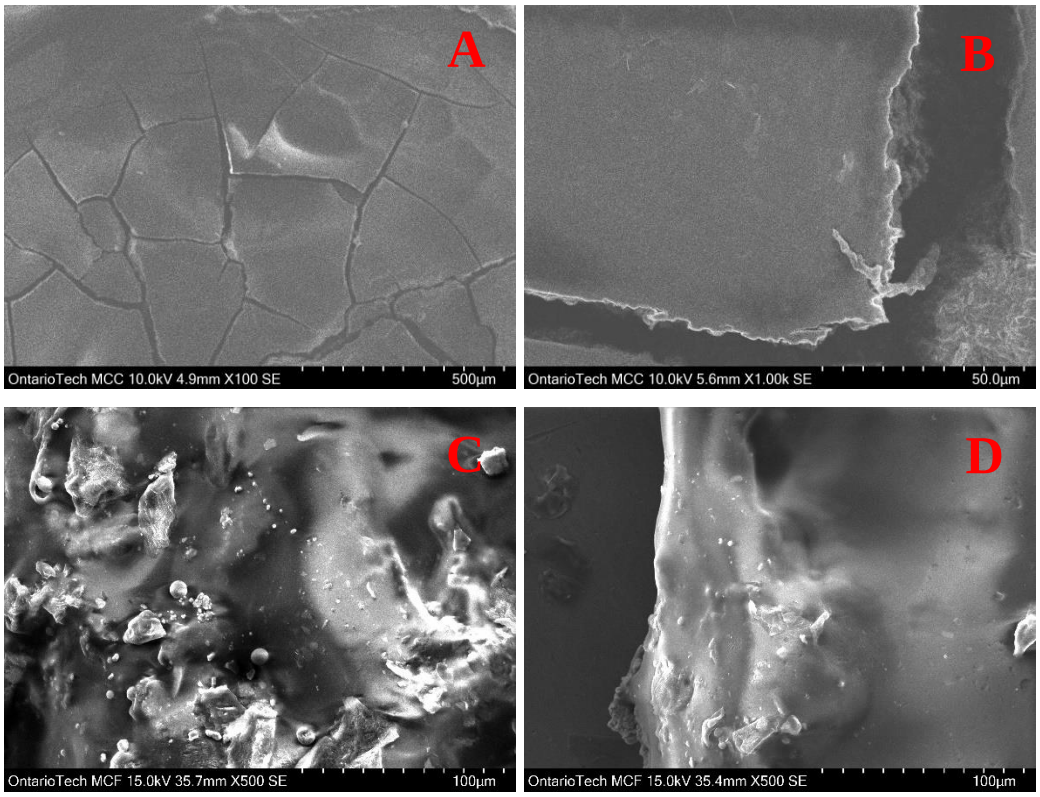

Figure 3.8: SEM images of blood film, image A shows the blood film on the electrode surface, image B magnifies on a crack formation and images C and D are magnified images taken from the center of the blood film.

The images from the SEM are consistent with the finding from the digital photographs of the blood films. In Figure 3.8, image A shows the blood film on the electrode surface under a low magnification. In this image, crack formations are visible and formed over the 2 days the blood was deposited on the electrode. Image B magnifies one of the cracks in this stain and possible RBC stacking is observed in the edges of the crack. Similar morphologies are seen in other SEM research involving whole blood [25]. Lastly, images C and D show the center of the film, where the majority of cellular content was confirmed. The SEM images of the center of the film has an irregular morphology with no distinctly visible RBCs. It is unclear what the surface features and irregularities are in images C and D. It is possible that these are fibrinogen proteins that are forming clots as the blood coagulates. As seen in the digital analysis and confirmed using SEM, most RBCs are aggregating in the center of the film. Direct cellular structure could not be seen and future characterization to better understand cell layering is supported.

Figure 3.7 shows a freshly deposited blood film that was aged for 2 days in controlled laboratory conditions. Over time, additional cracking and cellular damages are expected given environmental stresses such as temperature and humidity. Future work on blood film characterization on GC electrodes is supported as it relates to the use of electrochemistry to study Hb related redox reactions. The distribution and structure integrity of RBCs in a blood film at the time of deposition and over time are critical to electron transfer reactions. Applying techniques, such as spin coating, to evenly distribute blood on electrode surfaces and the effects of blood aging could improve reproducibility.

3.7 Characterization experiment conclusions

Understanding the mechanisms for these reactions and optimizing the methodologies for bovine blood electrochemical analysis was one of the main goals of this research. With forensic applications in mind, this research focusses on assessing the application of electrochemical analysis for blood samples. Determining a reproducible electrode preparation and electrochemical analysis method were the first steps before TSD estimates could be evaluated. The optimal experimental method was determined to be 1 μL of whole blood in a neutral pH phosphate buffer.

The results from the characterization studies compliment each other and together contribute to the understanding of blood analysis using electrochemical methods. The optimization experiment, along with the RDE study, were used characterize the electrochemical signals detected in DPVs. This was accomplished through the review of research literature in similar blood and Hb electrochemical analysis. Each of the adjusted independent variables, pH, volume and concentration in the optimization study had influencing effects on the measured responses. The electrode imaging studies demonstrate uneven film deposition with the RBCs settling in the center of the electrode.

Chapter 4: TSD Estimates for Bloodstains using DPV

4.1 Experimental design

Using the optimal experimental conditions from the factorial design experiment the methods were applied to TSD estimates of bovine blood. A total of nine time series were measured using DPV were completed. Five series were collected in laboratory conditions (22°C and 40% RH) and four at the following temperatures: -20°C, 3°C, 30°C, and 40°C, all at 40% RH. These studies were used to evaluate the applicability of electrochemical measurements on TSD estimates of bloodstains created on GC electrodes.

The laboratory condition time series were completed first and were used to evaluate the response variables correlated with time. Across all statistical analyses, the effect of biological replicate (i.e. blood from individual sources) was included. Understanding which electrochemical responses were correlated with time was followed by combining multiple responses into a principal component analysis (PCA).

Following the laboratory condition time series, the four other temperatures relevant to forensic science were compared to the laboratory condition data. At this point, only electrochemical measurements already determined to be correlated with time were assessed and used for further statistical analysis. The complete data set was used to complete a PCA and grouped the data by temperature to understand its effect on measured responses.

Following the combination of all the time studies and understanding the influence of temperature on Hb changes, an absolute dating technique is proposed. The dataset was divided based on before/after specific time points to further understand the changes relative to each other. Determining which time point the significant changes in electrochemical responses occur, led to the proposal of an electrochemistry-based absolute dating method for a bloodstain TSD estimation diagnostic test.

4.2 Time series experiment methodology

For the time series the electrodes were prepared throughout the morning of the blood collection day. A total of nine time series were conducted with the following

timepoints (hours): 0, 1, 3, 6, 9, 24 (1 day), 48 (2 days), 72 (3 days), 96 (4 days), 168 (1 week), 240 (10 days), 336 (2 weeks). Five time series were completed at standard laboratory conditions: 22°C and 40% RH. The other four time series were completed at the following temperatures with constant RH of 40%: -20°C, 3°C, 30°C, and 40°C. The 22°C, 30°C, and 40°C temperatures were maintained in an ESPEC SH-262 environmental chamber. The -20°C and 3°C temperatures were maintained in the freezer and refrigerator respectively. In the cold conditions, the electrodes were placed in a large glass beaker filled approximately a quarter volume with desiccant to maintain the desired 40% RH. A small dual temperature and humidity gauge was placed in the beaker with the electrodes to monitor any fluctuations. This method proved to keep a stable temperature and humidity across the two-week aging periods in both cold environments.

Electrode preparation and electrochemical analysis specifications can be found in Chapter 2. The same techniques and procedures from the characterization study were followed for the time studies using the optimal condition of 1 μL of whole blood in a neutral pH PBS.

4.2.1 Data analysis

OriginPro Software was used to find the peak potentials (V), heights (μA), and area (μW) in the DPVs. Ratios between the reduction and oxidations peak heights and areas were calculated. Following data collection, RStudio version 3.6.2 (2019) was used for statistical analysis and to generate linear regression plots.

For linear regression analysis, all the time studies were analyzed using the common Log(Time) scale. Pearson's correlation coefficients were calculated for each response variable in the standard time studies with Log(Time) and to other measured responses. This was used to understand how the electrochemical responses influence each other and the effect of time.

Linear mixed models against Log(Time) and with a random effect were determined for each of the measured electrochemical responses in the DPVs. These correlated variables were then used to build the PCA models to further investigate time affected correlations and temperature effects. This was completed with the standard time

series first (22°C and 40% RH) and then the temperature time series data was added to the models.

Absolute dating methods were completed for the laboratory condition time series (n = 5) and the complete time series data (n = 9) by conducting Wilcoxon T-tests for significance below/above respective time groups. The time groups chosen were: 24, 48, 72, 96, 168 hrs. Distribution box plots were used to visualize the separation of the time points within the groups with means, and confidence intervals calculated. This time separation data was then applied to the previously computed PCAs for data visualization.

4.3 Results and discussion

The blank subtracted and baseline corrected data from one of the standard time series is shown in Figure 4.1. The voltammograms from the other time studies can be found in Appendix C. Visual interpretations of voltammograms indicate no clear correlations to time and a large amount of variation is observed between time points. Generally speaking, it was noticed that low reduction peaks were often followed by low oxidation peaks. This supports the hypothesis of using peak ratios for correlations with time opposed to single peak metrics.

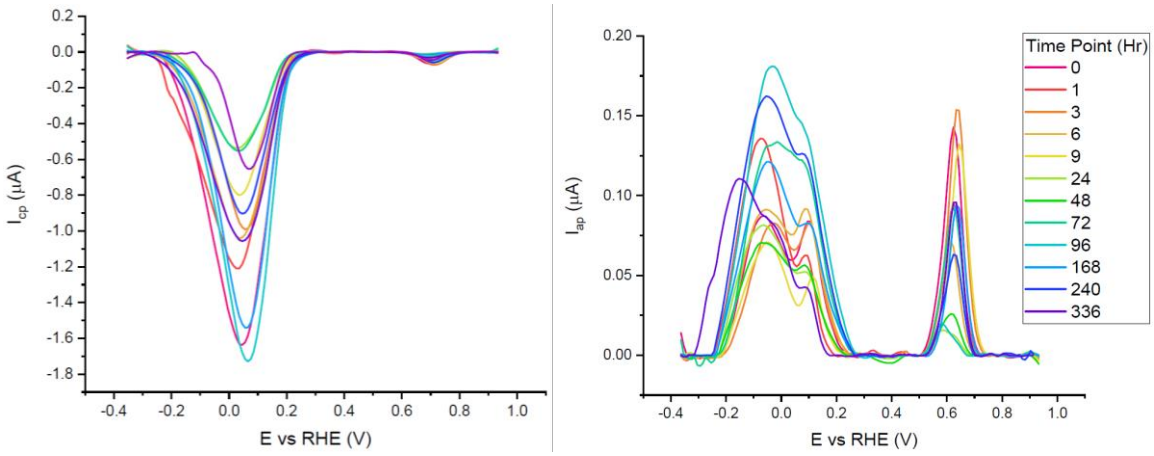

Figure 4.1: *Cathodic (left) and anodic (right) of Naf/Blood/Naf film deposited on GC electrodes over a two-week period, stored at 22°C and 40% RH. 10 mV/sec scan rate and purged with N_2.*

4.3.1 Correlation matrix

Using the standard time series data, a Pearson correlation matrix was constructed to visualize how the measured responses correlate to each other, independent of time. This matrix is found in Figure 4.2. The Pearson's correlation coefficient describes the

strength and direction of two chosen variables. The key finding from this matrix was that within a peak, the height and area were strongly correlated (Figure 4.2: outlined in red). This was expected and confirms that the general peak shapes are being maintained across increasing time points.

This correlation matrix was useful in determining how peak characteristics are changing with each other and was a starting point to begin assessing each of these dependent measurements with time. Another key finding was that the 2 Red peak height and area had a strong positive correlation with the 3 Ox and 4 Ox heights and areas, respectively (Figure 4.2: outlined in yellow). This confirms the hypothesis from the characterization experiments that the Hb molecules able to undergo reduction or facilitate the ORR can participate in oxidation in the anodic sweep. In other words, greater reduction signals correspond to greater oxidation signals in the Hb related peaks. This is also confirmed by the strong positive correlation seen between the height or area of the 2 Red peak and the height or area of the combined 3+4 Ox peak.

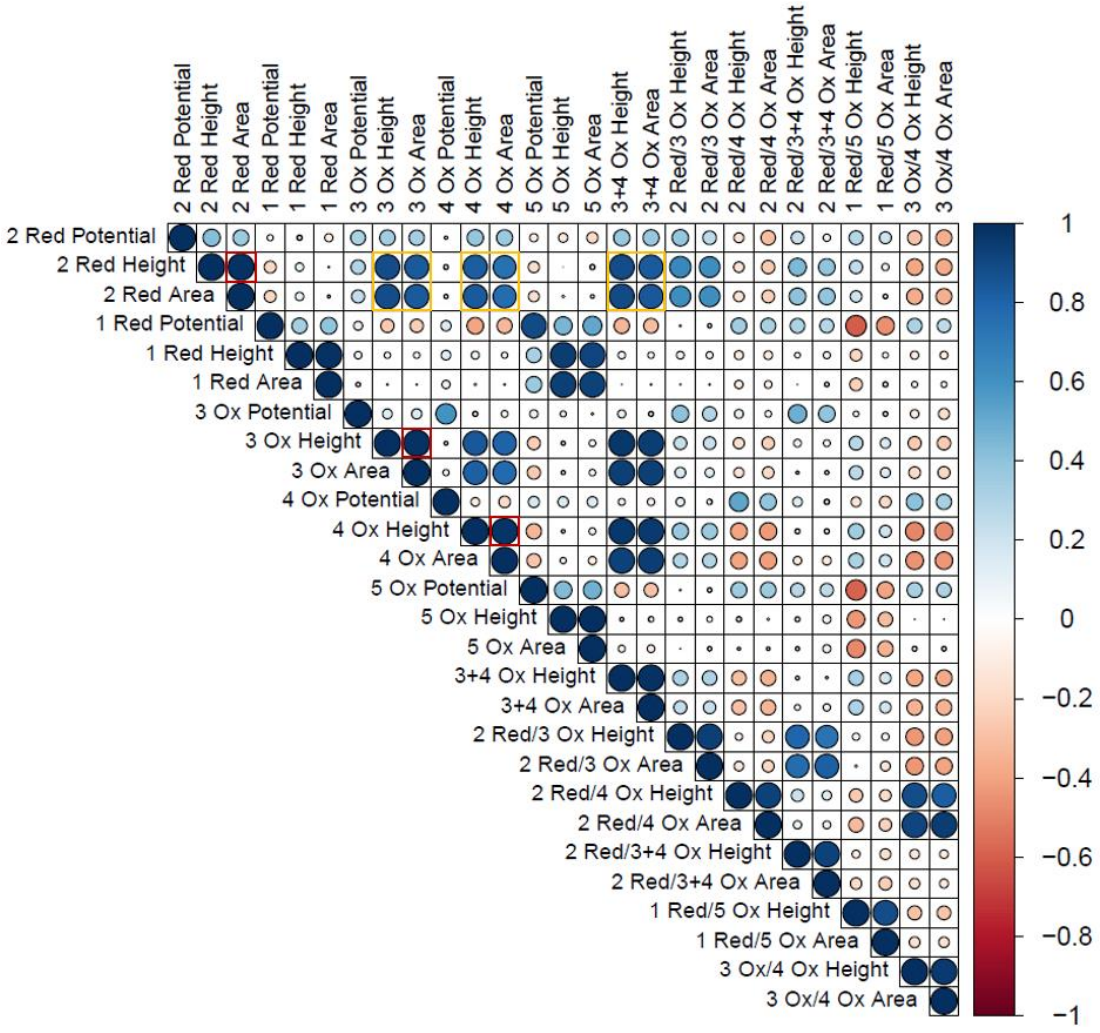

Figure 4.2: *Pearson's Correlation plot of measured response variables. The size and colour represent the strength and direction of correlation respectively. (Blue = positive correlation, Red = negative correlation).*

4.3.2 Standard time studies linear models

Each measured electrochemical response was fitted using a linear correlation with Log(Time). The common logarithm was used to transform the time point (in hours) to the respective Log(Time). The T0 time point was set to 6 minutes (0.1 hours) because it is likely a better representation of the time when the measurement was obtained. The reason for the transformation was to distribute the early time points and in turn improve linearity.

Table 4.1: *Mixed linear models of laboratory condition time series (n=5). All electrochemical responses were assessed. The bolded peak identifiers and corresponding variables that are significantly correlated with Log(Time) (p < 0.05).*

			Log(Time)			
Peak Identifier	**Variable**	**Marginal R^2/ Conditional R^2**	**Estimate**	**Confidence Interval**	**p-value**	**Pearson's Coefficient**
2 Red	**Potential**	0.066/0.310	0.00	0.00 – 0.01	**0.017**	0.2556
	Height	0.00/0.433	-0.01	-0.12 – 0.10	0.858	-0.0174
	Area	0.001/0.412	-0.00	-0.03 – 0.02	0.768	-0.0292
1 Red	Potential	0.002/0.036	0.00	-0.00 – 0.00	0.702	0.0484
	Height	0.003/0.263	0.00	-0.01 – 0.01	0.617	0.0554
	Area	0.003/0.250	0.00	-0.00 – 0.00	0.619	0.0555
3 Ox	Potential	0.003/0.193	-0.00	-0.01 – 0.00	0.622	-0.0572
	Height	0.015/0.248	0.01	-0.01 – 0.02	0.278	0.1214
	Area	0.031/0.234	0.00	-0.00 – 0.00	0.120	0.1755
4 Ox	Potential	0.009/0.027	-0.00	-0.01 – 0.00	0.479	-0.0892
	Height	0.012/0.320	0.01	-0.01 – 0.02	0.307	0.1088
	Area	0.032/0.239	0.00	-0.00 – 0.00	0.113	0.1787
5 Ox	Potential	0.001/0.049	0.00	-0.00 – 0.00	0.820	0.0286
	Height	0.005/0.137	0.00	-0.01 – 0.02	0.572	0.0678
	Area	0.002/0.142	0.00	-0.00 – 0.00	0.706	0.0451
3 Ox + 4 Ox	Height	0.015/0.300	0.01	-0.01 – 0.03	0.268	0.1197
	Area	0.036/0.271	0.00	-0.00 – 0.01	0.088	0.1879
2 Red/3 Ox	**Height**	0.044/0.425	-0.54	-1.03 – -0.04	**0.033**	-0.2088
	Area	0.079/0.344	-1.04	-1.81 – -0.28	**0.008**	-0.2797
2 Red/4 Ox	**Height**	0.098/0.308	-3.20	-5.40 – -0.99	**0.004**	-0.3005
	Area	0.127/0.238	-12.99	-21.24 – -4.73	**0.002**	-0.3471
2 Red/3 Ox + 4 Ox	**Height**	0.071/0.320	-0.39	-0.70 – -0.08	**0.013**	-0.2646
	Area	0.152/0.312	-0.97	-1.50 – -0.44	**<0.001**	-0.3868
1 Red/5 Ox	Height	0.001/0.022	0.01	-0.03 – 0.04	0.775	0.0364
	Area	0.005/0.029	0.01	-0.03 – 0.06	0.571	0.0721
3 Ox/4 Ox	Height	0.032/0.211	-0.33	-0.76 – 0.10	0.130	-0.1717
	Area	0.045/0.152	-1.23	-2.61 – 0.16	0.082	-0.2060

Table 4.1 summarizes data from the linear mixed models for the standard time series (n = 5). The bolded response variables represent the significantly correlated variable ($p < 0.05$). There were 7 significantly correlated variables: the peak potential of the 2 Red peak, and the height and area ratios of the Hb related redox peaks (2 Red/3 Ox, 2 Red/ 4 Ox, and 2 Red/3+4 Ox). As predicted, the peaks associated with quinone redox reactions (1 Red and 5 Ox) were not correlated with time since they are from the GC electrodes. Only one individual peak measurement was significantly correlated with Log(Time), that being the $HbFe^{3+}$ reduction and ORR peak potential (i.e. 2 Red peak). This potential shifted to more positive potentials over time possibly due to the degradation of cellular components leading to less resistant electron transfer pathways. This pattern is noticed in Figure 4.1 with the later time point cathodic sweeps having higher peak potentials.

As hypothesized, the ratios of heights and areas between Hb related peaks were found to be significantly correlated with Log(Time). The use of peak ratios between corresponding reduction and oxidation peaks mitigates variation between samples because the number of molecules participating in the reactions becomes relative. It was observed here that all of these ratios were decreasing over time, or in other words, the reduction peak was decreasing in magnitude and/or the collective oxidation peaks are increasing in magnitude. This makes sense with what is expected to be happening in the bloodstain as it ages. Natural oxidative damages are expected and the Hb bound O_2 is reduced to water with Fe^{2+}/Fe^{3+} oxidation [15,33]. This decreases the available O_2 to undergo reduction at the 2 Red peak and the increase in $HeFe^{3+}$ is able to participate in oxidation reactions during the 3 Ox and 4 Ox peaks.

Each of the measured electrochemical responses has a greater conditional R^2 value which means that more variability in the model is explained when the ‘time study’ (i.e. biological replicate) is considered as a random effect. This is critical information for forensic bloodstain TSD estimations since it means that the blood source influences the electrochemical measurements. This is consistent with other TSD research, finding that biological replicate influences the degradation rates of blood-related molecules studied for TSD purposes such as Hb, RNA, and RBCs [3,15,51].

The linear mixed model graphs can be found in Appendix C for the seven significantly correlated measurements with Log(Time). Figure 4.3 shows the linear mixed model for the 2 Red/3+4 Ox peak area ratio over Log(Time) with each line representing the line of best fit for each replicate time series. From the linear mixed model graphs, in all the cases the later time points had less variation between replicates. This highlights the applicability of this technique for older bloodstains and supports future research past the two-week mark. The later variation could be explained from the film morphology changing and allowing more complete redox reactions compared to the early time points where the blood is forming complex 3D networks.

The linear mixed models demonstrate weak correlations with time, even for the significantly correlated variables. Low Pearson correlation coefficients (i.e. 0.20 – 0.39) and R^2 (i.e. 0.30 – 0.49) values relate to this, however when biological replicate is taken into account the relationship to electrochemical response and Log(Time) increases. The statistics summarizing this are found in Table 4.1 under the bolded peak identifiers correlated with Log(Time).

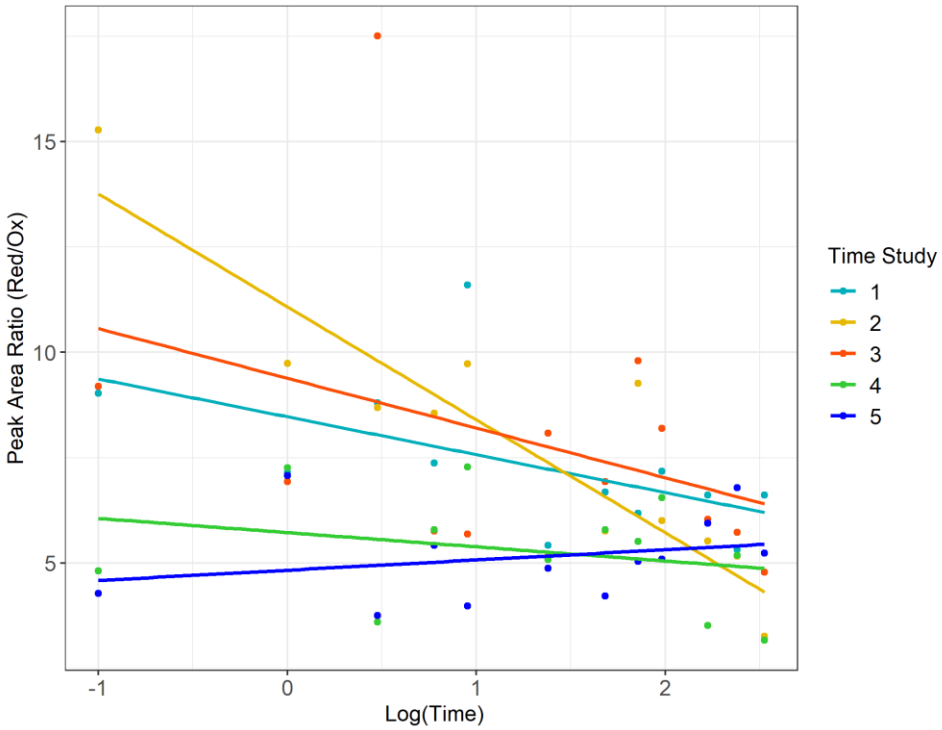

Figure 4.3: *Multiple linear regression of 2 Red/3+4 Ox peak area ratio over Log(Time) for each standard time series replicate.*

4.3.3 Effects of temperature

The four temperature variation time series had consistent peak shapes with the standard time series and the DPVs of the reduction and oxidation peaks can be found in Appendix C. For each of the temperature time series, only the 7 significantly correlated variables were assessed although the peak measurements for all the peaks were collected. Results from the linear models and Pearson's Correlations within each temperature group can be found in Table 4.2 and comprehensive results including the intercepts, confidence intervals and p-values can be found in Appendix C.

The majority of the measured electrochemical response variables were significant in the temperature time series. For the temperature time studies, the Pearson's correlation coefficients and R^2 values are similar to standard time studies demonstrating that consistent trends are observed. A major limitation to these reported statistics is the use of only one sample set for each temperature. For this reason, the R^2 and adjusted R^2 values are reported since a random effect of biological replicate could not be incorporated. Both of these values describe the percentage of variation in the regression with the adjusted R^2 only explaining the variation from the independent variables. For this analysis, only one independent variable is within the linear models, Log(Time), and the R^2 is considered reliable. Future experimental work replicating these studies would be beneficial and would likely give insight into more variation.

Table 4.2: *Data summary for linear models of temperature time series (standard time series included as a reference). Presented here are the Pearson's coefficients and the R^2/Adjusted R^2 values.*

Peak Identifier	Variable	22°C and 40% RH (n = 5)		-20°C and 40% RH (n = 1)		3°C and 40% RH (n = 1)		30°C and 40% RH (n = 1)		40°C and 40% RH (n = 1)	
		Pearson's Coefficient, Log(Time)	Marginal R^2/ Conditional R^2, Log(Time)	Pearson's Coefficient, Log(Time)	R^2/ Adjusted R^2, Log(Time)	Pearson's Coefficient, Log(Time)	R^2/ Adjusted R^2, Log(Time)	Pearson's Coefficient, Log(Time)	R^2/ Adjusted R^2, Log(Time)	Pearson's Coefficient, Log(Time)	R^2/ Adjusted R^2, Log(Time)
2 Red	Potential (V)	0.2556	0.066/0.310	0.7107456	0.505/0.456	0.6662	0.444/0.388	0.5141	0.264/0.191	0.5497	0.302/0.232
2 Red/3 Ox	Height Ratio	-0.2088	0.044/0.425	-0.4703872	0.221/0.143	-0.1934	0.037/-0.059	-0.7499	0.562/0.519	-0.7639	0.583/0.542
	Area Ratio	-0.2797	0.079/0.344	-0.6403454	0.410/0.351	-0.1814	0.033/-0.064	-0.7388	0.546/0.500	-0.8129	0.661/0.627
2 Red/4 Ox	Height Ratio	-0.3005	0.098/0.308	-0.2643495	0.070/-0.023	-0.5935	0.352/0.287	0.2465	0.061/-0.033	-0.6012	0.361/0.298
	Area Ratio	-0.3471	0.127/0.238	-0.3701841	0.137/0.051	-0.6245	0.390/0.329	0.1858	0.035/-0.062	-0.7790	0.607/0.567
2 Red/3 + 4 Ox	Height Ratio	-0.2646	0.071/0.320	-0.38118	0.145/0.060	-0.4957	0.246/0.170	-0.5475	0.300/0.230	-0.7237	0.524/0.476
	Area Ratio	-0.3868	0.152/0.312	-0.5824234	0.339/0.273	-0.7113	0.506/0.457	-0.6745	0.455/0.400	-0.8144	0.663/0.630

The temperature time series data was then incorporated into the standard time series data, effectively adding another independent measurement – temperature. This is referred to as levelling, where a particular independent variable condition is used as a reference to compare to the other conditions. In this analysis, the temperature data was levelled to the standard time studies (22°C) since this group had 5 replicates making it a more comprehensive regression model. This statistical analysis is useful in determining if temperature affects the measured electrochemical responses as it relates to the oxidative changes of Hb in a bloodstain.

The 7 measured responses were each assessed with Log(Time) and temperature was set to an independent effect with 'time study' (i.e. biological replicate) set to a random effect. Table 4.3 shows these results with many of the temperature groups being significantly different than the 22°C group ($p < 0.05$). Beside each variable the marginal and conditional R^2 values are listed, and in every case the conditional R^2 value is higher. Similar to the results with the standard time series alone, the incorporation of the random effect describes a greater portion of the variation. This highlights the significance of taking biological replicate into account regardless of temperature.

Table 4.3: *Influencing effects of Log(Time) and temperature (leveled to 22°C) for measured electrochemical responses significantly correlated with Log(Time).*

2 Red Potential (R^2 Marg/R^2 Cond: 0.386/0.422)			
Predictors	**Estimates**	**Confidence Interval**	**p-value**
(Intercept)	0.03	0.02 – 0.04	**<0.001**
Log(Time)	0.01	0.01 – 0.01	**<0.001**
Temperature -20	0.03	0.01 – 0.05	**<0.001**
Temperature 3	0.01	-0.00 – 0.03	0.145
Temperature 30	0.00	-0.01 – 0.02	0.633
Temperature 40	0.03	0.02 – 0.05	**<0.001**
2 Red/3 Ox Peak Height Ratio (R^2 Marg/R^2 Cond: 0.446/0.618)			
(Intercept)	8.88	7.68 – 10.07	**<0.001**
Log(Time)	-0.63	-0.95 – -0.30	**<0.001**
Temperature -20	-2.56	-5.31 – 0.18	0.068
Temperature 3	-3.59	-6.34 – -0.84	**0.010**
Temperature 30	-3.58	-6.33 – -0.84	**0.011**
Temperature 40	-4.17	-6.92 – -1.42	**0.003**
2 Red/3 Ox Peak Area Ratio (R^2 Marg/R^2 Cond: 0.444/0.583)			
(Intercept)	10.81	9.29 – 12.34	**<0.001**
Log(Time)	-0.97	-1.43 – -0.51	**<0.001**
Temperature -20	-4.22	-7.66 – -0.77	**0.016**
Temperature 3	-4.25	-7.69 – -0.80	**0.016**
Temperature 30	-4.76	-8.20 – -1.31	**0.007**
Temperature 40	-5.48	-8.93 – -2.04	**0.002**
2 Red/4 Ox Peak Height Ratio (R^2 Marg/R^2 Cond: 0.337/0.468)			
(Intercept)	21.09	17.19 – 24.99	**<0.001**
Log(Time)	-2.17	-3.47 – -0.86	**0.001**
Temperature -20	-6.18	-14.80 – 2.43	0.160
Temperature 3	-12.26	-20.88 – -3.65	**0.005**
Temperature 30	-9.46	-18.07 – -0.84	**0.031**
Temperature 40	-10.93	-19.54 – -2.31	**0.013**
2 Red/4 Ox Peak Area Ratio (R^2 Marg/R^2 Cond: 0.229/0.314)			
(Intercept)	47.02	35.27 – 58.77	**<0.001**
Log(Time)	-8.03	-12.73 – -3.34	**0.001**
Temperature -20	-18.05	-42.74 – 6.63	0.152
Temperature 3	-28.65	-53.34 – -3.97	**0.023**
Temperature 30	-23.00	-47.68 – 1.69	0.068
Temperature 40	-23.83	-48.52 – 0.85	0.058
2 Red/3 Ox + 4 Ox Peak Height Ratio (R^2 Marg/R^2 Cond: 0.532/0.623)			
(Intercept)	5.81	5.21 – 6.41	**<0.001**
Log(Time)	-0.41	-0.61 – -0.21	**<0.001**
Temperature -20	-1.53	-2.87 – -0.20	**0.024**
Temperature 3	-2.79	-4.13 – -1.46	**<0.001**
Temperature 30	-2.37	-3.71 – -1.04	**<0.001**
Temperature 40	-2.74	-4.08 – -1.41	**<0.001**
2 Red/3 Ox + 4 Ox Peak Area Ratio (R^2 Marg/R^2 Cond: 0.506/0.588)			
(Intercept)	7.73	6.85 – 8.60	**<0.001**
Log(Time)	-0.84	-1.15 – -0.53	**<0.001**
Temperature -20	-2.54	-4.45 – -0.62	**0.009**
Temperature 3	-3.67	-5.58 – -1.75	**<0.001**
Temperature 30	-3.27	-5.18 – -1.35	**0.001**
Temperature 40	-3.56	-5.47 – -1.65	**<0.001**

Figure 4.4 presents the 2 Red/3+4 Ox peak area ratio linear models, with the standard time studies in yellow and the temperatures time studies in blue or red for the cold or warm temperatures respectively. It is clear that the temperature conditions are separate from the standard time studies but it was not predicted that within the temperature variations the linear models would be relatively the same. This temperature grouping trend was observed for all 7 measured electrochemical responses. It was hypothesized that the warmer temperatures would have a greater decrease in Red/Ox peak ratios given accelerated natural Hb oxidation. The opposite was expected for the cold conditions, where the colder temperatures would slow the kinetic rate of Hb oxidation. One possible explanation is the low sample size and with more replicates greater variation would have been observed, adding more datapoints to the linear models.

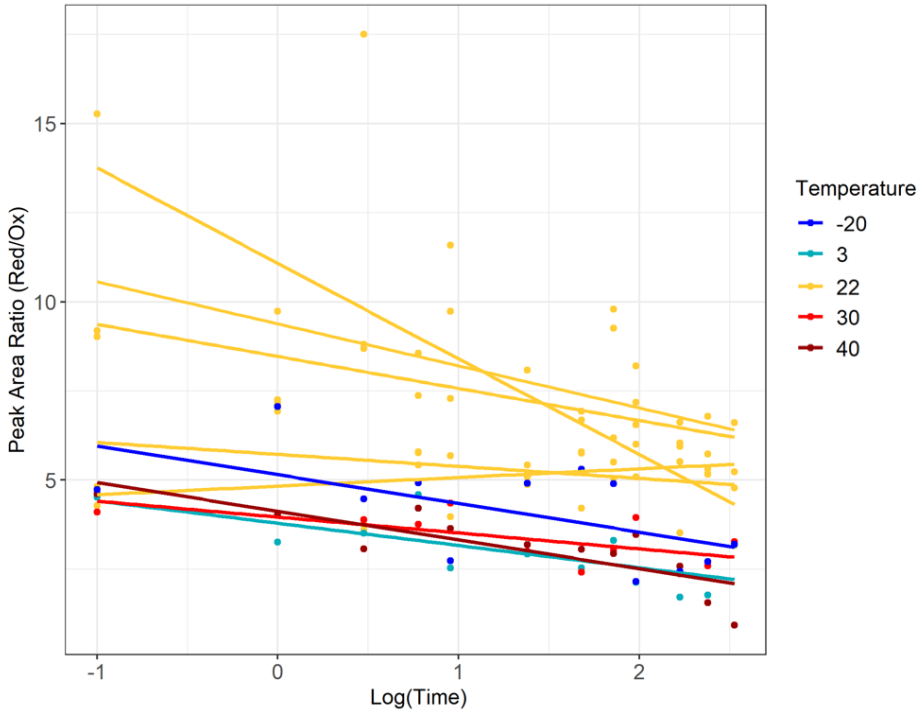

Figure 4.4: Multiple linear regression of 2 Red/3+4 Ox peak area ratio over Log(Time) for each time series replicate. Standard time series are in yellow and the temperature time series are in shades of blue or red for cold or warm temperatures respectively.

Accounting for temperature is an important consideration for Hb degradation. When considering TSD questions, understanding the effects the environment has on degradation is crucial when developing estimates. Other TSD studies that have

incorporated temperature into models have shown that warmer temperatures accelerate degradation in bloodstains and particularly the natural oxidation of Hb [15,43,57].

4.3.4 PCA for standard time series

Following the linear models from the standard time series, these data was used for a PCA. This included taking 4 of the 7 time-correlated variables for the analysis. PCA is a technique designed to reduce the dimensionality of data by combining variables to form better predictors. In this case, the height ratios were excluded from incorporation in the PCA. It was found that the height and area ratios for respective peaks were highly correlated and combining them both in the PCA would overfit the model. The PCA combined, the 2 Red potential and area ratios of the 2 Red/3 Ox, 2 Red/4 Ox, and 2 Red/3+4 Ox electrochemical responses. The full PCA separated by time point for the standard time studies can be found in Appendix C. The results of the PCA from the standard time series demonstrates that the later timepoints cluster together compared to the earlier time points and have narrower 95% confidence ellipses.

Each principal component (PC) is composed of contributions from the 4 included variables. The PCs were assessed individually by computing linear regressions with Log(Time). Table 4.4 summarizes these results with linear regression statistics and Pearson's correlation coefficients for each PC. PC1 and PC3 were found to be significantly correlated with Log(Time), ($p < 0.05$). The strongest contributing variables to PC1 were the 2 Red/3 Ox peak area ratio and the combined 2 Red/3+4 Ox peak area ratio. PC3 was the opposite; the strongest contributing variables were the 2 Red peak potential and the 2 Red/4 Ox peak area ratio. The linear models for PC1 and PC3 have stronger Pearson's coefficients compared to the single electrochemical measurement linear regressions, -0.3355 and -0.3889 respectively. This suggests that several peak measurements are important considerations when posed with TSD questions. Considering biological replicate improved the conditional R^2 values but had less of an effect on PC1. This suggests that PC1 removes most of the random effect from the biological replicate and could be applicable to scenarios where the blood source is unknown. To further test this hypothesis, a cross-validation study could be conducted with multiple biological replicates and compared to these data presented here.

Table 4.4: *Mixed linear models for the PCs with Log(Time) in the standard time series.*

	Log(Time)					
Principal Component	Strongest Contributing Variables	Marginal R^2/ Conditional R^2	Estimate	Confidence Interval	p-value	Pearson's Coefficient
PC1	2 Red/3 Ox Area Ratio and 2 Red/3+4 Ox Area Ratio	0.114/0.130	-1.19	-2.04 – -0.34	**0.006**	-0.3355
PC2	2 Red Potential and 2 Red/4 Ox Area Ratio	0.059/NA	-0.62	-1.27 – 0.02	0.059	-0.2403
PC3	2 Red Potential and 2 Red/4 Ox Area Ratio	0.161/0.376	-0.99	-1.50 – -0.49	**<0.001**	-0.3889
PC4	2 Red/3 Ox Area Ratio and 2 Red/3+4 Ox Area Ratio	0.001/NA	0.08	-0.67 – 0.82	0.842	0.0261

4.3.5 PCA for complete temperature dataset

Following the standard time series PCA, the temperature data was included in the dataset and the same analysis was completed. The inclusion of temperature as an independent variable allows data visualization where the effects of temperature can be seen in relation to the PCs. Grouping the PCA data by temperature can be used to determine if certain temperatures are different from each other or are clustering together. This in combination with the linear regression models is useful for determining the effects of temperature on the electrochemical measurements of bloodstains by measuring the changes to Hb.

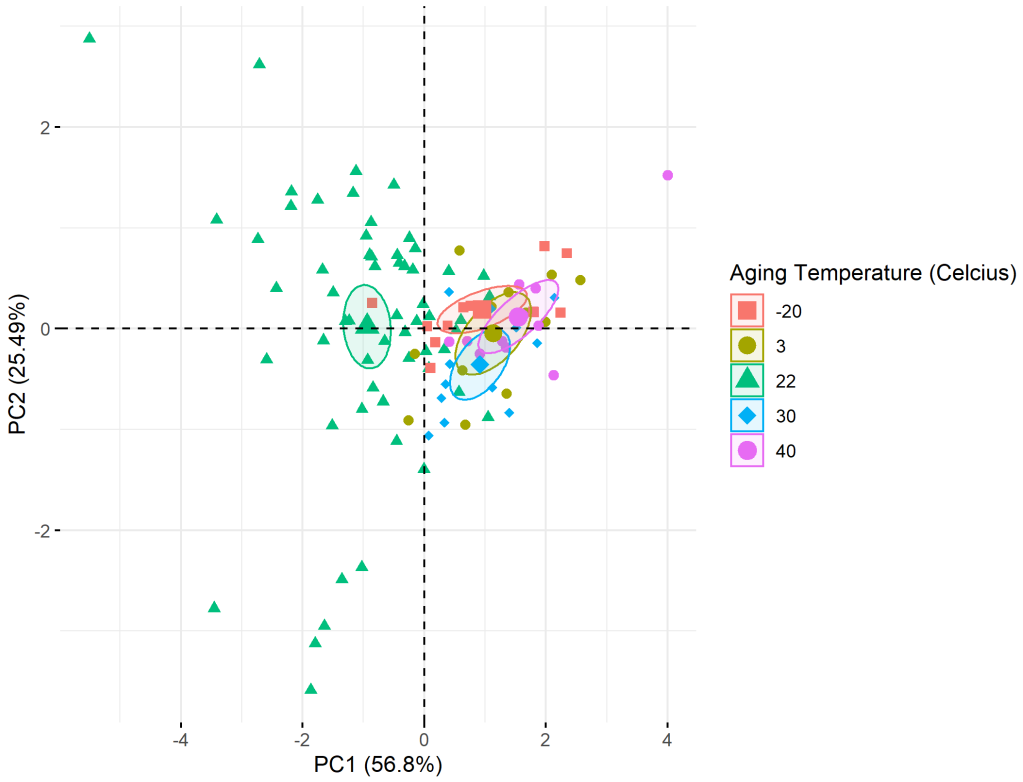

Figure 4.5: *PCA of complete time series dataset, including standard time series (n = 5) and 4 temperature variations (each n = 1).*

The complete dataset PCA containing all nine time studies is presented in Figure 4.5 and is grouped by temperature condition. In this PCA the variable temperature conditions are grouping together. This was an observation in the linear models comparing the temperature time series. The grouping of temperature variation series was not predicted and could be a result of the low sample size. The statistical analysis of the linear regressions demonstrated that each temperature condition is significantly different than the 22°C standard time series replicates which is visualized in the PCA. The addition of more replicates within these temperatures may shift the ellipses closer to the standard time series by introducing more variation. This is an interesting finding because it suggests that electrochemical methods are independent of temperature. Whether the blood deposited electrodes are aged in cold or warm conditions the same electrochemical signals are observed. This is not consistent with the bloodstain TSD literature surrounding Hb detection. Environmental conditions have been shown to influence Hb

oxidation, with warmer temperatures accelerating the kinetic oxidation rate compared to colder temperatures [15,32,44,56,57].

4.3.6 Absolute dating for diagnostic testing

The difference in 95% confidence ellipses between the early and later time points, in the standard time series PCA lead to the statistical analysis at cut off timepoints. The time series responses were divided by above or below chosen time points (*e.g.* above or below 24 hours) for data separation. This means of evidence dating can be insightful during criminal investigations when asked the approximate age of a sample, which can lead to more specific forensic questions. In the case for blood evidence, knowing if a blood sample is older than one day or one week is valuable information for investigators.

These data analysis was completed in similar means by looking at the standard time series followed by the combined dataset. The combined time series data is shown below but the same statistics for the standard time studies alone can be found in Appendix C. Table 4.5 summarize the significant differences between data groups in the standard and grouped time series data respectively. An unpaired two-sample Wilcoxon T-test was used to calculate the significance between the time separations of below/above: 24, 48, 72, 96, and 168 hours.

Table 4.5: *Unpaired two-sample Wilcoxon T-test for complete time series dataset. Bolded values represent significant differences ($p < 0.05$) between the blow and above data groups for each electrochemical measured response.*

Below and Above:		**24 Hours**	**48 Hours**	**72 Hours**	**96 Hours**	**168 Hours**
Peak Identifier	**Variable**	**p-value**	**p-value**	**p-value**	**p-value**	**p-value**
2 Red	Potential	**0.0008**	**0.0001**	**0.0001**	**0.0003**	**0.0079**
2 Red/3 Ox	Height	0.1164	0.2036	0.1155	0.1043	0.2570
	Area	0.0685	0.0832	0.0509	0.0541	0.1751
2 Red/4 Ox	Height	0.2580	0.3188	0.1114	**0.0431**	0.0949
	Area	**0.0241**	**0.0230**	**0.0081**	**0.0010**	**0.0069**
2 Red/3 Ox + 4 Ox	Height	0.0965	0.1865	0.0801	0.0510	0.1574
	Area	**0.0188**	**0.0261**	**0.0091**	**0.0051**	**0.0227**

The 96-hour separation time point had the most significant differences in electrochemical measurement, although many of the same responses were significant in

other time groups. This included the 2 Red peak potential, the 2 Red/4 Ox peak height and area ratios and the 2 Red/3+4 Ox peak area ratio. At this point, the mean and confidence intervals for each of the measured electrochemical responses were determined for the 96-hour time separation groups. The data is shown in Table 4.6 and is interpreted without the influence of temperature. In other words, a blood sample collected and analyzed using electrochemical methods by forensic investigators could compare results to Table 4.6 to correlate if the sample was below or above 96-hours if they did not know the temperature. These data shown here could serve as a training set for future experiments. Building on the model with more biological replicates and environmental conditions could strength confidence intervals for diagnostic applications.

Table 4.6: *The mean and confidence interval for the electrochemical responses, significantly different from the below/above 96-hour complete data set.*

		Below 96 Hours		**After 96 Hours**	
Peak Identifier	**Variable**	**Mean**	**Confidence Interval**	**Mean**	**Confidence Interval**
2 Red	**Potential**	0.0436	0.0385 – 0.0487	0.0673	0.0555 – 0.0792
2 Red/4 Ox	**Height**	15.0841	12.7873 – 17.3810	10.1999	8.0950 – 12.3047
	Area	30.1675	22.6607 – 37.6743	13.6662	10.1956 – 17.1368
2 Red/3 Ox + 4 Ox	**Area**	5.6332	5.0278 – 6.2387	3.9698	3.2725 – 4.6671

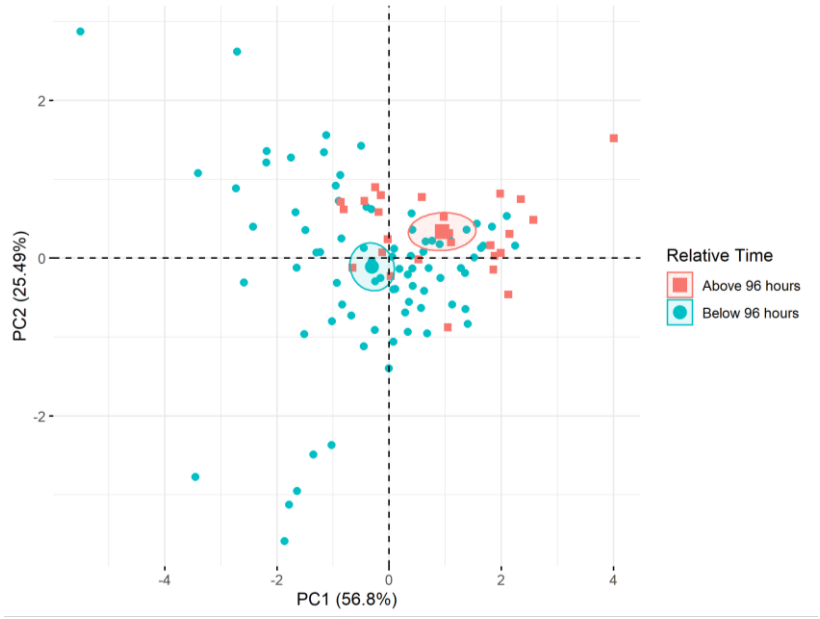

Figure 4.6: *Complete time series data PCA, grouped by below/above 96-hours, independent of aging temperature.*

The below/above 96-hour data separation was then applied to the complete dataset PCA. Using 95% confidence interval ellipses the below and above 96-hour groups are separated in Figure 4.6. This is independent of temperature and demonstrates that without knowing the temperature a bloodstain was stored in a sample can be dated to above or below 96-hours. Many of the forensic Hb related research acknowledges that the majority of Hb oxidation occurs in the first 4 days [15,44,53]. This research is consistent with other researchers findings and demonstrates that electrochemical methods can be used to study Hb changes in bloodstains deposited on GC electrodes [34,62,88]. The 2 Red/4 Ox peak height ($p < 0.043$) and area ($p < 0.001$) ratios statistically significant in the 96-hour time separation. This supports the hypothesis that cellular degradation events can be detected in bloodstains using DPV, given that the 4 Ox peak is attributed to lysed RBCs. Where many of the Hb related forensic TSD research has used absorbance and fluorescence spectroscopy to detect the changes in Hb, electrochemistry involves the direct electron transfers of the Hb. These techniques along with other blood related TSD methods complement each other and support future work where multiple techniques are combined for better TSD estimates.

4.4 TSD experimental conclusions

The application for electrochemistry to study bloodstains is novel research and its ability to be used for bloodstain TSD estimations was the primary focus of this thesis. The results presented here are paired well with other forensic bloodstain TSD research. The changes to Hb remain a primary target for TSD models because of its abundance in blood and the oxidative changes that occur to the central iron atom over time.

The results here demonstrate the applicability of electrochemistry for forensic bloodstain TSD analysis. Changes in the electrochemical signals of Hb related peaks have weak correlations with time. The decrease in O_2 within bloodstain was observed, highlighting DPV as a sensitive technique to detect the ORR within whole blood. These results promote the future study of DPV and other electrochemical techniques on forensic blood analysis. With advances in method optimization, real-world scenarios involving more complex environmental conditions could be studied. The greatest limitations to this research are the limited sample sizes and variation observed between replicates. The influence of temperature and other environmental conditions are important considerations that require further testing. The linear models, PCA, and absolute dating methods shown here demonstrate that correlations to time can be observed using DPV and support further study. Expansion into other electrochemical techniques and building on environmental conditions will benefit TSD estimates. Similar to other bloodstain TSD methods, these correlations are weak and consideration of biological replicate improves models. The absolute dating metrics demonstrate a separation between above and below 96-hours. An analysis technique such as this could aid forensic investigators by answering general TSD questions.

Chapter 5: Discussion and Future Directions

5.1 Bloodstain TSD through electrochemistry

The trends from the time series experiments were expected and are similar to other Hb related TSD techniques [16,33,43,51,56]. It was hypothesized that the oxidative changes in Hb could be detected in aged bloodstains, which we found in the time series experiments. It is suspected that not all of the Hb is accessible to electron transfers and the active Hb sites varies between bloodstains. Peak height and area ratios mitigate this variation and were found to be significantly correlated with time.

The DPVs demonstrate the natural oxidation of $HbFe^{2+}$ to $HbFe^{3+}$ and O_2 reduction in older bloodstains compared to fresher stains. This research presents an application for blood detection as well as TSD estimates using electrochemical methods such as DPV. The oxidative changes of Hb in bloodstains remains the primary analyte for bloodstain aging. Redox reaction potentials, such as $HbFe^{3+}$ reduction or the ORR, can be used to presumptively characterize blood related electron transfer reactions in evidence samples collected at a crime scene.

The Hb related reactions detected using electrochemical methods have a relationship with bloodstain degradation, and time. The redox changes in Hb and the structural changes in RBCs influence the electrochemical signals which could provide insight into TSD estimates. As a bloodstain ages, these structural changes affect the morphology of the bloodstain which influences the electron transfer reactions occurring within the cells. Medical research has observed similar voltammogram shapes and potentials when compared with this research; where older or structurally damaged cells have multiple weaker peak signals [62,88]. Damages to cellular and/or protein structures creates differences in electron transfer pathways within RBCs for Hb based on varying layered 3D networks. This phenomenon also highlights applicability to TSD bloodstain estimates. The magnitude of redox reactions measured is proportional to the Hb molecules that can facilitate electron transfers. The physical and chemical structural changes in RBCs and Hb respectively present promising TSD estimation targets for forensic analysis.

In this research, the use of peak ratios demonstrates linear correlations with Log(Time). Individual peak metrics such as height or area, when compared with different biological replicates, were not found to be significantly correlated with Log(Time). Peak ratios improved correlations because it mitigates the variation between replicates. This was observed especially in the later time points of the time series where the majority of O_2 has left the bloodstain. It is hypothesized that variation in film morphology affects the magnitude of redox reactions and limits the participation of Hb molecules that are either buried deep in the film or are too far from the electrode surface. Peak ratios only consider the Hb molecules able to participate in the reduction and oxidation reactions during the cathodic and anodic sweeps respectively.

The ability to detect the Hb related reactions demonstrates that these reactions can occur without modifications to blood samples and that the cell membrane from the RBCs is not inhibiting the electron transfers. It is suspected that the variation in electrochemical signals is a result of drying of the film. As the RBCs assemble and agglomerate towards the center of the electrode they create a complex 3D network. Cells trapped further from the electrode surface have to overcome higher resistances to electron transfer to produce a signal. Peak height/area ratios help to mitigate this variation in signal intensity across replicates; demonstrated in Figure 3.4 of the 2 Red/3+4 Ox Peak area ratio distribution boxplot.

Similar to other forensic blood time studies, considering the biological replicate as a random effect improved correlation [51]. The variation of blood between individuals is a major obstacle for real work scenarios where the blood source may not be known. Bloodstains from different individuals result in different drying and degradation processes [15]. Analytical techniques independent of blood source are desirable, but this level of sensitivity has not been reached. Advances and further study of analytical methods applied to blood TSD research may be able to quantify this variation but with real-world cases in mind, the identity of the blood source must be known.

Another important consideration in TSD estimates is the effect of environmental conditions such as temperature, humidity, sunlight, and daily condition fluctuations. Many blood TSD researchers take into account these metrics when developing models

and interpreting results [3,33,51,56]. Understanding the effects of these factors on bloodstains is critical for TSD estimates when answering temporal questions for bloodstains aged in various conditions. With the development of analytical techniques to study bloodstains, the application to TSD estimates in diverse and fluctuating environmental conditions remains an important area of study.

Across the bloodstain TSD literature, similar correlations with time and associated challenges are discussed. Researchers have yet to pinpoint a universal method to accurately date a bloodstain. For this reason, the combination of various techniques that focus on different physical and biochemical changes in degrading bloodstains is proposed. The shift to multivariate statistical analysis from single variable analysis is a part of the bloodstain TSD timeline. These trends will likely continue, with spectrographic methods being paired with PCR methods to monitor changes in Hb and RNA within a bloodstain [26,47,50,51,56]. The combining of variables may prove effective in mitigating biological replicate variation and have stronger correlations with time when environmental conditions are considered.

This research highlights the use of electrochemical techniques for blood TSD applications. Oxygen electrodes were among the first to be used when posed with the bloodstain TSD question in 1995 by Matsuoka *et al.* [57]. Promising results were presented with changes to fractional oxyHb and metHb over time; however, no further research using this technique has been published. The research by Matsuoka *et al.* focused on aging bloodstains in various temperature conditions to estimate bloodstain age (0 – 216 hours) through oxyHb to metHb conversion. Bloodstains were aged in ceramic wells and then dissolved in a saline solution. The oxyHb was oxidized to metHb by potassium ferricyanide and the released O_2 was measured with an oxygen electrode. Total Hb and metHb concentrations were determined with respective commercial Hb test kits and then the ratio of oxyHb and metHb to total Hb was analyzed. The main findings were that most of the Hb changes in the bloodstains occurred in the early time points (0 – 20 hours) with a gradual decrease in fractional oxyHb over time. Additionally, higher temperatures were found to increase the rates of Hb oxidation. After this publication, much of the research shifted to spectrographic techniques. The work by Matsuoka *et al.*

[57] and this research are both sensing changes in Hb through electrodes. What differentiates the two is that the research presented here studies the direct Hb electron transfer reactions on the electrode surface as opposed to the loss of bound oxygen in a bloodstain. Matsuoka and colleagues measured the O_2 released from the bloodstain and coupled that with Hb concentration kits to indirectly measure the conversion of oxyHb to metHb. Despite different in experimental methods, similar findings of the decrease in oxyHb over time are demonstrated, supporting applicability to TSD estimation.

The results presented here demonstrate the proof-of-concept foundations for electrochemical applications to bloodstain TSD. Weak correlations to Hb related redox peaks were observed and statistical analysis shows promising applications to absolute dating metrics. This research proposes the use of peak ratios for linear models when using electrochemical methods, making the signals relative between analyses. Reliable conclusions can be drawn to demonstrate changes between below and above 96 hours. For forensic investigators, this can be useful when asked to infer the chronological order of events. The applicability of electrochemical techniques to blood analysis are relatively unexplored and this research demonstrates one possible application. Advances in electrochemistry over the decades and the use of whole blood as a sample matrix have been demonstrated. This research supports future research in bloodstain estimates using electrochemical methods.

5.2 BPA and electrochemistry

Electrochemical techniques have been growing in popularity for forensic applications. Several forensic samples are being researched, such as drugs [60,66,69] and explosives [58]. Biomedical research has expanded the utility of electrochemical biosensors for the identification and quantification of various drugs, macromolecules, and metals in blood samples over recent decades. High specificity and selectivity of many analytes have been validated and show promise for implementation in clinical and forensic science settings. While electrochemical methods have demonstrated analytical sensitivity for identifying drugs in the laboratory, detecting individual or drugs mixtures in blood would be valuable in forensic cases [61,67,69]. Presumptive on-site drug identification testing presents a strong starting research opportunity to utilize these sensors in a forensic context and possibly lead to confirmatory tests once accurate

methods are thoroughly understood. The low cost, quick analysis, and portability of electrochemical techniques are advantageous traits for forensic investigators who could perform presumptive analysis at the scene. Future work on testing the LOD, specificity, and an optimization of these technologies for whole blood samples is on the horizon [58,60,61,70,72].

Electrochemical techniques for whole blood analysis have been researched for medical applications. The majority of these works focus on the Hb/ORR redox system to diagnosis blood related diseases [34,62,88,89]. When electrochemical techniques were first being applied to blood analysis, the Hb electron mediated transfer was thought to be a slow and relatively difficult process to monitor due to the electroactive components being buried inside the cell membrane [34,116]. For this reason, purified Hb and pretreated blood samples were primarily used for analysis. This, along with the risk of biofouling dissuaded the use of whole blood as a sample matrix. Given these early challenges, researchers have explored many variations of electrode materials and sample immobilization techniques to effectively study Hb redox reactions and have shown that direct electron transfer is possible through the cell membrane. A number of articles report a quasi-reversible to nearly reversible Hb corresponding redox peak using many electrode materials, including the well-studied GC electrode [84,101,102,115,123].

The characterization experiments, presented in Chapter 3, show similar peak shapes and electrochemical signals seen in related research [34,85,88,93]. The GC electrodes and simple immobilization techniques of layering Naf proved to be suitable for electrochemical analysis of whole blood. Future work on improving uniformity in the blood film across the electrode surface would likely be useful in achieving greater Hb sensitivity and reproducibility. The methods presented here are not limited to forensic science research. The use of whole blood for analysis overlaps with medical and environmental disciplines. Within the medical field, whole blood electrochemistry for Hb/ORR reactions has been studied and presents promising applications to non-invasive, fast, and portable diagnostic tests for blood related conditions. Blood electrochemical analysis could be used in environmental field testing where blood is detected in water treatment plants or the run-off from abattoirs. The electrode preparation methodologies

and data analysis are not limited to forensic science but other fields that encounter biological samples.

5.3 Conclusions

The goals of this project were to evaluate the applicability of DPV on blood analysis with forensic perspectives in mind. This was accomplished by characterizing the redox reactions present and determining a reproducible method for electrochemical analysis using bovine blood deposited on GC electrodes. From a forensic perspective, the application of this technique was used to study the changes in Hb over time and contribute to the bloodstain TSD literature.

This thesis project proposes a new research avenue for bloodstain TSD estimates. Electrochemical methods have been used for blood analysis in medical fields and have many desirable characteristics for forensic analysis. Research design and proof-of-concept methodologies using electrochemical methods are the first steps toward applying electrochemical methods to TSD estimates. Future applications to case-specific experimentation are encouraged. Additionally, research in optimizing electrode preparation methods and understanding the sensitivity of these methods when environmental conditions are changed is required. The question of a bloodstain's age is unanswered in forensic science, and one that has likely been posed to forensic experts before. The studied TSD techniques have yet to obtain forensic level accuracy and precision. Many analytical techniques are increasing in sensitivity to study blood evidence and researchers are incorporating mathematics to strengthen models. Understanding the environmental effects on degradation and blood source variation are high priorities for researchers focussed on TSD questions. The assemblage of other bloodstains TSD analytical methods to form multivariate statistical analysis is on the path ahead. Presenting new analytical techniques, such as electrochemistry, opens the door to new and exciting perspectives on the toolkit of useful for techniques to age a bloodstain.

References

[1] R.J. Dinis-Oliveira, F. Carvalho, J.A. Duarte, F. Remião, A. Marques, A. Santos, T. Magalhães, Collection of biological samples in forensic toxicology, Toxicol. Mech. Methods. 20 (2010) 363–414. https://doi.org/10.3109/15376516.2010.497976.

[2] K. Virkler, I.K. Lednev, Analysis of body fluids for forensic purposes: From laboratory testing to non-destructive rapid confirmatory identification at a crime scene, Forensic Sci. Int. 188 (2009) 1–17. https://doi.org/10.1016/j.forsciint.2009.02.013.

[3] D.R. Cavalcanti, L.P. Silva, Application of atomic force microscopy in the analysis of time since deposition (TSD) of red blood cells in bloodstains: A forensic analysis, Forensic Sci. Int. 301 (2019) 254–262. https://doi.org/10.1016/j.forsciint.2019.05.048.

[4] T.Y. Chen, V. Mani, S.T. Huang, P.C. Chang, C.H. Huang, N.M. Huang, Synthesis of robust electrochemical substrate and fabrication of immobilization free biosensors for rapid sensing of salicylate and β-hydroxybutyrate in whole blood, Anal Chim Acta. 990 (2017) 78–83. https://doi.org/10.1016/j.aca.2017.08.051.

[5] F.Y. Kong, S.X. Gu, W.W. Li, T.T. Chen, Q. Xu, W. Wang, A paper disk equipped with graphene/polyaniline/Au nanoparticles/glucose oxidase biocomposite modified screen-printed electrode: Toward whole blood glucose determination, Biosens. Bioelectron. 56 (2014) 77–82. https://doi.org/10.1016/j.bios.2013.12.067.

[6] E. Matysiak, M. Donten, A. Kowalczyk, M. Bystrzejewski, I.P. Grudzinski, A.M. Nowicka, A novel type of electrochemical sensor based on ferromagnetic carbon-encapsulated iron nanoparticles for direct determination of hemoglobin in blood samples, Biosens. Bioelectron. 64 (2015) 554–559. https://doi.org/10.1016/j.bios.2014.09.079.

[7] J. Vacek, Z. Andrysík, L. Trnková, R. Kizek, Determination of azidothymidine - An antiproliferative and virostatic drug by square-wave voltammetry, Electroanalysis. 16 (2004) 224–230. https://doi.org/10.1002/elan.200302787.

[8] D. Brutin, B. Sobac, B. Loquet, J. Sampol, Pattern formation in drying drops of blood, J. Fluid Mech. 667 (2011) 85–95. https://doi.org/10.1017/S0022112010005070.

[9] F. Barni, S.W. Lewis, A. Berti, G.M. Miskelly, G. Lago, Forensic application of the luminol reaction as a presumptive test for latent blood detection, Talanta. 72 (2007) 896–913. https://doi.org/10.1016/j.talanta.2006.12.045.

[10] A. Sparer, B. Serp, L. Schwarz, U. Windberger, Storability of porcine blood in forensics: How far should we go?, Forensic Sci. Int. 311 (2020) 110268. https://doi.org/10.1016/j.forsciint.2020.110268.

[11] C.A. Streeting, J. Chaseling, M.N. Krosch, K. Wright, A comparison of ABAcard® Hematrace® and RSIDTM-Blood tests on dried, diluted bloodstains treated with leucocrystal violet or luminol, Aust. J. Forensic Sci. (2020). https://doi.org/10.1080/00450618.2020.1781256.

[12] D. Attinger, C. Moore, A. Donaldson, A. Jafari, H.A. Stone, Fluid dynamics topics in bloodstain pattern analysis: Comparative review and research opportunities, Forensic Sci. Int. 231 (2013) 375–396. https://doi.org/10.1016/j.forsciint.2013.04.018.

[13] J.Y. Liu, C. Zhong, A. Holt, R. Lagace, M. Harrold, A.B. Dixon, M.G. Brevnov, J.G. Shewale, L.K. Hennessy, AutoMate Express™ Forensic DNA Extraction System for the Extraction of Genomic DNA from Biological Samples, J. Forensic Sci. 57 (2012) 1022–1030. https://doi.org/10.1111/j.1556-4029.2012.02084.x.

[14] K. Phillips, N. McCallum, L. Welch, A comparison of methods for forensic DNA extraction: Chelex-100 ® and the QIAGEN DNA Investigator Kit (manual and automated), Forensic Sci. Int. Genet. 6 (2012) 282–285. https://doi.org/10.1016/j.fsigen.2011.04.018.

[15] G. Zadora, A. Menżyk, In the pursuit of the holy grail of forensic science – Spectroscopic studies on the estimation of time since deposition of bloodstains, TrAC - Trends Anal. Chem. 105 (2018) 137–165. https://doi.org/10.1016/j.trac.2018.04.009.

[16] K.C. Doty, C.K. Muro, I.K. Lednev, Predicting the time of the crime: Bloodstain aging estimation for up to two years, Forensic Chem. 5 (2017) 1–7. https://doi.org/10.1016/j.forc.2017.05.002.

[17] S.S. Simões, A. Casta, M.J. Dias, Dried blood spots combined to an UPLC – MS / MS method for the simultaneous determination of drugs of abuse in forensic toxicology, J. Pharm. Biomed. Anal. 147 (2018) 634–644. https://doi.org/10.1016/j.jpba.2017.02.046.

[18] H.H.M. T, Multi-analyte procedures for screening for and quantification of drugs in blood, plasma, or serum by liquid chromatography-single stage or tandem mass spectrometry (LC-MS or LC-MS/MS) relevant to clinical and forensic toxicology, Clin. Biochem. 38 (2005) 310–318. https://doi.org/10.1016/j.clinbiochem.2005.01.014.

[19] F. Peters, Staility of analytes in biosamples - an important issue in clinical and forensic toxicology?, Anal. Bioanal. Chem. 388 (2007) 1505–1519. https://doi.org/10.1007/s00216-007-1267-2.

[20] N. Laan, F. Smith, C. Nicloux, D. Brutin, Morphology of drying blood pools, Forensic Sci. Int. 267 (2016) 104–109. https://doi.org/10.1016/j.forsciint.2016.08.005.

[21] F. Ramsthaler, J. Schlote, C. Wagner, J. Fiscina, M. Kettner, The ring phenomenon of diluted blood droplets, Int. J. Legal Med. 130 (2016) 731–736. https://doi.org/10.1007/s00414-015-1304-1.

[22] D. Brutin, B. Sobac, C. Nicloux, Influence of Substrate Nature on the Evaporation of a Sessile Drop of Blood, J. Heat Transfer. 134 (2012) 1–7. https://doi.org/10.1115/1.4006033.

[23] A. Pal, A. Gope, J.D. Obayemi, G.S. Iannacchione, Concentration-driven phase transition and self-assembly in drying droplets of diluting whole blood, Sci. Rep. 10 (2020) 1–12. https://doi.org/10.1038/s41598-020-76082-6.

[24] P. Hortola, Using digital anaglyphy to improve the relief effect of SEM micrographs of bloodstains, Micron. 40 (2009) 409–412. https://doi.org/10.1016/j.micron.2008.09.008.

[25] P. Hortola, SEM examination of human erythrocytes in uncoated bloodstains on stone: use of conventional as environmental-like SEM in a soft biological tissue (and hard inorganic material), J. Microsc. 218 (2005) 94–113. https://doi.org/10.1111/j.1365-2818.2005.01477.x.

[26] S. Boyd, M.F. Bertino, S.J. Seashols, Raman spectroscopy of blood samples for forensic applications, Forensic Sci. Int. 208 (2011) 124–128. https://doi.org/10.1016/j.forsciint.2010.11.012.

[27] M. Asghari-Khiavi, A. Mechler, K.R. Bambery, D. McNaughton, B.R. Wood, A resonance Raman spectroscopic investigation into the effects of fixation and dehydration on heme environment of hemoglobin, J. Raman Spectrosc. 40 (2009) 1668–1674. https://doi.org/10.1002/jrs.2317.

[28] S.L. Forbes, L. Rust, K. Trebilcock, K.A. Perrault, L.T. McGrath, Effect of age and storage conditions on the volatile organic compound profile of blood, Forensic Sci. Med. Pathol. 10 (2014) 570–582. https://doi.org/10.1007/s12024-014-9610-3.

[29] L.T. Rust, K.D. Nizio, S.L. Forbes, The influence of ageing and surface type on the odour profile of blood-detection dog training aids, Anal. Bioanal. Chem. 408 (2016) 6349–6360. https://doi.org/10.1007/s00216-016-9748-9.

[30] K.K. Hussain, J.M. Moon, D.S. Park, Y.B. Shim, Electrochemical Detection of Hemoglobin: A Review, Electroanalysis. 29 (2017) 2190–2199. https://doi.org/10.1002/elan.201700308.

[31] C. Bonaventura, R. Henkens, A.I. Alayash, S. Banerjee, A.L. Crumbliss, Molecular controls of the oxygenation and redox reactions of hemoglobin, Antioxidants Redox Signal. 18 (2013) 2298–2313. https://doi.org/10.1089/ars.2012.4947.

[32] R.H. Bremmer, K.G. De Bruin, M.J.C. Van Gemert, T.G. Van Leeuwen, M.C.G. Aalders, Forensic quest for age determination of bloodstains, Forensic Sci. Int. 216 (2012) 1–11. https://doi.org/10.1016/j.forsciint.2011.07.027.

[33] R.H. Bremmer, D.M. de Bruin, M. de Joode, W.J. Buma, T.G. van Leeuwen, M.C.G. Aalders, Biphasic oxidation of Oxy-Hemoglobin in bloodstains, PLoS One. 6 (2011) 1–6. https://doi.org/10.1371/journal.pone.0021845.

[34] R.J. Toh, W.K. Peng, J. Han, M. Pumera, Direct in vivo electrochemical detection

of haemoglobin in red blood cells, Sci. Rep. 4 (2014) 1–7. https://doi.org/10.1038/srep06209.

[35] P. Lemler, W.R. Premasiri, A. DelMonaco, L.D. Ziegler, NIR Raman spectra of whole human blood: Effects of laser-induced and in vitro hemoglobin denaturation, Anal. Bioanal. Chem. 406 (2014) 193–200. https://doi.org/10.1007/s00216-013-7427-7.

[36] K. Shikama, The molecular mechanism of autoxidation for myoglobin and hemoglobin: A venerable puzzle, Chem. Rev. 98 (1998) 1357–1373. https://doi.org/10.1021/cr970042e.

[37] T. Kassa, S. Jana, F. Meng, A.I. Alayash, Differential heme release from various hemoglobin redox states and the upregulation of cellular heme oxygenase-1, FEBS Open Bio. 6 (2016) 876–884. https://doi.org/10.1002/2211-5463.12103.

[38] S. Lociciro, L. Dujourdy, W. Mazzella, P. Margot, E. Lock, Dynamic of the ageing of ballpoint pen inks: Quantification of phenoxyethanol by GC-MS, Sci. Justice - J. Forensic Sci. Soc. 44 (2004) 165–171. https://doi.org/10.1016/S1355-0306(04)71709-8.

[39] C. Weyermann, D. Kirsch, C.C. Vera, B. Spengler, A GC/MS study of the drying of ballpoint pen ink on paper, Forensic Sci. Int. 168 (2007) 119–127. https://doi.org/10.1016/j.forsciint.2006.06.076.

[40] C. Weyermann, C. Roux, C. Champod, Initial Results on the Composition of Fingerprints and its Evolution as a Function of Time by GC/MS Analysis, J. Forensic Sci. 56 (2011) 102–108. https://doi.org/10.1111/j.1556-4029.2010.01523.x.

[41] R.K. Shukla, Forensic application of comet assay: an emerging technique, Forensic Sci. Res. 2 (2017) 180–184. https://doi.org/10.1080/20961790.2017.1379893.

[42] C. Salzmann, Andrea Patrizia; Russo, Giancarlo; Kreutzer, Susanne; Haas, Degradation of human mRNA transcripts over time as an indicator of the time since deposition (TsD) in biological crime scene traces, Forensic Sci. Int. 53 (2021) 102524. https://doi.org/10.1016/j.fsigen.2021.102524.

[43] R.H. Bremmer, A. Nadort, T.G. van Leeuwen, M.J.C. van Gemert, M.C.G. Aalders, Age estimation of blood stains by hemoglobin derivative determination using reflectance spectroscopy, Forensic Sci. Int. 206 (2011) 166–171. https://doi.org/10.1016/j.forsciint.2010.07.034.

[44] A.R. Weber, I.K. Lednev, Crime clock – Analytical studies for approximating time since deposition of bloodstains, Forensic Chem. 19 (2020) 100248. https://doi.org/10.1016/j.forc.2020.100248.

[45] E. Hanson, A. Albornoz, J. Ballantyne, Validation of the hemoglobin (Hb) hypsochromic shift assay for determination of the time since deposition (TSD) of dried bloodstains, Forensic Sci. Int. Genet. Suppl. Ser. 3 (2011) e307–e308. https://doi.org/10.1016/j.fsigss.2011.09.016.

[46] C. Fang, J. Zhao, J. Li, J. Qian, X. Liu, Q. Sun, W. Liu, Massively parallel sequencing of microRNA in bloodstains and evaluation of environmental in fl uences on miRNA candidates using realtime polymerase chain reaction, Forensic Sci. Int. 38 (2019) 32–38. https://doi.org/10.1016/j.fsigen.2018.10.001.

[47] J. Fu, R.W. Allen, A method to estimate the age of bloodstains using quantitative PCR, Forensic Sci. Int. 39 (2019) 103–108. https://doi.org/10.1016/j.fsigen.2018.12.004.

[48] N. Heneghan, J. Fu, J. Pritchard, M. Payton, R.W. Allen, The effect of environmental conditions on the rate of RNA degradation in dried blood stains, Forensic Sci. Int. 51 (2021) 102456. https://doi.org/10.1016/j.fsigen.2020.102456.

[49] S. Alshehhi, N.A. McCallum, P.R. Haddrill, Quantification of RNA degradation of blood-specific markers to indicate the age of bloodstains, Forensic Sci. Int. Genet. Suppl. Ser. 6 (2017) e453–e455. https://doi.org/10.1016/j.fsigss.2017.09.175.

[50] S. Anderson, B. Howard, G.R. Hobbs, C.P. Bishop, A method for determining the age of a bloodstain, Forensic Sci. Int. 148 (2005) 37–45. https://doi.org/10.1016/j.forsciint.2004.04.071.

[51] M.L. Cossette, T. Stotesbury, A.B.A. Shafer, Quantifying visible absorbance changes and DNA degradation in aging bloodstains under extreme temperatures, Forensic Sci. Int. 318 (2021) 110627. https://doi.org/10.1016/j.forsciint.2020.110627.

[52] S. Alshehhi, P.R. Haddrill, Estimating time since deposition using quantification of RNA degradation in body fluid-specific markers, Forensic Sci. Int. 298 (2019) 58–63. https://doi.org/10.1016/J.FORSCIINT.2019.02.046.

[53] S. Mc Shine, K. Suhling, A. Beavil, B. Daniel, N. Frascione, The applicability of fluorescence lifetime to determine the time since the deposition of biological stains, Anal. Methods. 9 (2017) 2007–2013. https://doi.org/10.1039/c6ay03099h.

[54] B. Li, P. Beveridge, W. O'Hare, M. Islam, The age estimation of blood stains up to 30 days old using visible wavelength hyperspectral image analysis and linear discriminant analysis, Sci. Justice. 53 (2013) 270–277. https://doi.org/10.1016/j.scijus.2013.04.004.

[55] Y. Fujita, K. Tsuchiya, S. Abe, Y. Takiguchi, S. Kubo, H. Sakurai, Estimation of the age of human blodstains by electron paramagnetic resonance spectroscopy: Long-term controlled experiment on the effects of environmental factors, Forensic Sci. Int. 152 (2005) 39–43. https://doi.org/10.1016/j.forsciint.2005.02.029.

[56] E.K. Hanson, J. Ballantyne, A blue spectral shift of the hemoglobin soret band correlates with the age (time since deposition) of dried bloodstains, PLoS One. 5 (2010) 1–11. https://doi.org/10.1371/journal.pone.0012830.

[57] T. Matsuoka, T. Taguchi, J. Okuda, Estimation of bloodstain age by rapid determinations of oxyhemoglobin by use of oxygen electrode and total hemoglobin, Biol Pharm Bull. 18 (1995) 1031–1035.

https://doi.org/10.1248/bpb.18.1031.

[58] H.A. Yu, D.A. Detata, S.W. Lewis, D.S. Silvester, Recent developments in the electrochemical detection of explosives: Towards field-deployable devices for forensic science, Trends Anal. Chem. 97 (2017) 374–384. https://doi.org/10.1016/j.trac.2017.10.007.

[59] A. Harshey, A. Srivastava, T. Das, K. Nigam, R. Shrivastava, V.K. Yadav, Trends in Gunshot Residue Detection by Electrochemical Methods for Forensic Purpose, J. Anal. Test. (2021). https://doi.org/10.1007/s41664-020-00152-x.

[60] É. Naomi Oiye, J. Midori Toia Katayama, M. Fernanda Muzetti Ribeiro, L. Oka Duarte, R. de Castro Baker Botelho, A. José Ipólito, B. Royston McCord, M. Firmino de Oliveira, Voltammetric detection of 3,4-methylenedioxymethamphetamine (mdma) in saliva in low cost systems, Forensic Chem. 20 (2020) 100268. https://doi.org/10.1016/j.forc.2020.100268.

[61] N. Samyn, K. De Wael, Electrochemical Strategies for Adulterated Heroin Samples, Anal. Chem. 91 (2019) 7920–7928. https://doi.org/10.1021/acs.analchem.9b01796.

[62] K. Amreen, A.S. Kumar, Electrochemical redox signaling of hemoglobin in human whole blood and its relevance to anemia and thalassemia diagnosis, Analyst. 141 (2016) 2145–2149. https://doi.org/10.1039/c5an02646f.

[63] Y. Xu, C. Hu, S. Hu, Direct electron-transfer of native hemoglobin in blood: kinetics and catalysis, Bioelectrochemistry. 72 (2008) 135–140. https://doi.org/10.1016/j.bioelechem.2008.01.002.

[64] D. Moher, A. Liberati, J. Tetzlaff, D.G. Altman, T.P. Group, Preferred Reporting Items for Systematic Reviews and Meta-Analyses : The PRISMA Statement, 6 (2009). https://doi.org/10.1371/journal.pmed.1000097.

[65] P. Luo, G. Xie, Y. Liu, H. Xu, S. Deng, F. Song, Electrochemical detection of blood alcohol concentration using a disposable biosensor based on screen-printed electrode modified with Nafion and gold nanoparticles, Clin. Chem. Lab. Med. 46 (2008) 1641–1647. https://doi.org/10.1515/CCLM.2008.308.

[66] J. Aymerich, A. Marquez, L. Teres, X. Munoz-Berbel, C. Jimenez, C. Dominguez, F. Serra-Graells, M. Dei, Cost-effective smartphone-based reconfigurable electrochemical instrument for alcohol determination in whole blood samples, Biosens. Bioelectron. 117 (2018) 736–742. https://doi.org/10.1016/j.bios.2018.06.044.

[67] L.F. Mendes, Â.R. Souza e Silva, R.P. Bacil, S.H.P. Serrano, L. Angnes, T.R.L.C. Paixão, W.R. de Araujo, Forensic electrochemistry: Electrochemical study and quantification of xylazine in pharmaceutical and urine samples, Electrochim. Acta. 295 (2019) 726–734. https://doi.org/10.1016/j.electacta.2018.10.120.

[68] H.M. Elbardisy, A. García-Miranda Ferrari, C.W. Foster, O.B. Sutcliffe, D.A.C. Brownson, T.S. Belal, W. Talaat, H.G. Daabees, C.E. Banks, Forensic

Electrochemistry: The Electroanalytical Sensing of Mephedrone Metabolites, ACS Omega. 4 (2019) 1947–1954. https://doi.org/10.1021/acsomega.8b02586.

[69] E.R. Darzi, N.K. Garg, Toward an Optical and Electrochemical Method for Marijuana Detection : A Simple Electrochemical Oxidation of Δ 9 -THC, ChemRxiv. December 2 (n.d.). https://doi.org/10.26434/chemrxiv.11259437.v1.

[70] E.R. Darzi, N.K. Garg, Electrochemical Oxidation of Δ9 - Tetrahydrocannabinol: A Simple Strategy for Marijuana Detection, Org. Lett. 22 (2020) 3951–3955. https://doi.org/10.1021/acs.orglett.0c01241.

[71] J.P. Smith, J.P. Metters, O.I.G. Khreit, O.B. Sutcli, C.E. Banks, Forensic Electrochemistry Applied to the Sensing of New Psychoactive Substances: Electroanalytical Sensing of Synthetic Cathinones and Analytical Validation in the Quantification of Seized Street Samples, Anal. Chem. 86 (2014) 9985–9992. https://doi.org/10.1021/ac502991g.

[72] S.A. Goodchild, L.J. Hubble, R.K. Mishra, Z. Li, K.Y. Goud, A. Bar, R. Shah, K.S. Bagot, A.J.S. Mcintosh, J. Wang, Ionic Liquid-Modified Disposable Electrochemical Sensor Strip for Analysis of Fentanyl, Anal. Chem. 91 (2019) 3747–3753. https://doi.org/10.1021/acs.analchem.9b00176.

[73] E. Garcia-gutierrez, C. Lledo-fernandez, Electroanalytical Sensing of Flunitrazepam Based on Screen Printed Graphene Electrodes, Chemosensors. 1 (2013) 68–77. https://doi.org/10.3390/chemosensors1030068.

[74] J.P. Smith, J.P. Metters, D.K. Kampouris, C. Lledo-fernandez, O.B. Sutcli, C.E. Banks, Forensic electrochemistry : the electroanalytical sensing, Analyst. 138 (2013) 6185–6191. https://doi.org/10.1039/c3an01352a.

[75] E.P. Nahirny, M.F. Bergamini, L.H. Marcolino-junior, Improvement in the performance of an electrochemical sensor for ethanol determination by chemical treatment of graphite, J. Electroanal. Chem. 877 (2020) 114659. https://doi.org/10.1016/j.jelechem.2020.114659.

[76] S. Cinti, M. Basso, D. Moscone, F. Arduini, A paper-based nanomodi fi ed electrochemical biosensor for ethanol detection in beers, Anal. Chim. Acta. 960 (2017) 123–130. https://doi.org/10.1016/j.aca.2017.01.010.

[77] E. Pargoletti, A. Tricoli, V. Pi, S. Orsini, M. Longhi, V. Guglielmi, G. Cerrato, An electrochemical outlook upon the gaseous ethanol sensing by graphene, Appl. Surf. Sci. 483 (2019) 1081–1089. https://doi.org/10.1016/j.apsusc.2019.04.046.

[78] E.B. Easton, M.R. Rahman, J.T.S. Allan, H.L. Geoffrey, The Design of Low Pt Loading Electrodes for Use in Fuel Cell-Based Breath Alcohol Sensors, J. Electrochem. Soc. 167 (2020) 147509. https://doi.org/10.1149/1945-7111/abc5de.

[79] W. Li, J. Lü, S. Gao, Q. Li, R. Cao, Electrochemical preparation of metal – organic framework films for fast detection of nitro explosives, J. Mater. Chem. A. 2 (2014) 19473–19478. https://doi.org/10.1039/c4ta04203d.

[80] T. Trejos, C. Vander, K. Menking-hoggatt, A. Lorena, L.E. Arroyo, Fast

identification of inorganic and organic gunshot residues by LIBS and electrochemical methods, Forensic Chem. 8 (2018) 146–156. https://doi.org/10.1016/j.forc.2018.02.006.

[81] A.M.O. Mahony, J. Wang, Electrochemical Detection of Gunshot Residue for Forensic Analysis: A Review, Electroanalysis. 25 (2013) 1341–1358. https://doi.org/10.1002/elan.201300054.

[82] R. Rosa, R. Giovanardi, A. Bozza, P. Veronesi, C. Leonelli, Electrochemical impedance spectroscopy: A deeper and quantitative insight into the fingermarks physical modifications over time, Forensic Sci. Int. 273 (2017) 144–152. https://doi.org/10.1016/j.forsciint.2017.02.016.

[83] E.I. Naik, H.S.B. Naik, B.E.K. Swamy, R. Viswanath, I.K.S. Gowda, M.C. Prabhakara, K. Chetankumar, Influence of Cu doping on ZnO nanoparticles for improved structural, optical, electrochemical properties and their applications in efficient detection of latent fingerprints, Chem. Data Collect. 33 (2021) 100671. https://doi.org/10.1016/j.cdc.2021.100671.

[84] A. Safavi, N. Maleki, O. Moradlou, M. Sorouri, Direct electrochemistry of hemoglobin and its electrocatalytic effect based on its direct immobilization on carbon ionic liquid electrode, Electrochem. Commun. 10 (2008) 420–423. https://doi.org/10.1016/j.elecom.2007.12.026.

[85] K. Amreen, A.S. Kumar, Bio-electrocatalytic reduction of dissolved oxygen by whole blood chemically modified electrode and its application, J. Electroanal. Chem. 809 (2018) 36–43. https://doi.org/10.1016/j.jelechem.2017.12.047.

[86] W.W. Yao, C. Lau, Y. Hui, H.L. Poh, R.D. Webster, Electrode-supported biomembrane for examining electron-transfer and ion-transfer reactions of encapsulated low molecular weight biological molecules, J. Phys. Chem. C. 115 (2011) 2100–2113. https://doi.org/10.1021/jp1096037.

[87] S. Goines, J.E. Dick, Review—Electrochemistry's Potential to Reach the Ultimate Sensitivity in Measurement Science, J. Electrochem. Soc. 167 (2020) 037505. https://doi.org/10.1149/2.0052003jes.

[88] A. Domenech-Carbo, E. Villamon, I. Luna, D. Ramos, C. Domenech-Casasus, G. Cebrian-Torrejon, Transmembrane electrochemistry of erythrocytes: Direct electrochemical test for detecting hemolysis in whole blood, Sensors and Actuators B-Chemical. 226 (2016) 419–428. https://doi.org/10.1016/j.snb.2015.12.001.

[89] M. Ogunlesi, W. Okiei, A.S. Akanmu, T. Popoola, K. Okafor, O. Akore, Novel Method for the Determination of Haemoglobin Phenotypes by Cyclic Voltammetry using Glassy Carbon Electrode, Int. J. Electrochem. Sci. 4 (2009) 1593–1606.

[90] Y. Ayato, K. Sakurai, S. Fukunaga, T. Suganuma, K. Yamagiwa, H. Shiroishi, J. Kuwano, A simple biofuel cell cathode with human red blood cells as electrocatalysts for oxygen reduction reaction, Biosens. Bioelectron. 55 (2014) 14–18. https://doi.org/10.1016/j.bios.2013.11.063.

[91] H.H. Liu, Y.Q. Wan, G.L. Zou, Direct electrochemistry and electrochemical catalysis of immobilized hemoglobin in an ethanol-water mixture, Anal. Bioanal. Chem. 385 (2006) 1470–1476. https://doi.org/10.1007/s00216-006-0588-x.

[92] Y. Wang, J. Guo, H. Gu, A novel nano-sized bionic function interface for enhancing the ability of red blood cells to carry oxygen, Microchim Acta. 171 (2010) 179–186. https://doi.org/10.1007/s00604-010-0392-3.

[93] K. Amreen, A.S. Kumar, A human whole blood chemically modified electrode for the hydrogen peroxide reduction and sensing: Real-time interaction studies of hemoglobin in the red blood cell with hydrogen peroxide, J. Electroanal. Chem. 815 (2018) 189–197. https://doi.org/10.1016/j.jelechem.2018.03.023.

[94] T.L.T. Ho, N.T.T. Hoang, J. Lee, J.H. Park, B.K. Kim, Determining mean corpuscular volume and red blood cell count using electrochemical collision events, Biosens. Bioelectron. 110 (2018) 155–159. https://doi.org/10.1016/j.bios.2018.03.053.

[95] R.K. Khan, S.P. Gadiraju, M. Kumar, G.A. Hatmaker, B.J. Fisher, R. Natarajan, J.E. Reiner, M.M. Collinson, Redox Potential Measurements in Red Blood Cell Packets Using Nanoporous Gold Electrodes, ACS Sensors. 3 (2018) 1601–1608. https://doi.org/10.1021/acssensors.8b00498.

[96] L. Sepunaru, S. V. Sokolov, J. Holter, N.P. Young, R.G. Compton, Electrochemical Red Blood Cell Counting: One at a Time, Angew. Chemie - Int. Ed. 55 (2016) 9768–9771. https://doi.org/10.1002/anie.201605310.

[97] X.Y. Lin, L.L. Wu, Z.Q. Pan, C.G. Shi, N. Bao, H.Y. Gu, Paper-based analytical devices for electrochemical study of the breathing process of red blood cells, Talanta. 135 (2015) 23–26. https://doi.org/10.1016/j.talanta.2014.12.040.

[98] X. Liu, Z. Pan, Z. Dong, Y. Lu, Q. Sun, T. Wu, N. Bao, H. He, H. Gu, Amperometric oxygen biosensor based on hemoglobin encapsulated in nanosized grafted starch particles, Microchim. Acta. 183 (2016) 353–359. https://doi.org/10.1007/s00604-015-1655-9.

[99] R. Rastogi, S. Tuteja, S.K. Tripathi, I. Kaur, L.M. Bharadwaj, In-Situ Direct Electrochemistry of Hemoglobin Using Vertically Aligned Carbon Nanotube Ropes, Adv. Sci. Lett. 4 (2011) 3390–3397. https://doi.org/10.1166/asl.2011.1914.

[100] S. V Sokolov, L. Sepunaru, R.G. Compton, Taking cues from nature: Hemoglobin catalysed oxygen reduction, Appl. Mater. Today. 7 (2017) 82–90. https://doi.org/10.1016/j.apmt.2017.01.005.

[101] L. Wang, N. Hu, Direct electrochemistry of hemoglobin in layer-by-layer films with poly(vinyl sulfonate) grown on pyrolytic graphite electrodes, Bioelectrochemistry. 53 (2001) 205–212. https://doi.org/10.1016/S0302-4598(01)00095-2.

[102] J. Xu, C. Liu, Z. Wu, Direct electrochemistry and enhanced electrocatalytic activity of hemoglobin entrapped in graphene and ZnO nanosphere composite

film, Microchim. Acta. 172 (2011) 425–430. https://doi.org/10.1007/s00604-010-0515-x.

[103] R.K. Khan, V.K. Yadavalli, M.M. Collinson, Flexible Nanoporous Gold Electrodes for Electroanalysis in Complex Matrices, Chemelectrochem. 6 (2019) 4660–4665. https://doi.org/10.1002/celc.201900894.

[104] H. Fini, K. Kerman, Revisiting the nitrite reductase activity of hemoglobin with differential pulse voltammetry, Anal. Chim. Acta. 1104 (2020) 38–46. https://doi.org/10.1016/j.aca.2019.12.071.

[105] M. Amayreh, M. Hourani, Direct Electrochemical Determination of Hemoglobin in Blood Using Iodine-Coated Platinum Polycrystalline Electrode, Anal. Bioanal. Chem. Res. 6 (2019) 59–68. https://doi.org/10.22036/abcr.2018.125953.1198.

[106] Z.Q. Pan, J. Xie, X.J. Liu, N. Bao, H.Y. Gu, Direct electron transfer from native human hemoglobin using a glassy carbon electrode modified with chitosan and a poly(N,N-diethylacrylamide) hydrogel containing red blood cells, Microchim. Acta. 181 (2014) 1215–1221. https://doi.org/10.1007/s00604-014-1222-9.

[107] R.J. Toh, W.K. Peng, J. Han, M. Pumera, Haemoglobin electrochemical detection on various reduced graphene surfaces: Well-defined glassy carbon electrode outperforms the graphenoids, RSC Adv. 4 (2014) 8050–8054. https://doi.org/10.1039/c3ra45417g.

[108] A. Orr, R. Gualdieri, M.L. Cossette, A.B.A. Shafer, T. Stotesbury, Whole bovine blood use in forensic research: Sample preparation and storage considerations, Sci. Justice. 61 (2021) 214–220. https://doi.org/10.1016/j.scijus.2021.02.004.

[109] T.C. de Castro, M.C. Taylor, D.J. Carr, J. Athens, J.A. Kieser, Storage life of whole porcine blood used for bloodstain pattern analysis, J. Can. Soc. Forensic Sci. 49 (2016) 26–37. https://doi.org/10.1080/00085030.2015.1108770.

[110] M.T. Huynh, C.W. Anson, A.C. Cavell, S.S. Stahl, S. Hammes-Schiffer, Quinone 1 e– and 2 e–/2 H+ Reduction Potentials: Identification and Analysis of Deviations from Systematic Scaling Relationships, J. Am. Chem. Soc. 138 (2016) 15903–15910. https://doi.org/10.1021/jacs.6b05797.

[111] M. Rafiee, D. Nematollahi, Voltammetry of electroinactive species using quinone/hydroquinone redox: A known redox system viewed in a new perspective, Electroanalysis. 19 (2007) 1382–1386. https://doi.org/10.1002/elan.200703864.

[112] G.C. Sedenho, D. De Porcellinis, Y. Jing, E. Kerr, L.M. Mejia-Mendoza, Á. Vazquez-Mayagoitia, A. Aspuru-Guzik, R.G. Gordon, F.N. Crespilho, M.J. Aziz, Effect of Molecular Structure of Quinones and Carbon Electrode Surfaces on the Interfacial Electron Transfer Process, ACS Appl. Energy Mater. 3 (2020) 1933–1943. https://doi.org/10.1021/acsaem.9b02357.

[113] M. Lu, R.G. Compton, Voltammetric pH sensing using carbon electrodes: glassy carbon behaves similarly to EPPG, Analyst. 139 (2014) 4599–4605. https://doi.org/10.1039/c4an00866a.

[114] K. Wedege, E. Dražević, D. Konya, A. Bentien, Organic Redox Species in Aqueous Flow Batteries : Redox Potentials , Chemical Stability and Solubility, Nat. Publ. Gr. 6 (2016) 1–13. https://doi.org/10.1038/srep39101.

[115] W. Sun, D. Wang, G. Li, Z. Zhai, R. Zhao, K. Jiao, Direct electron transfer of hemoglobin in a CdS nanorods and Nafion composite film on carbon ionic liquid electrode, Electrochim. Acta. 53 (2008) 8217–8221. https://doi.org/10.1016/j.electacta.2008.06.021.

[116] C. Yu, L. Wang, Z. Zhu, N. Bao, H. Gu, Trans-membrane electron transfer in red blood cells immobilized in a chitosan film on a glassy carbon electrode, Microchim. Acta. 181 (2014) 55–61. https://doi.org/10.1007/s00604-013-1060-1.

[117] A.C. Onuoha, X. Zu, J.F. Rusling, Electrochemical Generation and Reactions of Ferrylmyoglobins in Water and Microemulsions, J. Am. Chem. Soc. 119 (1997) 3979–3986. https://doi.org/10.1021/ja964007l.

[118] F.W. Scheller, N. Bistolas, S. Liu, M. Jänchen, M. Katterle, U. Wollenberger, Thirty years of haemoglobin electrochemistry, Adv. Colloid Interface Sci. 116 (2005) 111–120. https://doi.org/10.1016/j.cis.2005.05.006.

[119] Y. Yuan, X. Ni, Y. Cao, Electrochemical determination of hemoglobin on a magnetic electrode modified with chitosan based on electrocatalysis of oxygen, J. Electroanal. Chem. 837 (2019) 219–225. https://doi.org/10.1016/j.jelechem.2019.01.066.

[120] C. Cai, J. Chen, Direct electron transfer and bioelectrocatalysis of hemoglobin at a carbon nanotube electrode, Anal. Biochem. 325 (2004) 285–292. https://doi.org/10.1016/j.ab.2003.10.040.

[121] X. Ge, A. Sumboja, D. Wuu, T. An, B. Li, F.W.T. Goh, T.S.A. Hor, Y. Zong, Z. Liu, Oxygen Reduction in Alkaline Media: From Mechanisms to Recent Advances of Catalysts, ACS Catal. 5 (2015) 4643–4667. https://doi.org/10.1021/acscatal.5b00524.

[122] M. Rauf, Y. Zhao, Y. Wang, Y. Zheng, C. Chen, X. Yang, Z. Zhou, S. Sun, Insight into the different ORR catalytic activity of Fe/N/C between acidic and alkaline media: Protonation of pyridinic nitrogen SNW-Fe/N/C, Electrochem. Commun. 73 (2016) 71–74. https://doi.org/10.1016/j.elecom.2016.10.016.

[123] H. Yao, N. Li, J.Z. Xu, J.J. Zhu, Direct electrochemistry and electrocatalysis of hemoglobin in gelatine film modified glassy carbon electrode, Talanta. 71 (2007) 550–554. https://doi.org/10.1016/j.talanta.2006.04.025.

[124] X. Chen, C. Ruan, J. Kong, R. Yang, J. Deng, Direct Reduction of Oxyhemoglobin on a Bare Glassy Carbon Electrode, Electroanalysis. 10 (1998) 695–699. https://doi.org/10.1002/(SICI)1521-4109(199808)10:10<695::AID-ELAN695>3.0.CO;2-7.

[125] I.T. Ivanov, Low pH-induced hemolysis of erythrocytes is related to the entry of the acid into cytosole and oxidative stress on cellular membranes, Biochim.

Biophys. Acta - Biomembr. 1415 (1999) 349–360. https://doi.org/10.1016/S0005-2736(98)00202-8.

[126] J. Tom, P.J. Jakubec, H.A. Andreas, Enhanced hemoglobin electroactivity on carbon in electrolytes or binders containing water-miscible primary alcohols, Sensors Actuators, B Chem. 272 (2018) 425–432. https://doi.org/10.1016/j.snb.2018.05.164.

[127] L. Lee Hamm, N. Nakhoul, K.S. Hering-Smith, Acid-base homeostasis, Clin. J. Am. Soc. Nephrol. 10 (2015) 2232–2242. https://doi.org/10.2215/CJN.07400715.

[128] N. Laan, C. Compain, L. Seyve, B. Polack, C. Nicloux, F. Caton, The influence of coagulation on the drying dynamics of blood pools, Forensic Sci. Int. 305 (2019) 1–5. https://doi.org/10.1016/j.forsciint.2019.110008.

[129] F.R. Smith, D. Brutin, Wetting and spreading of human blood: Recent advances and applications, Curr. Opin. Colloid Interface Sci. 36 (2018) 78–83. https://doi.org/10.1016/j.cocis.2018.01.013.

[130] T. V Skiba, A.R. Tsygankova, N.S. Borisova, K.N. Narozhnykh, T. V Konovalova, O.I. Sebezhko, O.S. Korotkevich, V.L. Petukhov, L. V Osadchuk, Direct determination of copper, lead and cadmium in the whole bovine blood using thick film modified graphite electrodes, J. Pharm. Sci. Res. 9 (2017) 958–964.

[131] W. Xing, G. Yin, J.J. Zhang, Rotating Electrode Methods and Oxygen Reduction Electrocatalysis, Elsevier, Amsterdam, 2014.

[132] S. Treimer, A. Tang, D.C. Johnson, A consideration of the application of Koutecký-Levich plots in the diagnoses of charge-transfer mechanisms at rotated disk electrodes, Electroanalysis. 14 (2002) 165–171. https://doi.org/10.1002/1521-4109(200202)14:3<165::AID-ELAN165>3.0.CO;2-6.

[133] M. Lefèvre, E. Proietti, F. Jaouen, J.-P. Dodelet, Iron-Based Catalysts with Improved Oxygen Reduction Activity in Polymer Electrolyte Fuel Cells, Science. 324 (2009) 71–74. https://doi.org/10.1126/science.1170051

[134] W. Chen, J. Kim, S. Sun, S. Chen, Electrocatalytic Reduction of Oxygen by FePt Alloy Nanoparticles, J. Phys. Chem. 112 (2008) 1891–3898. https://doi.org/10.1021/jp7110204.

[135] G. Lu, H. Yang, Y. Zhu, T. Huggins, Z.J. Ren, Z. Liu, W. Zhang, Synthesis of a conjugated porous Co(II) porphyrinylene – ethynylene framework through alkyne metathesis and its catalytic activity study, J. Mater. Chem. A. 3 (2015) 4954–4959. https://doi.org/10.1039/c4ta06231k.

[136] R. Zhou, Y. Zheng, M. Jaroniec, S. Qiao, Determination of the Electron Transfer Number for the Oxygen Reduction Reaction: From Theory to Experiment, ACS Catal. 6 (2016) 4720–4728. https://doi.org/10.1021/acscatal.6b01581.

[137] U. Windberger, A. Bartholovitsch, R. Plasenzetti, K.J. Korak, G. Heinze, Whole blood viscosity, plasma viscosity and erythrocyte aggregation in nine mammalian species: Reference values and comparison of data, Exp. Physiol. 88 (2003) 431–

440. https://doi.org/10.1113/eph8802496.

[138] X. Min, Y. Chen, M.W. Kanan, Alkaline O2 Reduction on Oxide-Derived Au: High Activity and 4e Selectivity without (100) Facets, Phys. Chem. Chem. Phys. 16 (2014) 13601–13604. https://doi.org/10.1039/c4cp01337a.

[139] Y. Ayato, K. Sakurai, S. Fukunaga, T. Suganuma, K. Yamagiwa, H. Shiroishi, J. Kuwano, A simple biofuel cell cathode with human red blood cells as electrocatalysts for oxygen reduction reaction, Biosens. Bioelectron. 55 (2014) 14–18. https://doi.org/10.1016/j.bios.2013.11.063.

[140] R. Iqbal, A.Q. Shen, A.K. Sen, Understanding of the role of dilution on evaporative deposition patterns of blood droplets over hydrophilic and hydrophobic substrates, J. Colloid Interface Sci. 579 (2020) 541–550. https://doi.org/10.1016/j.jcis.2020.04.109.

[141] L. Lanotte, D. Laux, B. Charlot, M. Abkarian, Role of red cells and plasma composition on blood sessile droplet evaporation, Phys. Rev. 96 (2017) 1–8. https://doi.org/10.1103/PhysRevE.96.053114.

[142] M. Mukhopadhyay, R. Ray, M. Ayushman, P. Sood, M. Bhattacharyya, D. Sarkar, S. DasGupta, Interfacial energy driven distinctive pattern formation during the drying of blood droplets, J. Colloid Interface Sci. 573 (2020) 307–316. https://doi.org/10.1016/j.jcis.2020.04.008.

Appendices

Appendix A:

Figure A1: License for re-use for of figure 1.1, published by Zadora and Menżyk 2018.

Posting licensed content on Electronic reserve: In addition to the above the following clauses are applicable: The web site must be password-protected and made available only to bona fide students registered on a relevant course. This permission is granted for 1 year only. You may obtain a new license for future website posting.

17. **For journal authors:** the following clauses are applicable in addition to the above:

Preprints:

A preprint is an author's own write-up of research results and analysis, it has not been peer-reviewed, nor has it had any other value added to it by a publisher (such as formatting, copyright, technical enhancement etc.).

Authors can share their preprints anywhere at any time. Preprints should not be added to or enhanced in any way in order to appear more like, or to substitute for, the final versions of articles however authors can update their preprints on arXiv or RePEc with their Accepted Author Manuscript (see below).

If accepted for publication, we encourage authors to link from the preprint to their formal publication via its DOI. Millions of researchers have access to the formal publications on ScienceDirect, and so links will help users to find, access, cite and use the best available version. Please note that Cell Press, The Lancet and some society-owned have different preprint policies. Information on these policies is available on the journal homepage.

Accepted Author Manuscripts: An accepted author manuscript is the manuscript of an article that has been accepted for publication and which typically includes author-incorporated changes suggested during submission, peer review and editor-author communications.

Authors can share their accepted author manuscript:

- immediately
  - via their non-commercial person homepage or blog
  - by updating a preprint in arXiv or RePEc with the accepted manuscript
  - via their research institute or institutional repository for internal institutional uses or as part of an invitation-only research collaboration work-group
  - directly by providing copies to their students or to research collaborators for their personal use
  - for private scholarly sharing as part of an invitation-only work group on commercial sites with which Elsevier has an agreement
- After the embargo period
  - via non-commercial hosting platforms such as their institutional repository
  - via commercial sites with which Elsevier has an agreement

In all cases accepted manuscripts should:

- link to the formal publication via its DOI
- bear a CC-BY-NC-ND license - this is easy to do
- if aggregated with other manuscripts, for example in a repository or other site, be shared in alignment with our hosting policy not be added to or enhanced in any way to appear more like, or to substitute for, the published journal article.

Published journal article (JPA): A published journal article (PJA) is the definitive final record of published research that appears or will appear in the journal and embodies all

The author(s) must be appropriately credited and we ask that you include the end user license and a DOI link to the formal publication on ScienceDirect.

If any part of the material to be used (for example, figures) has appeared in our publication with credit or acknowledgement to another source it is the responsibility of the user to ensure their reuse complies with the terms and conditions determined by the rights holder.

Additional Terms & Conditions applicable to each Creative Commons user license:

CC BY: The CC-BY license allows users to copy, to create extracts, abstracts and new works from the Article, to alter and revise the Article and to make commercial use of the Article (including reuse and/or resale of the Article by commercial entities), provided the user gives appropriate credit (with a link to the formal publication through the relevant DOI), provides a link to the license, indicates if changes were made and the licensor is not represented as endorsing the use made of the work. The full details of the license are available at http://creativecommons.org/licenses/by/4.0.

CC BY NC SA: The CC BY-NC-SA license allows users to copy, to create extracts, abstracts and new works from the Article, to alter and revise the Article, provided this is not done for commercial purposes, and that the user gives appropriate credit (with a link to the formal publication through the relevant DOI), provides a link to the license, indicates if changes were made and the licensor is not represented as endorsing the use made of the work. Further, any new works must be made available on the same conditions. The full details of the license are available at http://creativecommons.org/licenses/by-nc-sa/4.0.

CC BY NC ND: The CC BY-NC-ND license allows users to copy and distribute the Article, provided this is not done for commercial purposes and further does not permit distribution of the Article if it is changed or edited in any way, and provided the user gives appropriate credit (with a link to the formal publication through the relevant DOI), provides a link to the license, and that the licensor is not represented as endorsing the use made of the work. The full details of the license are available at http://creativecommons.org/licenses/by-nc-nd/4.0. Any commercial reuse of Open Access articles published with a CC BY NC SA or CC BY NC ND license requires permission from Elsevier and will be subject to a fee.

Commercial reuse includes:

- Associating advertising with the full text of the Article
- Charging fees for document delivery or access
- Article aggregation
- Systematic distribution via e-mail lists or share buttons

Posting or linking by commercial companies for use by customers of those companies.

20. **Other Conditions**:

v1.10

Questions? customercare@copyright.com or +1-855-239-3415 (toll free in the US) or +1-978-646-2777.

value-adding publishing activities including peer review co-ordination, copy-editing, formatting, (if relevant) pagination and online enrichment.

Policies for sharing publishing journal articles differ for subscription and gold open access articles:

Subscription Articles: If you are an author, please share a link to your article rather than the full-text. Millions of researchers have access to the formal publications on ScienceDirect, and so links will help your users to find, access, cite, and use the best available version.

Theses and dissertations which contain embedded PJAs as part of the formal submission can be posted publicly by the awarding institution with DOI links back to the formal publications on ScienceDirect.

If you are affiliated with a library that subscribes to ScienceDirect you have additional private sharing rights for others' research accessed under that agreement. This includes use for classroom teaching and internal training at the institution (including use in course packs and courseware programs), and inclusion of the article for grant funding purposes.

Gold Open Access Articles: May be shared according to the author-selected end-user license and should contain a CrossMark logo, the end user license, and a DOI link to the formal publication on ScienceDirect.

Please refer to Elsevier's posting policy for further information.

18. **For book authors** the following clauses are applicable in addition to the above: Authors are permitted to place a brief summary of their work online only. You are not allowed to download and post the published electronic version of your chapter, nor may you scan the printed edition to create an electronic version. **Posting to a repository:** Authors are permitted to post a summary of their chapter only in their institution's repository.

19. **Thesis/Dissertation**: If your license is for use in a thesis/dissertation your thesis may be submitted to your institution in either print or electronic form. Should your thesis be published commercially, please reapply for permission. These requirements include permission for the Library and Archives of Canada to supply single copies, on demand, of the complete thesis and include permission for Proquest/UMI to supply single copies, on demand, of the complete thesis. Should your thesis be published commercially, please reapply for permission. Theses and dissertations which contain embedded PJAs as part of the formal submission can be posted publicly by the awarding institution with DOI links back to the formal publications on ScienceDirect.

Elsevier Open Access Terms and Conditions

You can publish open access with Elsevier in hundreds of open access journals or in nearly 2000 established subscription journals that support open access publishing. Permitted third party re-use of these open access articles is defined by the author's choice of Creative Commons user license. See our open access license policy for more information.

Terms & Conditions applicable to all Open Access articles published with Elsevier:

Any reuse of the article must not represent the author as endorsing the adaptation of the article nor should the article be modified in such a way as to damage the author's honour or reputation. If any changes have been made, such changes must be clearly indicated.

Figure A2: License for re-use for of figure 1.2, published by Zadora and Menżyk 2018.

ELSEVIER LICENSE
TERMS AND CONDITIONS

Aug 28, 2021

This Agreement between OntarioTech University -- Mitchell Tiessen ("You") and Elsevier ("Elsevier") consists of your license details and the terms and conditions provided by Elsevier and Copyright Clearance Center.

License Number	5137790461647
License date	Aug 28, 2021
Licensed Content Publisher	Elsevier
Licensed Content Publication	TrAC Trends in Analytical Chemistry
Licensed Content Title	In the pursuit of the holy grail of forensic science – Spectroscopic studies on the estimation of time since deposition of bloodstains
Licensed Content Author	Grzegorz Zadora,Alicja Menżyk
Licensed Content Date	Aug 1, 2018
Licensed Content Volume	105
Licensed Content Issue	n/a
Licensed Content Pages	29
Start Page	137
End Page	165

Type of Use	reuse in a thesis/dissertation
Portion	figures/tables/illustrations
Number of figures/tables/illustrations	2
Format	both print and electronic
Are you the author of this Elsevier article?	No
Will you be translating?	No
Title	Electrochemical characterization and forensic applications of blood films on glassy carbon electrodes
Institution name	OntarioTech University
Expected presentation date	Dec 2021
Portions	Figure 2, on page 140. Caption: "Pathway of ex vivo hemoglobin degradation."
Requestor Location	OntarioTech University 7 Pinewood Ave Grimsby, ON L3M 1W2 Canada Attn: OntarioTech University
Publisher Tax ID	GB 494 6272 12
Total	0.00 CAD

Terms and Conditions

INTRODUCTION

1. The publisher for this copyrighted material is Elsevier. By clicking "accept" in connection with completing this licensing transaction, you agree that the following terms and conditions apply to this transaction (along with the Billing and Payment terms and conditions established by Copyright Clearance Center, Inc. ("CCC"), at the time that you opened your Rightslink account and that are available at any time at http://myaccount.copyright.com).

GENERAL TERMS

2. Elsevier hereby grants you permission to reproduce the aforementioned material subject to the terms and conditions indicated.

3. Acknowledgement: If any part of the material to be used (for example, figures) has appeared in our publication with credit or acknowledgement to another source, permission must also be sought from that source. If such permission is not obtained then that material may not be included in your publication/copies. Suitable acknowledgement to the source must be made, either as a footnote or in a reference list at the end of your publication, as follows:

"Reprinted from Publication title, Vol /edition number, Author(s), Title of article / title of chapter, Pages No., Copyright (Year), with permission from Elsevier [OR APPLICABLE SOCIETY COPYRIGHT OWNER]." Also Lancet special credit - "Reprinted from The Lancet, Vol. number, Author(s), Title of article, Pages No., Copyright (Year), with permission from Elsevier."

4. Reproduction of this material is confined to the purpose and/or media for which permission is hereby given.

5. Altering/Modifying Material: Not Permitted. However figures and illustrations may be altered/adapted minimally to serve your work. Any other abbreviations, additions, deletions and/or any other alterations shall be made only with prior written authorization of Elsevier Ltd. (Please contact Elsevier's permissions helpdesk here). No modifications can be made to any Lancet figures/tables and they must be reproduced in full.

6. If the permission fee for the requested use of our material is waived in this instance, please be advised that your future requests for Elsevier materials may attract a fee.

7. Reservation of Rights: Publisher reserves all rights not specifically granted in the combination of (i) the license details provided by you and accepted in the course of this licensing transaction, (ii) these terms and conditions and (iii) CCC's Billing and Payment terms and conditions.

8. License Contingent Upon Payment: While you may exercise the rights licensed immediately upon issuance of the license at the end of the licensing process for the transaction, provided that you have disclosed complete and accurate details of your proposed use, no license is finally effective unless and until full payment is received from you (either by publisher or by CCC) as provided in CCC's Billing and Payment terms and conditions. If full payment is not received on a timely basis, then any license preliminarily granted shall be deemed automatically revoked and shall be void as if never granted. Further, in the event that you breach any of these terms and conditions or any of CCC's Billing and Payment terms and conditions, the license is automatically revoked and shall be void as if never granted. Use of materials as described in a revoked license, as well as any use of the materials beyond the scope of an unrevoked license, may constitute copyright infringement and publisher reserves the right to take any and all action to protect its copyright in the materials.

9. Warranties: Publisher makes no representations or warranties with respect to the licensed material.

10. Indemnity: You hereby indemnify and agree to hold harmless publisher and CCC, and their respective officers, directors, employees and agents, from and against any and all claims arising out of your use of the licensed material other than as specifically authorized pursuant to this license.

11. No Transfer of License: This license is personal to you and may not be sublicensed, assigned, or transferred by you to any other person without publisher's written permission.

12. No Amendment Except in Writing: This license may not be amended except in a writing signed by both parties (or, in the case of publisher, by CCC on publisher's behalf).

13. Objection to Contrary Terms: Publisher hereby objects to any terms contained in any purchase order, acknowledgment, check endorsement or other writing prepared by you, which terms are inconsistent with these terms and conditions or CCC's Billing and Payment terms and conditions. These terms and conditions, together with CCC's Billing and Payment terms and conditions (which are incorporated herein), comprise the entire agreement between you and publisher (and CCC) concerning this licensing transaction. In the event of any conflict between your obligations established by these terms and conditions and those established by CCC's Billing and Payment terms and conditions, these terms and conditions shall control.

14. Revocation: Elsevier or Copyright Clearance Center may deny the permissions described in this License at their sole discretion, for any reason or no reason, with a full refund payable to you. Notice of such denial will be made using the contact information provided by you. Failure to receive such notice will not alter or invalidate the denial. In no event will Elsevier or Copyright Clearance Center be responsible or liable for any costs, expenses or damage incurred by you as a result of a denial of your permission request, other than a refund of the amount(s) paid by you to Elsevier and/or Copyright Clearance Center for denied permissions.

LIMITED LICENSE

The following terms and conditions apply only to specific license types:

15. **Translation**: This permission is granted for non-exclusive world **English** rights only unless your license was granted for translation rights. If you licensed translation rights you may only translate this content into the languages you requested. A professional translator must perform all translations and reproduce the content word for word preserving the integrity of the article.

16. **Posting licensed content on any Website**: The following terms and conditions apply as follows: Licensing material from an Elsevier journal: All content posted to the web site must maintain the copyright information line on the bottom of each image; A hyper-text must be included to the Homepage of the journal from which you are licensing at http://www.sciencedirect.com/science/journal/xxxxx or the Elsevier homepage for books at http://www.elsevier.com; Central Storage: This license does not include permission for a scanned version of the material to be stored in a central repository such as that provided by Heron/XanEdu.

Licensing material from an Elsevier book: A hyper-text link must be included to the Elsevier homepage at http://www.elsevier.com . All content posted to the web site must maintain the copyright information line on the bottom of each image.

Posting licensed content on Electronic reserve: In addition to the above the following clauses are applicable: The web site must be password-protected and made available only to bona fide students registered on a relevant course. This permission is granted for 1 year only. You may obtain a new license for future website posting.

17. **For journal authors:** the following clauses are applicable in addition to the above:

Preprints:

A preprint is an author's own write-up of research results and analysis, it has not been peer-reviewed, nor has it had any other value added to it by a publisher (such as formatting, copyright, technical enhancement etc.).

Authors can share their preprints anywhere at any time. Preprints should not be added to or enhanced in any way in order to appear more like, or to substitute for, the final versions of articles however authors can update their preprints on arXiv or RePEc with their Accepted Author Manuscript (see below).

If accepted for publication, we encourage authors to link from the preprint to their formal publication via its DOI. Millions of researchers have access to the formal publications on ScienceDirect, and so links will help users to find, access, cite and use the best available version. Please note that Cell Press, The Lancet and some society-owned have different preprint policies. Information on these policies is available on the journal homepage.

Accepted Author Manuscripts: An accepted author manuscript is the manuscript of an article that has been accepted for publication and which typically includes author-incorporated changes suggested during submission, peer review and editor-author communications.

Authors can share their accepted author manuscript:

- immediately
  - via their non-commercial person homepage or blog
  - by updating a preprint in arXiv or RePEc with the accepted manuscript
  - via their research institute or institutional repository for internal institutional uses or as part of an invitation-only research collaboration work-group
  - directly by providing copies to their students or to research collaborators for their personal use
  - for private scholarly sharing as part of an invitation-only work group on commercial sites with which Elsevier has an agreement
- After the embargo period
  - via non-commercial hosting platforms such as their institutional repository
  - via commercial sites with which Elsevier has an agreement

In all cases accepted manuscripts should:

- link to the formal publication via its DOI
- bear a CC-BY-NC-ND license - this is easy to do
- if aggregated with other manuscripts, for example in a repository or other site, be shared in alignment with our hosting policy not be added to or enhanced in any way to appear more like, or to substitute for, the published journal article.

Published journal article (JPA): A published journal article (PJA) is the definitive final record of published research that appears or will appear in the journal and embodies all

The author(s) must be appropriately credited and we ask that you include the end user license and a DOI link to the formal publication on ScienceDirect.

If any part of the material to be used (for example, figures) has appeared in our publication with credit or acknowledgement to another source it is the responsibility of the user to ensure their reuse complies with the terms and conditions determined by the rights holder.

Additional Terms & Conditions applicable to each Creative Commons user license:

CC BY: The CC-BY license allows users to copy, to create extracts, abstracts and new works from the Article, to alter and revise the Article and to make commercial use of the Article (including reuse and/or resale of the Article by commercial entities), provided the user gives appropriate credit (with a link to the formal publication through the relevant DOI), provides a link to the license, indicates if changes were made and the licensor is not represented as endorsing the use made of the work. The full details of the license are available at http://creativecommons.org/licenses/by/4.0.

CC BY NC SA: The CC BY-NC-SA license allows users to copy, to create extracts, abstracts and new works from the Article, to alter and revise the Article, provided this is not done for commercial purposes, and that the user gives appropriate credit (with a link to the formal publication through the relevant DOI), provides a link to the license, indicates if changes were made and the licensor is not represented as endorsing the use made of the work. Further, any new works must be made available on the same conditions. The full details of the license are available at http://creativecommons.org/licenses/by-nc-sa/4.0.

CC BY NC ND: The CC BY-NC-ND license allows users to copy and distribute the Article, provided this is not done for commercial purposes and further does not permit distribution of the Article if it is changed or edited in any way, and provided the user gives appropriate credit (with a link to the formal publication through the relevant DOI), provides a link to the license, and that the licensor is not represented as endorsing the use made of the work. The full details of the license are available at http://creativecommons.org/licenses/by-nc-nd/4.0. Any commercial reuse of Open Access articles published with a CC BY NC SA or CC BY NC ND license requires permission from Elsevier and will be subject to a fee.

Commercial reuse includes:

- Associating advertising with the full text of the Article
- Charging fees for document delivery or access
- Article aggregation
- Systematic distribution via e-mail lists or share buttons

Posting or linking by commercial companies for use by customers of those companies.

20. **Other Conditions**:

v1.10

Questions? customercare@copyright.com or +1-855-239-3415 (toll free in the US) or +1-978-646-2777.

value-adding publishing activities including peer review co-ordination, copy-editing, formatting, (if relevant) pagination and online enrichment.

Policies for sharing publishing journal articles differ for subscription and gold open access articles:

Subscription Articles: If you are an author, please share a link to your article rather than the full-text. Millions of researchers have access to the formal publications on ScienceDirect, and so links will help your users to find, access, cite, and use the best available version.

Theses and dissertations which contain embedded PJAs as part of the formal submission can be posted publicly by the awarding institution with DOI links back to the formal publications on ScienceDirect.

If you are affiliated with a library that subscribes to ScienceDirect you have additional private sharing rights for others' research accessed under that agreement. This includes use for classroom teaching and internal training at the institution (including use in course packs and courseware programs), and inclusion of the article for grant funding purposes.

Gold Open Access Articles: May be shared according to the author-selected end-user license and should contain a CrossMark logo, the end user license, and a DOI link to the formal publication on ScienceDirect.

Please refer to Elsevier's posting policy for further information.

18. **For book authors** the following clauses are applicable in addition to the above: Authors are permitted to place a brief summary of their work online only. You are not allowed to download and post the published electronic version of your chapter, nor may you scan the printed edition to create an electronic version. **Posting to a repository:** Authors are permitted to post a summary of their chapter only in their institution's repository.

19. **Thesis/Dissertation**: If your license is for use in a thesis/dissertation your thesis may be submitted to your institution in either print or electronic form. Should your thesis be published commercially, please reapply for permission. These requirements include permission for the Library and Archives of Canada to supply single copies, on demand, of the complete thesis and include permission for Proquest/UMI to supply single copies, on demand, of the complete thesis. Should your thesis be published commercially, please reapply for permission. Theses and dissertations which contain embedded PJAs as part of the formal submission can be posted publicly by the awarding institution with DOI links back to the formal publications on ScienceDirect.

Elsevier Open Access Terms and Conditions

You can publish open access with Elsevier in hundreds of open access journals or in nearly 2000 established subscription journals that support open access publishing. Permitted third party re-use of these open access articles is defined by the author's choice of Creative Commons user license. See our open access license policy for more information.

Terms & Conditions applicable to all Open Access articles published with Elsevier:

Any reuse of the article must not represent the author as endorsing the adaptation of the article nor should the article be modified in such a way as to damage the author's honour or reputation. If any changes have been made, such changes must be clearly indicated.

Table A1: Summary of the results from the systematic literature review search strategy. Bolded numbers indicate retained articles from the searches containing the word 'forensic' that were included in this review.

Sr. No.	Search Strategy	PubMed		Scopus		Web of Science	
		Hits	Selected	Hits	Selected	Hits	Selected
1	Electrochemistry AND Whole Blood	186	7	205	12	58	9
2	Electrochemistry AND Red Blood Cells	67	4	115	7	28	8
3	Electrochemistry AND Arterial Blood	26	0	36	0	7	0
4	Cyclic Voltammetry AND Whole Blood	20	4	41	6	64	7
5	Cyclic Voltammetry AND Red Blood Cells	9	1	21	9	27	8
6	Cyclic Voltammetry AND Arterial Blood	2	0	2	0	4	1
7	Differential Pulse Voltammetry AND Whole Blood	19	8	45	7	52	9
8	Differential Pulse Voltammetry AND Red Blood Cells	2	1	2	1	7	1
9	Differential Pulse Voltammetry AND Arterial Blood	3	0	4	0	5	0
10	Potentiometry AND Whole Blood	50	2	151	13	38	2
11	Potentiometry AND Red Blood Cells	6	1	43	5	8	2
12	Potentiometry AND Arterial Blood	5	0	26	0	2	0
13	Electrochemistry AND Whole Blood AND Forensic	2	**0**	2	**0**	0	**0**
14	Electrochemistry AND Red Blood Cells AND Forensic	0	**0**	0	**0**	0	**0**
15	Electrochemistry AND Arterial Blood AND Forensic	0	**0**	0	**0**	0	**0**
16	Electrochemistry AND Blood AND Forensic	29	**1**	29	**2**	5	**0**

17	Electrochemistry AND Hemoglobin AND Forensic	1	**1**	2	**1**	0	**0**
18	Cyclic Voltammetry AND Hemoglobin AND Forensic	1	**0**	1	**0**	0	**0**
19	Differential Pulse Voltammetry AND Hemoglobin AND Forensic	0	**0**	0	**0**	0	**0**
20	Potentiometry AND Hemoglobin AND Forensic	0	**0**	0	**0**	0	**0**

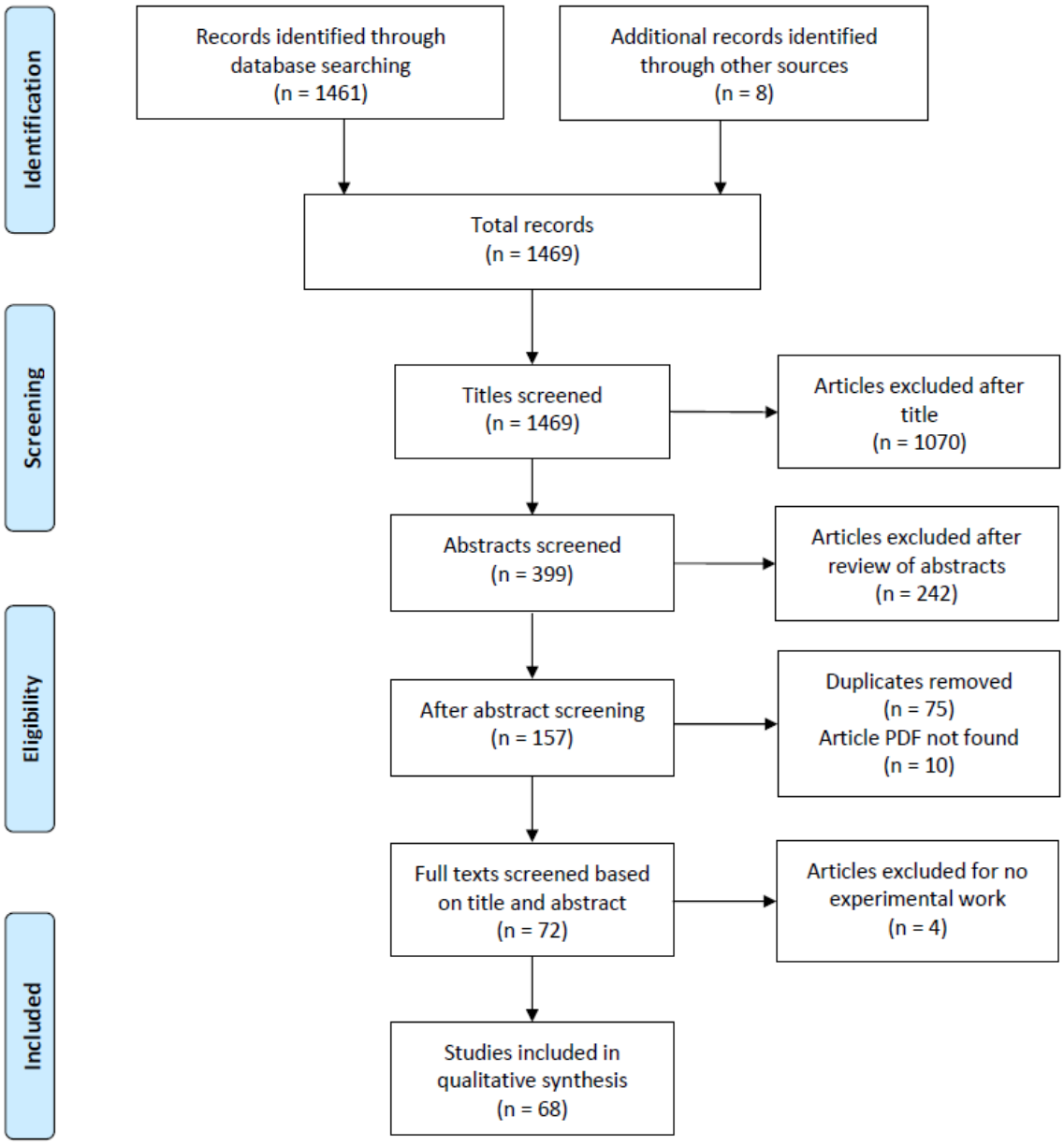

Figure A3: PRISMA flowchart for article inclusion.

Table A2: The following pages contain a summary of literature involving the electrochemical detection of blood from the systematic review. All 68 articles can be found in this table, with the blood source, electrochemical methods, electrode preparation steps, and a brief summary of results/findings. Abbreviations: CV – Cyclic voltammetry, DPV – Differential pulse voltammetry, LSV – Linear scan voltammetry, SWV – Square wave voltammetry, ASV – Anodic stripping voltammetry, EIS - Electrochemical impedance spectroscopy

Author (Year)	Starting Sample	Electrochemical method	Working Electrode	Analyte(s)	Review Category	Comments
Amayreh et al. (2019)	Whole human blood	CV	Iodine coated platinum electrode	Hb	Cells and Hb	Focusses on determining the concentration of Hb in clinical samples. Includes optimization and method validation for real-time blood analysis. Linear relationship between anodic peak signal and Hb concentration is reported. The voltammetric method is simple, fast, accurate, and can be developed to a hand-held device for determination of hemoglobin.
Amreen et al. (2016)	Whole human blood	CV	Glassy carbon electrode coated with graphitized mesoporous carbon	Hb	Cells and Hb	Focusses on developing a protocol for human blood disease diagnosis through electrochemical characterization of Hb redox peaks. Clinical and Biomedical application to real time monitoring of Hb in whole blood. High degree of linearity between Hb concentration and redox signals. Clear changes in Hb electroactivity between healthy and Hb-faulty blood samples.
Amreen et al. (2018)	Whole human blood	CV and LSV (rotating electrode)	Glassy carbon electrode coated with graphitized mesoporous carbon	Hb and H_2O_2	Cells and Hb	Studies the interaction between Hb in RBCs with H_2O_2. Demonstrate well define redox peaks when immobilizing whole blood on electrodes. Blood-modified electrode mediates the 2-electron reduction of dissolved H_2O_2 with common interference molecules not influencing redox characteristics.
Amreen et al. (2018)	Whole human blood	CV and LSV (rotating electrode)	Glassy carbon electrode coated with graphitized mesoporous carbon	Hb and oxygen	Cells and Hb	Studies the direct electrochemical reactions in blood related to the Hb-Fe(III)/Fe(II) redox system. Explores the interaction of Hb and oxygen in blood at physiological conditions, interested in direct electron transfers occurring between Hb and oxygen. Proposes reaction scheme where Hb catalyzes oxygen to water in 4 electron process.
Attar et al. (2013)	Diluted and decomposed whole blood	Adsorptive cathodic stripping voltammetry	Hanging mercury drop electrode	Copper	Metals	Applies established methods for copper (II) determination in digested blood samples to diluted blood. Reports a fast, simple analysis with a low detection limit (0.001 ng/mL) making it applicable to real blood samples in clinical setting. Reports significant improvements to LOD, linear dynamic range, and deposition time compared to alternative methods.
Ayato et al. (2014)	RBCs from human group AB treated with glutaraldehyde 4%(m/m), RBCs suspended in PBS and bovine hemoglobin	CV	Indium tin oxide electrode	Hb and oxygen	Cells and Hb	Reports a direct electron transform mechanism for oxygen reduction using RBCs on an electrode surface. Changes in scan rates show that electron transfer is dominated by surface-controlled electrode processes – RBC electrode adsorption. Proposed as an electrocatalysis for biofuels.

Aymerich et al. (2018)	Whole human blood	CV and chronoamperometry	Silicon substrate Lab-on-a-chip concept	Ethanol	Drugs	This work focusses on the determination of ethanol in blood samples for medical and law enforcement professionals using portable technologies. Develops a smart-phone based electrochemical method with specifications and architecture explained. Electrochemical current and ethanol concentration have linear relationship offering a sensitive, portable and fast *in situ* determination method.
Brainina et al. (1996)	Whole blood, pretreated whole blood, plasma, and erythrocyte mass	Differential pulse stripping voltammetry	Ultra-trace epoxy impregnated graphite electrode and disposable thick film graphite electrode	Copper, Lead, and Cadmium	Metals	This work focusses on the biofouling issues associated with whole blood analysis. Two electrodes were used for the quantitative analysis of copper, lead and cadmium in blood samples. All analytes could be determined on thick film graphite electrode without sample pretreatment and on ultra-trace electrode with sample pretreatment due to blood adsorbing onto the electrode surface.
Canovas et al. (2020)	Whole human blood	Electromotive force measurements	Platinized paper-based electrode with glucose oxidase entrapped between two layers of Aquivion	Glucose	Biomolecules	Presents a glucose biosensor using a designed polymer that enhances ion-exchange and enhances transport properties. Offers low cost glucose determination in whole blood samples in applicable range with no biofouling of electrodes. Possesses applications to environmental monitoring and security, early diagnosis, pharmaceutical and food industries.
Chen et al. (2005)	Whole human blood	SWV	Disposable screen-printed electrode in a 3-electrode configuration with carbon as the working and reference electrodes	Uric acid	Biomolecules	Research objective includes developing a sensitive detection method for uric acid in untreated whole blood. Showed stable uric acid oxidation peaks with little interferences from the blood matrix. Tested using clinical samples and results were consistent with clinical test procedures.
Chen et al. (2017)	10% whole blood mixed with Tris-H Buffer (pH 8.0)	DPV	Glassy carbon electrode	Salicylic acid and β-hydroxybutyrate	Biomolecules	Designed and characterized a latent redox substrate for monitoring salicylate hydroxylase activity. Specific and sensitive response to analytes of interest in blood samples, offering applications to real-time medical diagnosis of SA poisoning or diabetes related conditions.
Ci et al. (1998)	White rabbit blood with heparin anticoagulant, centrifuged and resuspended in PBS	CV	Graphite working electrode	Erythrocytes and leukocytes	Cells and Hb	Reports an irreversible redox process for erythrocytes and leukocytes, likely affected by cell membrane. The anodic wave has two peaks for erythrocytes (0.73 V) and leukocytes (0.32 V) (both vs. SCE). Demonstrates a successful application to detecting and quantifying pure erythrocytes and leukocytes.

Coon et al. (1998)	Whole human blood and blood serum	CV	Nickel electrode chemically modified with ferricyanide	Sodium and potassium ions	Biomolecules	Demonstrates a well-defined oxidation peak in whole blood samples, with intrinsic antifouling properties and free of biological anion interferences. Electrodes do show a short lifetime (8 assays) and research to develop electrode stability is encouraged. Presents possibilities of *in vivo* blood monitoring.
Dennouni-Medjati et al. (2012)	Pretreated whole human blood	Differential pulse cathodic stripping voltammetry	Hanging mercury drop electrode	Selenium	Metals	Assess the levels of selenium in whole blood samples from 300 people in four regions in Algeria. Uses previously described analysis methods and largely focusses on geographical interpretations of results.
Domenech-Carbo et al. (2016)	Whole blood from health and anemic patients	CV and SWV	Glassy carbon electrode and screen-printed electrode	Hb	Cells and Hb	Developed a direct method for detecting hemolysis in blood samples through the Hb-Fe voltammetric response, specifically in individuals with anemia. Healthy individuals did not show any changes in free heme over the 7 days, unlike patients with anemia. These different voltammetric signals are attributed to changes in transmembrane electrochemistry of erythrocytes. With the described methods the LOD of free Hb is 0.02 g/L in blood samples.
Fini et al. (2020)	Lyophilized human Hb and lyophilized sickle cell Hb	CV and DPV	Glassy carbon electrode	Nitrite	Cells and Hb	This is a comprehensive study on the nitrite reductase activity of Hb. Results shows that nitrite is reversible reduced by two Hb states – Fe(II) and Fe(III). Complete reaction mechanisms are proposed for the two systems. The developed biosensor was found to have high linearity, easy to produce, and time efficient for nitrite quantification.
Ho et al. (2018)	Whole human blood	Chronoamperometry	Platinum ultramicroelectrode (UME)	RBCs	Cells and Hb	Explores a electrochemical collision method with RBCs on UME to detect the number of RBCs and the size of RBCs with applications for anemia diagnosis. Concentration and size of RBCs was able to be determined with accuracy and precision based on collision events on the electrode surface. Demonstrates a simple procedure to diagnose different classifications of anemias in clinical samples.
Hoyer et al. (1987)	Whole human blood	ASV	Glassy carbon electrode	Lead	Metals	Focusses on the determination of trace metals in various biological fluids (lead in blood samples), particularly looking at the antifouling properties of the electrode coating and the minimal sample preparation required. Validate a more sensitive and easier method at the time for lead determination in whole blood using ASV. Dilution in acid causes the complete release of lead in the sample and removes interferences from the blood matrix.
Ilie et al. (2019)	Whole human blood	DPV	Modified graphite paste on a silver wire electrode	L-tryptophan	Biomolecules	Studies an assay for the determination of L-tryptophan (L-Trp), an essential amino acid, in PBS solution (pH=7.5) and whole blood samples. The average recovery of L-Trp in whole blood was 93.72% (N=5).

Inam et al. (1998)	Pretreated whole human blood	Differential pulse polarography	Hanging mercury drop electrode	Lead (II) and Selenium (IV)	Metals	Focusses on determining the concentrations of lead and selenium in synthetic samples and apply it to the determination of these trace metals in a blood sample after acid digestion. Polarograms of digested blood samples had peaks corresponding to lead ions, selenite, and most likely an intermetallic PbSe compound. Replicates of 5 digested blood samples from the same individual were used to calculate metal concentrations and was found to give reproducible results
Jain et al. (2016)	Whole blood samples from non-diabetic and diabetic patients	CV	Modified indium tin oxide glass plate electrode	Glycated hemoglobin (HbA1c)	Cells and Hb	Researchers develop an electrochemical biosensor for glycated Hb as it related to diabetic patient diagnosis. The modified working electrode showed fast response (3s), wide linear range (0.5-2000 mM), low detection limit (0.5 mM), good reproducibility (100 times), and long-term stability (4 months). The biosensor was tested with healthy and diabetic blood.
Khan et al. (2018)	Whole human blood	CV	Nano porous gold electrode	RBCs	Cells and Hb	This research explores the redox potential of packed RBCs over a 56-day storage period. Assessed large and small volume electrochemical analysis of RBCs and showed that RBCs redox potential shifts more positive over time. The addition of Vitamin C was added to stored samples in various concentrations to study its improvements to redox stability and storage duration.
Khan et al. (2019)	Packed RBC solution and RBC blood storage bag	CV	Flexible Nano porous gold or planar gold electrodes	Uric acid	Biomolecules	This work focusses on the fabrication of NPG electrodes for electrochemical sensing of complex matrices such as blood. High sensitivity and linear relationship between uric acid concentration and oxidation current across electrode replicates. Electrode is easy to fabricate, and is biocompatible making it applicable to study a wide range of biological samples.
Khandekor et al. (1987)	Pretreated whole human blood	Differential pulse ASV	Not specified	Lead, cadmium, zinc, and copper	Metals	Researchers wanted to study the concentration of metals in the population of the Greater Bombay area. Focusses on geographical/urbanization, and age of participants with respect to blood trace metal concentrations and compares with other studies done around the world.
Kong et al. (2014)	Whole human blood	DPV	Modified screen-printed carbon electrode	Glucose	Biomolecules	This research studies a paper-base, reagent-less glucose sensor that was successfully applied to whole blood. Found a strong linear relationship between glucose concentration in whole blood and DPV intensity. Peak potential shifted more positive in whole blood samples, likely due to the whole bloods buffer systems. This method is proposed for monitoring other analytes in blood including cholesterol and alcohol.
Li et al. (2013)	Whole human blood	Lab-on-a-CD system with	Modified gold working electrode	Glucose, uric acid, and lactate	Biomolecules	A proof-of-concept study that developed a simple Lab-on-a-CD system for whole blood analyte analysis, combining plasma separation and quantitative analysis on one platform. This method

		chronoamperometry measurements				is highly efficient in terms of time and reagents, and possesses the accuracy of conventional methods for each analyte tested. Changing the enzyme on the electrode allows this method to be adapted to other analytes in biological matrices.
Lin et al. (2015)	Whole human blood	DPV	Indium-tin oxide glass slide with carbon and transparent tape as the working electrode	Hb	Cells and Hb	This work Apply paper-based electroanalytical sensing methods to study the breathing of RBCs in oxygen and nitrogen rich environments. When nitrogen was added the reduction current decreased and with oxygen added the reduction current increases. The electrochemical signal is attributed to oxyhemoglobin reduction. Cycling between oxygen and nitrogen saw a decrease in reduction current likely due to the formation of oxygen radical species.
Liu et al. (2006)	Pure Hemoglobin samples and clinical blood samples	CV and flow injection analysis-electrochemically determination	Glassy carbon electrode and PCQDs chemically modified electrode	Hb	Cells and Hb	Explore the electron transfer characteristics of hemoglobin using quantum dot chemically modified electrodes. Chemically modified electrode had good biocompatibility and reduction responses were seen for Hb. The LOD of detection reported is: 5.0×10^{-9} M. flow injection analysis was used to show the biosensor has high sensitivity, stability and working life.
Liu et al. (2016)	PBS and whole blood samples spiked with glucose	Amperometry	Carbon coating polyester thread electrode	Glucose and lactate	Biomolecules	This work develops an electrochemical sensor fabricated on conductive threads that can be built into 2D arrays while maintaining structural integrity. Embroidered thread electrodes proved to be provided high linear responses for both analytes in PBS and whole blood with low background noise from complex samples. The electrodes-maintained accuracy after several bending cycles and were shows to be appropriate when sewn into fabric.
Liu et al. (2016)	Bovine hemoglobin encapsulated in long chain fatty acids grafted starch (GS-Hb)	CV, amperometric measurements and EIS	Chitosan-coated glassy carbon electrode	Hb and Oxygen	Cells and Hb	Develop an oxygen biosensor using grafted starch and hemoglobin for improving the performance of mediator-free biosensors in medical fields. Found that encapsulated hemoglobin retained its chemical structure and bioactivity, exhibiting fast electrode transfer. Demonstrates high oxyegn carrying capacity with reversible binding making it applicable for transfusions.
Luo et al. (2008)	Centrifuged blood samples diluted in PBS	CV and chronoamperometry	Meldola's blue modified screen printed electrode with immobilized alcohol dehydrogenase	Ethanol	Drugs	Develops a biosensor using alcohol dehydrogenase for blood alcohol determination. This method eliminates laborious sample pretreatment and has low interferences from other electrochemical active components within blood serum. Biosensor has good precision, accuracy, and stability. Article offers manufacturing and optimization steps for SPE.
Matsuoka et al. (2019)	Whole human blood	Polarographic oxygen analyzer	Oxygen electrode	oxyhemoglobin and	Cells and Hb	Focusses on determining the age of bloodstains by measuring the percentage of oxyhemoglobin to the total hemoglobin in

				deoxyhemoglobin in bloodstains		bloodstains. Shows aging curves for bloodstains aged up to 216 hours, demonstrating the change in fractional HbO_2 over time with a rapid decay in the early time points followed by slow degradation past the 10-hour mark.
Matysiak et al. (2015)	Human Hb and hemolyzed human blood	CV, LSV, and electrochemical quartz microbalance measurements	Gold electrode consisting of quartz crystal resonator covered by carbon layer	Hb	Cells and Hb	Develop a reliable, fast, and simple method of the direct electrochemical determination of hemoglobin in human blood samples. Reports 0.7 pM as the limit for Hb detection and quantification. The complexity of the blood matrix slows electrode-reaction rate, and increases reduction potentials but does not change their intensity.
Moldoveanu et al. (2014)	Whole human blood (individuals with and without HER-1 growth factor)	DPV and Stochastic chronoamperometric technique	Three electrode pasts tested: maltodextrin (MD)/C60 fullrene, MD/graphite, and Mn(III)P/diamond paste	HER-1	Biomolecules	Develop a new molecular screening method based on multimode sensing for identification and quantification of HER-1 in whole blood samples and propose this method for early detection of cancers. This method has quick analysis time, requires low samples and each of the electrode modifications and quantify low concentrations of HER-1 (280 fg/ml to 4.86 ng/ml). MD/C60 and Mn(III)P/DA pastes had the highest sensitivity for the stochastic and DPV method respectively.
Nicolai et al. (2017)	Blood collected from anesthetized swine and heparinized, spiked with norepinephrine	Fast scan CV	Carbon fiber microelectrode	Norepinephrine	Biomolecules	This work contributes to the development of *in vivo* biosensors to measure central nervous system biomolecules such as norepinephrine. Tested analyte detection in saline buffer solution and compared to whole blood measurements. Biofouling was found to drastically reduce sensitivity both immediately and over time but redox peaks were still overaerate.
Novell et al. (2014)	Blood and serum samples	Electromotive force potentiometry	Paper based lithium ion selective electrode	Lithium	Metals	Presents a novel approach for lithium monitoring in blood outside of the lab. Details electrochemical method construction and method validation. Results were comparable to traditional AES methods and were found not to be influenced by the blood matrix or other drugs in samples. The system requires one drop of whole blood and offers fast results for lithium determination.
Ogunlesi et al. (2009)	Whole human blood samples for known hemoglobin phenotypes	CV	Glassy carbon electrode	Hb phenotypes A, S, AS, and AC	Cells and Hb	This work focusses on characterizing the electrochemical nature of Hb and oxygen for the discrimination of Hb phenotypes. Minimal sample treatment is preformed and differences in peak current for four Hb phenotypes are reported at fixed concentrations. Applied a bind study with 20 samples of undisclosed Hb phenotypes and phenotypes were assigned with 100% accuracy.
Okochi et al. (1999)	Whole human blood	CV	Gold array microelectrode	Serotonin as allergen chemical mediator	Biomolecules	This work developed an allergen sensor using electrochemical detection methods for 20 µL whole blood samples. Blood samples exposed to cedar pollen allergen show an increase in current at 350 mV (vs Ag/AgCl) attributed to serotonin release and the

						levels of antibody immunoglobin E were measured to confirm allergic symptoms.
Ostapczuk (1992)	Whole human blood	Potentiometric stripping analysis	Mercury plated glassy carbon electrode	Lead and Cadmium	Metals	Determination of lead and cadmium in whole blood samples with simple pretreatment steps. Analysis method has no background interference form organic electroactive sample components. Lead and cadmium levels could be detected simultaneously with the detection limit changing based on deposition time and volume of blood. For 1 mL of blood with 1-minute deposition time the LOD was 1 μg/L for both elements.
Pan et al. (2014)	Human RBCs	CV, EIS, and amperometry	Chitosan-coated glassy carbon electrode	Hb and H_2O_2	Cells and Hb	This work focusses on the development of high-performance hydrogen peroxide biosensors using hydrogel-like materials. high stability and analytical accuracy for hydrogen peroxide quantification. This biosensor benefits for the membrane porosity and conductivity it also has low LOD (0.055×10^{-6} M). Oxygen is noted as the only significant interference.
Park et al. (2012)	Whole blood and serum from healthy individuals spiked with glucose	Amperometry	Coated Nano porous platinum thin film on platinum wire electrode	Glucose	Biomolecules	This article describes the first nonenzymatic electrochemical glucose sensor in whole human blood and serum. This method offers several advantages to traditional enzyme-based glucose sensor including better quality control, prolonged shelf life and the ability to be sterilized. Demonstrated that the sensor works for up to a month and does not loose sensitivity, offers advances to in vivo continuous glucose monitoring.
Popa-Tudor et al. (2019)	Human blood spiked dilute zinc solution	DPV	Graphite past modified with 2,6-bis(thiophen-3-yl)-4-(4,6,8-trimethylazulen-1-yl) pyridine	Zinc	Metals	This work proposes an electrochemical sensor for zinc ions in whole blood samples. High linearity, with high accuracy and precision reported for zinc quantification in whole blood. Reports LOD of 1.26×10^{-6} M. No interference from other cations.
Qu et al. (2009)	Whole blood samples. Hemoglobin and glycated hemoglobin (HbA1c)	Ion sensitive field-effect transistors (ISFET) differential voltage measurements	Antibody immobilization onto micro-gold electrodes	Hemoglobin and Glycated Hemoglobin	Cells and Hb	This work proposes an electrochemical sensor for simultaneous determination of hemoglobin and glycated hemoglobin in clinical whole blood samples. For whole blood samples a linear range for Hb concentrations were 125-197 μg/mL. Further improvements in reproducibility and stability of electrode surface characteristics are required but this research shows clinical applications to this biosensor.
Raghunath et al. (2002)	Whole blood samples (n =35) and serum samples (n = 201) from healthy adults	Differential pulse cathodic stripping voltammetry	Static mercury drop electrode	Selenium	Metals	This work focusses on the determination of selenium in a variety of biological samples of adults in the Mumbai population. This work quantifies the level of selenium in whole blood samples with an average of 99.6 ng/mL. Geographical interpretations are given based off of results obtained.

Rastogi et al. (2011)	Whole blood samples, red blood cells, lyophilized Hb and serum samples	CV	Single walled carbon nanotubes (SWNTs) ropes on indium tin oxide (ITO) working electrode	Hb	Cells and Hb	This work focusses on devising an efficient, quick, and sensitive biosensor for hemoglobin through the electrochemical reaction of the central iron atom. Pure hemoglobin samples had high linearity with the cathodic peak current. When applied to whole blood, RBCs, and serum only the RBC sample showed linear behaviour to cathodic peak current. Found that 91.5% of Hb was participating in the reaction. Not a completely reversible reaction but significantly increase electron transfer rate of Hb in solution.
Safavi et al. (2008)	Hemoglobin from bovine blood	CV	Carbon ionic liquid working electrode	Hb	Cells and Hb	This work investigates the application of ionic liquids to study the electrochemistry and electrocatalytic activity of Hb. Ionic liquids improved Hb immobilization and found the iron redox reaction to be completely reversible. The Hb modified electrode was also sensitive to oxygen, hydrogen peroxide, and nitrite reduction
Sepunaru et al. (2016)	Sheep red blood cells	CV and Chronoamperometry	Edge-plane pyrolytic graphite or carbon fiber working electrodes	RBCs	Cells and Hb	This work focusses on the counting of RBCs through the detection of oxygen and hydrogen peroxide reduction by Hb. Found that a solution with an unknown cell count can be drop cast onto an electrode and the magnitude of oxygen reduction can be use to determine the cell count with high accuracy.
Shulka et al. (2019)	Whole blood and serum	DPV	Chitosan-carbon nanotube modified titanium/gold microelectrode	Clozapine	Drugs	This work enables the rapid and minimally invasive detection of antipsychotic drug clozapine in whole blood and serum for point-of-care analysis. The modified electrodes showed redox capabilities of clozapine in all samples with a better LOD in serum compared to whole blood but still within the clinical range. Presents a fast, simple and sensitive sensor with reproducible electrochemical signals and high stability.
Skiba et al. (2017)	Whole and mineralized bovine blood with EDTA	ASV	Thick film modified graphite electrode	Copper, Lead, and Cadmium	Metals	This article describes a direct and rapid analysis approach for metals in whole bovine blood. Under specific circumstances the metal concentrations could be determined simultaneously but in low cadmium samples, separate copper determination must be separate. No significant difference was determined between the mineralized and whole blood sample metal determination.
Sokolov et al. (2017)	Pure Hb	CV	Glassy carbon electrode	Hb and oxygen	Cells and Hb	This work focusses on understanding the oxygen reduction reaction mechanism through immobilized Hb on an electrode surface. Found this to be a four-electron process, creating H_2O_2, and that Nafion increased catalytic activity. Changes in Hb concentrations, Nafion thickness, the effects of scan rate, dissolved oxygen and dissolved hydrogen peroxide are discussed.
Soleymani et al. (2017)	Whole blood and serum samples, diluted in	CV and DPV	Poly-arginine fabricated glassy carbon electrode	Doxorubicin	Drugs	This research develops a one-step electrodeposition method for doxorubicin in whole blood, cell lysate and untreated-plasma samples. The simplicity, fast electron transport, high repeatability and low limit of quantification (0.1 nM) make this method

	electrolyte solution					desirable for real samples. Highlights method for electrochemical analysis in complex biological samples.
Sun et al. (2013)	Whole human blood samples	DPV	Glassy carbon electrode modified with glucose oxidase	Glucose	Biomolecules	Focusses on the development of a glucose biosensor in whole blood that eliminates biofouling and other problems associated with blood analysis. Discusses optimization including pH change, scan rate, and concentrations of glucose oxidase and PU-F127. Applied to whole blood the senor had a low detection limit of 1.14×10^{-5} M.
Sun et al. (2013)	Whole human blood samples	DPV	Glassy carbon electrode modified with glucose oxidase	Glucose	Biomolecules	This work investigates the use of carboxymethyl- PEG-carboxymethyl biomaterial film on electrodes for glucose determination in whole blood samples. The biosensor was found to be electrochemically active and have a low LOD (1.24×10^{-5} M), high linearity for glucose and no associated biofouling in whole blood samples. The senor was tested with blood samples from a hospital with accurate results.
Thuerlemann et al. (2009)	Whole human blood (diluted)	Chronoamperometry	Single used microelectrode test strips	Thrombin	Biomolecules	Develops a new biosensor for the electrochemical detection of thrombin in plasma and whole blood samples as low as 10 µL. Increasing thrombin concentrations gave standard curves with increasing current, however peak shape and area under the curve is not fully understood at this time.
Toh et al. (2014)	Lyophilized hemoglobin, dry powder glutaraldehyde treated sheep RBCs, Lyophilized human whole blood, and live human RBCs	CV	Glassy carbon electrode	Hb	Cells and Hb	A simple protocol for the immobilization of RBCs on glassy carbon electrodes is presented. Good reproducibility is achieved with comparable results to live RBCs and lyophilized RBCs. Discusses optimization of electrochemical analysis and the effects of changing RBC/Hb concentrations. Discusses Hb reaction mechanisms, peak attributions and the effects of sample matrix on electrochemical analysis.
Toh et al. (2014)	Hemoglobin in the form of lyophilized powder from human blood	CV and DPV	Carbon nanomaterial working electrodes	Hb	Cells and Hb	This work focusses on the optimization of carbon-based electrodes for hemoglobin detection in solution by assessing 6 different electrode materials. This research studies the iron redox reactions of human Hb dissolved in the supporting electrolyte with the bare glassy carbon electrode had the superior performance for the electrochemical sensing of hemoglobin in solution.
Tom et al. (2018)	Hemoglobin in the form of lyophilized	DPV	Glassy carbon working electrode	Hb	Cells and Hb	This study focusses on the influence of alcohol exposure on Hb electrochemistry on carbon electrodes. The type of Nafion used to immobilize Hb strongly impacted the Hb electrochemistry. The

	powder from bovine blood					addition of primary alcohols increases Hb electroactivity, likely by modifying the Hb structure and accessibility to active sites.
Vacek et al. (2004)	Whole human blood	CV, DPV, SWV, and constant current chronopotentiometry stripping analysis	Hanging drop mercury electrode	3-azido-3-deoxythymidine (AZT)	Drugs	This work develops a simple and fast electrochemical detection method for AZT in biological samples and study the effects of ssDNA and albumin on electrochemical signal. Confirms AZT undergoes irreversible redox reduction with no anodic peak, SWV had the most sensitive results and was used for whole blood, urine, and serum analysis. Determined to be a rapid and simple analysis without sample preparations. ssDNA and BSA did not affect results due to different reduction potentials.
Viksna et al. (1997)	Pretreated whole blood samples	Stripping potentiometry	Glassy carbon electrode	Lead and Cadmium	Metals	This work focusses on the quantification of lead and cadmium in mothers and their babies' blood from Swedish and Polish populations. Compares electrochemical results with graphite furnace atomic adsorption spectrometry and found the methods recorded similar results. The study focusses on the geographical interpretations of the data.
Wang et al. (2010)	Whole human blood (RBCs centrifuged and resuspended)	EIS, CV, and amperometric measurements	Gold colloid-Cysteamine modified silver electrode	Hb and oxygen	Cells and Hb	This work focusses on studying the oxygen carrying ability of RBCs. RBCs containing hemoglobin were successfully immobilized on electrodes to study the reduction of oxygen. It was found that RBCs immobilized on the interface were able to store and carry oxygen for longer compared to normal RBCs
Wang et al. (2016)	Whole human blood	DPV	Screen printed carbon electrode	Leukocytes	Cells and Hb	This aim of this work was to develop and evaluate a method to identify hematologic malignancies and solid tumors based on leukocyte electrochemical characteristics. Differences in electrochemical peak shape and peak potential are seen across the healthy, hematologic malignancies, and solid tumor groups. Recommends further research for clinical applications
Wang et al. (2001)	Pure Hb	Cyclic and SWV	Pyrolytic graphite disk electrode	Hb	Cells and Hb	Explores electrochemical behaviour of Hb immobilized in layers on a graphite disk electrode with applications to biosensors and bioreactors. Demonstrate strong dependence on buffer pH for Hb redox reactions. Films in buffers at pH 5.5 showed symmetric and roughly equal reduction and oxidation peaks.
Xu et al. (2008)	Whole human blood, pure hemoglobin samples, and blood from grass carp and *Carassius auratus*	CV	Glassy carbon electrode	Hb, H_2O_2 and nitrite (NO_2^-)	Cells and Hb	This work explores the direct electron transfer characteristics of Hb in a variety of blood related samples. Reports that whole blood retains the ability to reduce hydrogen dioxide and nitrite on the electrode surface. Among the first research to present direct Hb electrochemical behaviour in blood deposited on a GCE. Show that the RBCs in whole blood maintain structure and have reversible redox reactions attributed to iron(II)/iron(III) couple.

Xu et al. (2011)	Hemoglobin from bovine blood	CV and chronoamperometry	Gold disk electrode with Hb entrapped in graphene–ZnO nanosphere	Hb and H_2O_2	Cells and Hb	This work focusses on establishing a biocompatible composite to study the catalytic reduction of hydrogen peroxide with Hb. Quasi-reversible iron redox peaks were observed, and the biosensor had excellent sensitivity and reproducibility for hydrogen peroxide sensing. A wide linear range, low detection limit, fast response and good long-term stability make it a good biosensor for biocatalysis.
Xu et al. (2010)	Hemoglobin from bovine blood	Cyclic voltammetric experiments and EIS	Hb entrapped in graphene-chitosan composite film modified glassy carbon electrode	Hb and H_2O_2	Cells and Hb	focusses on developing an effective biosensor for Hb by providing a favorable microenvironment for immobilization and electron transport. Concluded Hb entrapped in graphene-chitosan film retained native structure and enhanced the effective acceleration of electron transfers between the matrix and Hb. Demonstrates capabilities of being an effective biosensor for hydrogen peroxide
Yu et al. (2014)	Whole human blood centrifuged and RBC layer diluted	CV, amperometric measurements and EIS	Glassy carbon electrode with chitosan film	Hb and oxygen	Cells and Hb	Focusses on studying the electrochemical activity of Hb in RBCs. Details the coupled Hb and ORR reaction mechanism and highlights the direct electron transfer within RBCs on the electrode surface. RBCs maintained electrochemical activity compared to pure Hb samples and could be used to determine H_2O_2 concentration to a limit of 0.085 μM.
Yuan et al. (2019)	Pure hemoglobin and whole human blood	CV, DPV, and EIS	Chitosan magnetic glassy carbon electrode	Hb	Cells and Hb	Develops a simple biosensor for Hb that can be applied to clinical samples with a limit of detection of 0.01 μg/mL. Can be applied to diluted whole blood samples. Method is described as simple, robust, and reproducible method for Hb determination and found an increase of 13.7% with the magnetic electrode due to the paramagnetic properties of Hb and oxygen.
Zhou et al. (2015)	Whole human blood samples	DPV	Modified glassy carbon electrode	Glycated hemoglobin (HbA1c)	Cells and Hb	This study focusses on the development of a glycated hemoglobin biosensor that is applicable to clinical whole blood samples where limited pretreatment is needed. Found linear response between glycated hemoglobin percentage and measured current for real blood samples in the appropriate clinical range (9.4–65.8 μg/mL).

Appendix B:

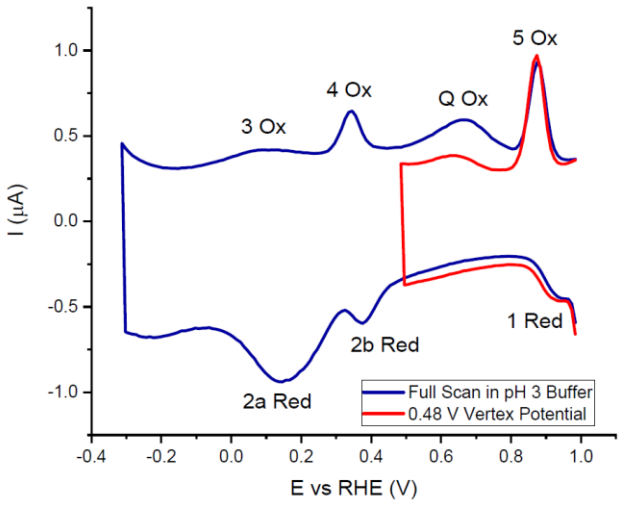

Figure B1: DPV of Naf/Blood/Naf film in pH 3 buffer. The blue trace is the full scan and the red trace is with the vertex potential of 0.48 V vs RHE. This was used to characterize the Q Ox peak.

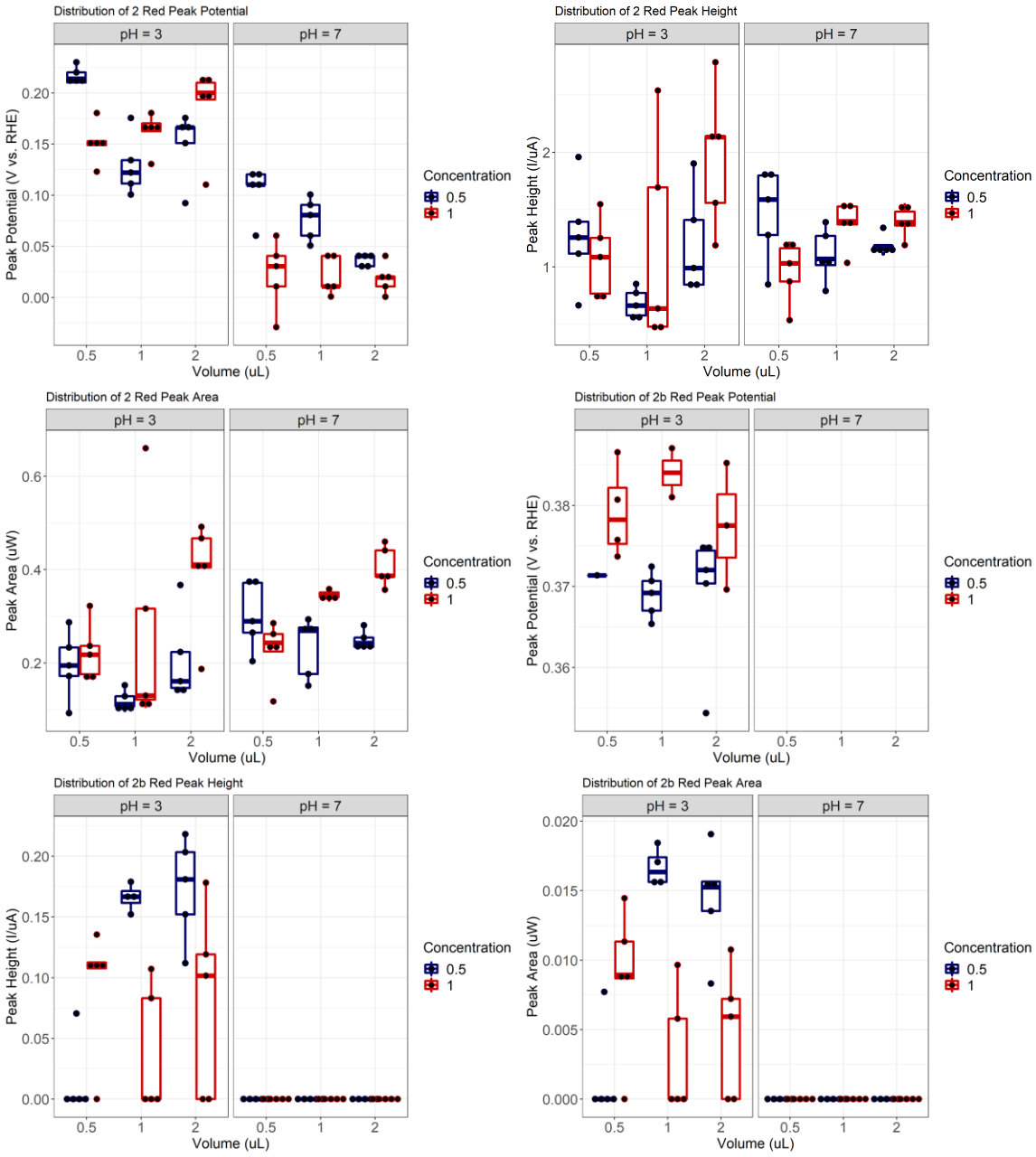
Distribution of 2 Red Peak Potential
pH = 3
pH = 7
Peak Potential (V vs. RHE)
0.20
0.15
0.10
0.05
0.00
0.5
1
2
Volume (uL)
Concentration
0.5
1
Distribution of 2 Red Peak Height
Peak Height (I/uA)
2
1
Distribution of 2 Red Peak Area
Peak Area (uW)
0.6
0.4
0.2
Distribution of 2b Red Peak Potential
0.38
0.37
0.36
Distribution of 2b Red Peak Height
Distribution of 2b Red Peak Area
0.020
0.015
0.010
0.005
0.000

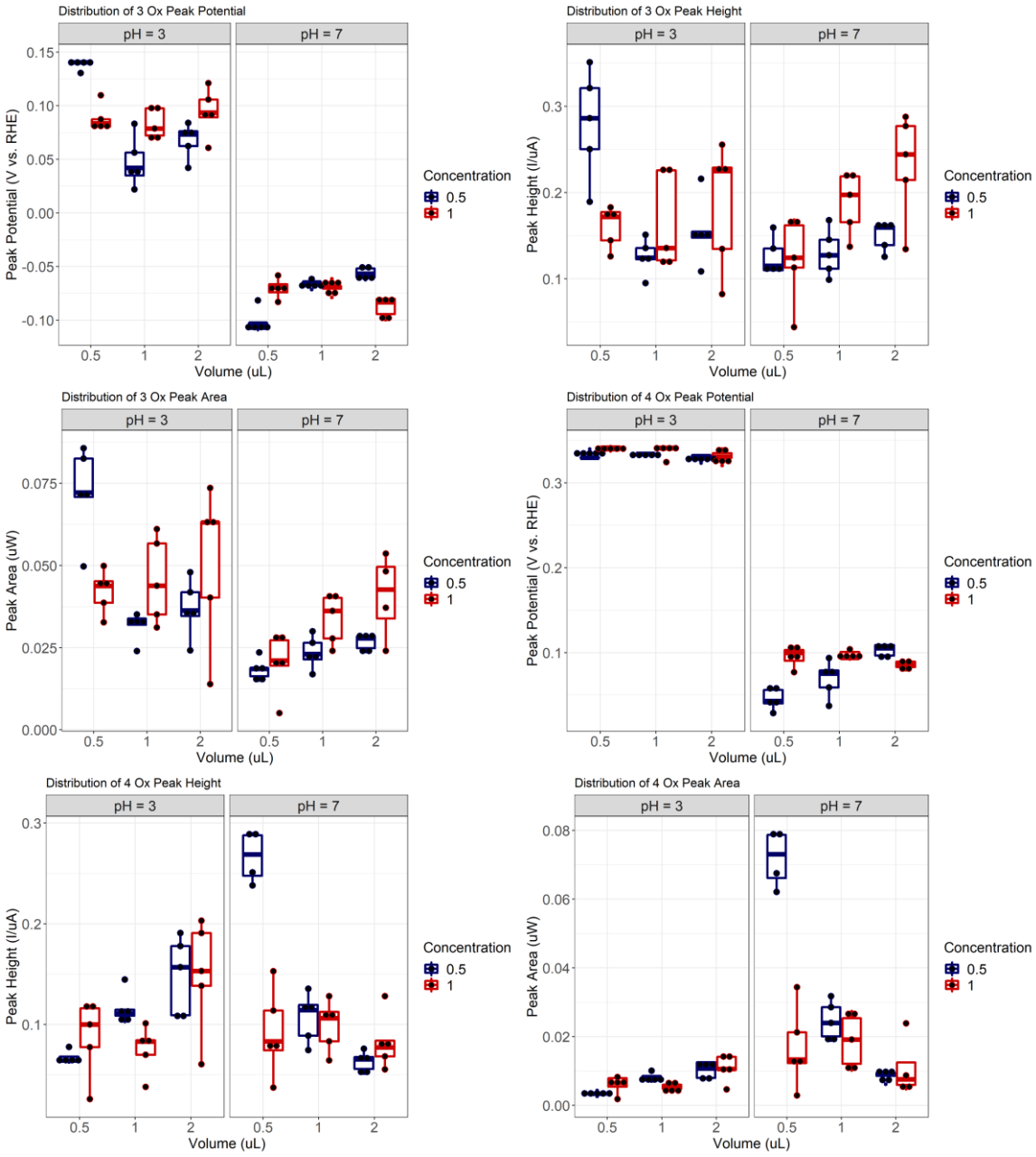
Distribution of 3 Ox Peak Potential
pH = 3
pH = 7
Peak Potential (V vs. RHE)
0.15
0.10
0.05
0.00
-0.05
-0.10
0.5
1
2
Volume (uL)
Concentration
0.5
1
Distribution of 3 Ox Peak Height
Peak Height (I/uA)
0.3
0.2
0.1
Distribution of 3 Ox Peak Area
Peak Area (uW)
0.075
0.050
0.025
0.000
Distribution of 4 Ox Peak Potential
Distribution of 4 Ox Peak Height
Distribution of 4 Ox Peak Area
0.08
0.06
0.04
0.02
0.00

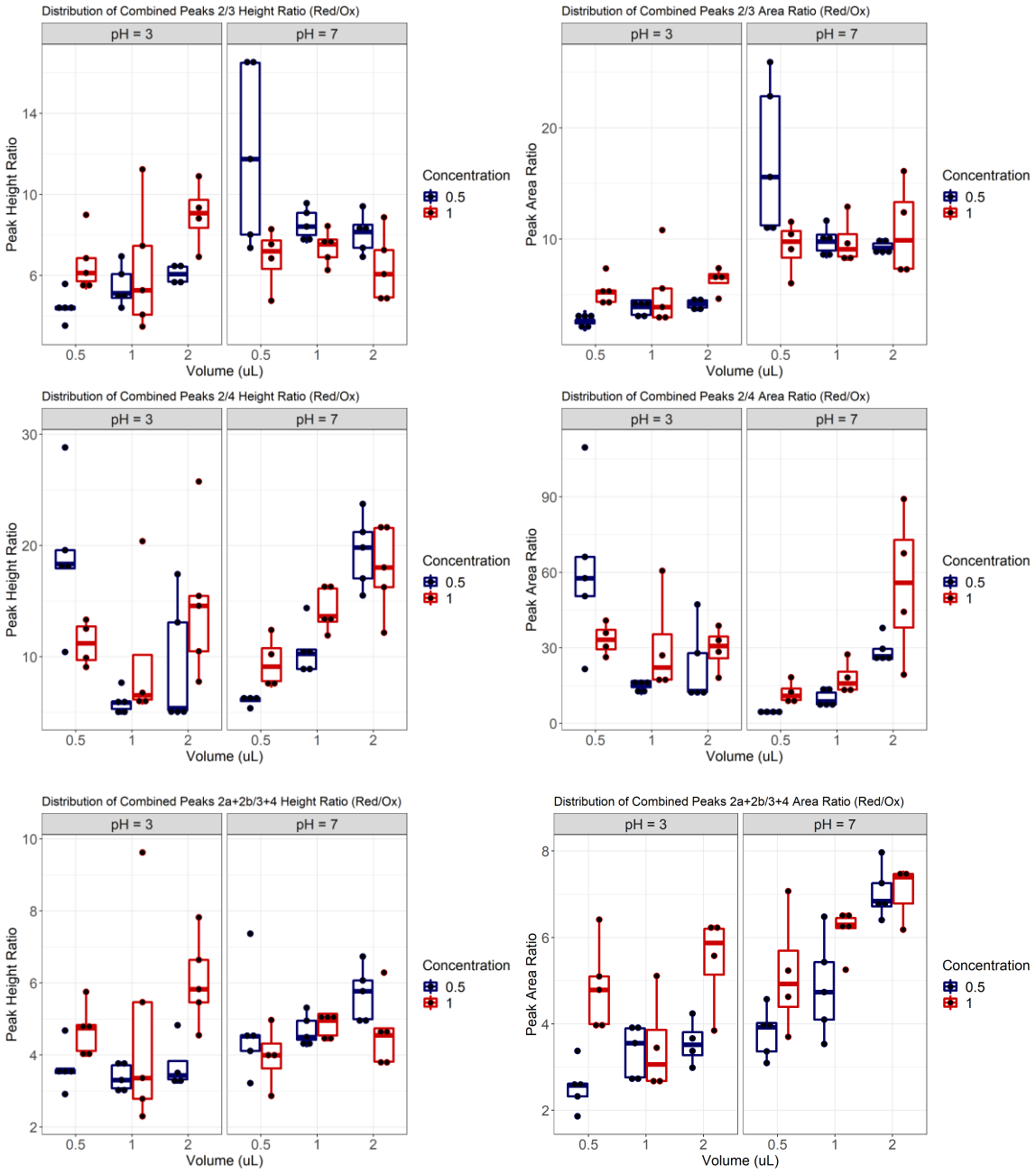

Figure B2: Distribution boxplots for the Hb related peaks in the factorial design experiment. Included here are the peak potenial (V), height (μA) and area (μW) for the 2a Red, 2b Red, 3 Ox, and 4 Ox peaks. Also included are the peak height and area ratios for the 2a Red/3 Ox, 2a Red/4 Ox and combined 2 Red/3+4 Ox peaks.

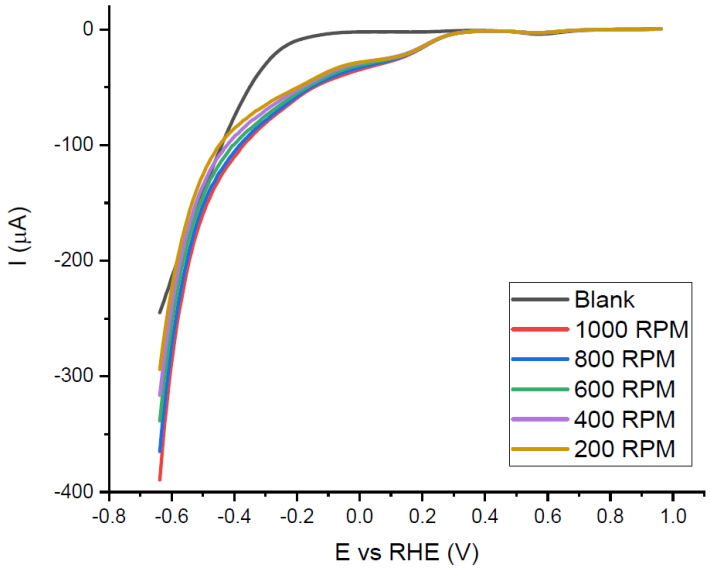

Figure B3: LSV scans of Naf/Blood/Naf film on GC-RDE in 0.1 M H_2SO_4 buffer (pH = 1.25) with different RPM (50-1000), purging gas O_2.

Appendix C:

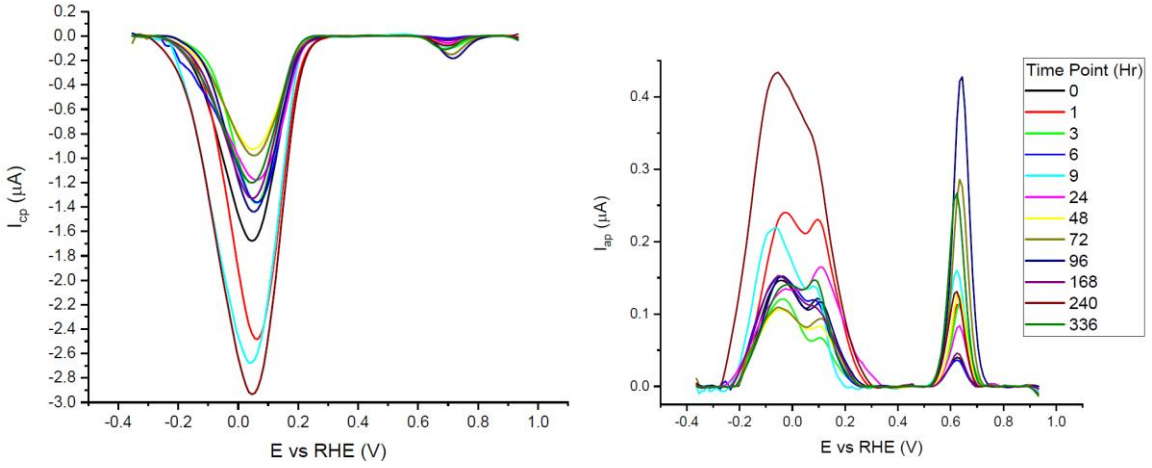

Figure C1: DPVs of reduction and oxidation sweeps of laboratory conditons time series (Replicate 2)

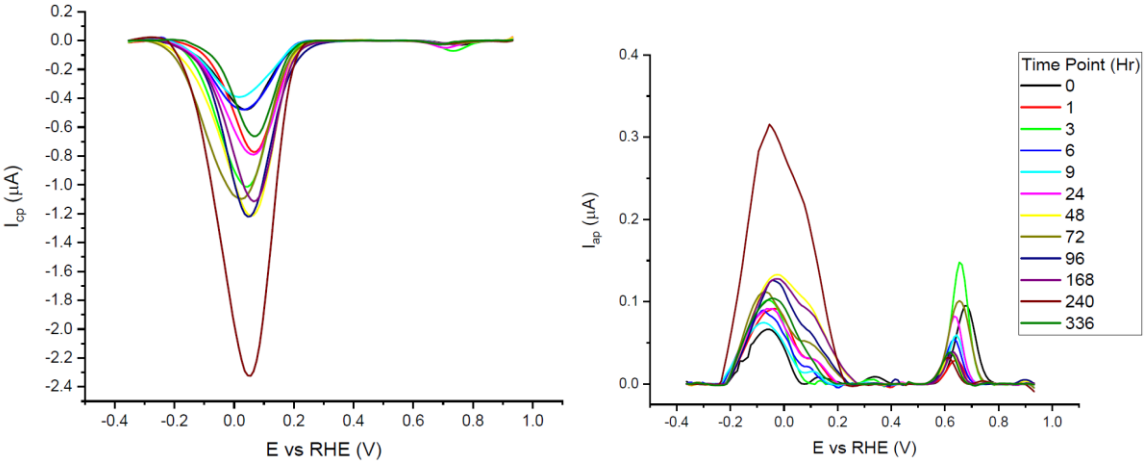

Figure C2: DPVs of reduction and oxidation sweeps of laboratory conditons time series (Replicate 3)

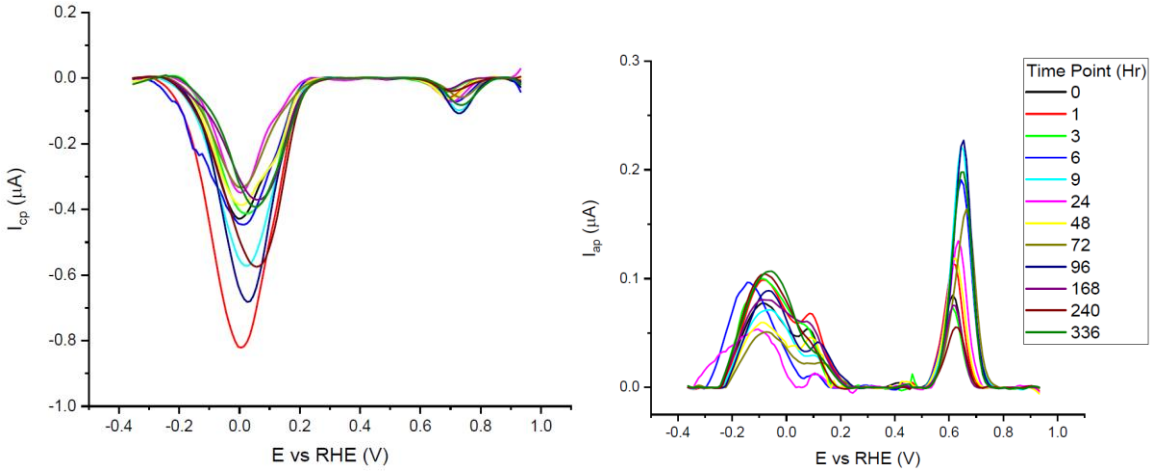

Figure C3: DPVs of reduction and oxidation sweeps of laboratory conditons time series (Replicate 4)

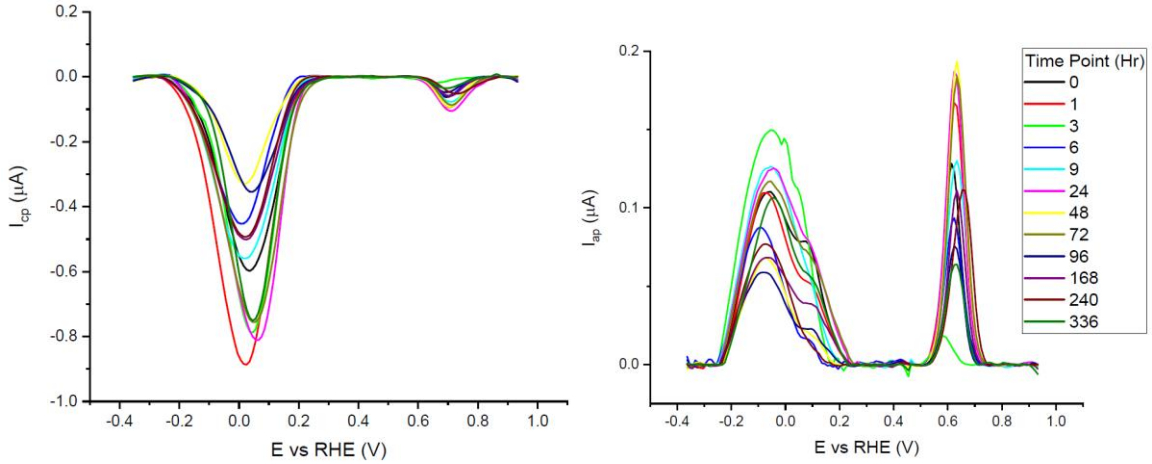

Figure C4: DPVs of reduction and oxidation sweeps of laboratory conditons time series (Replicate 5)

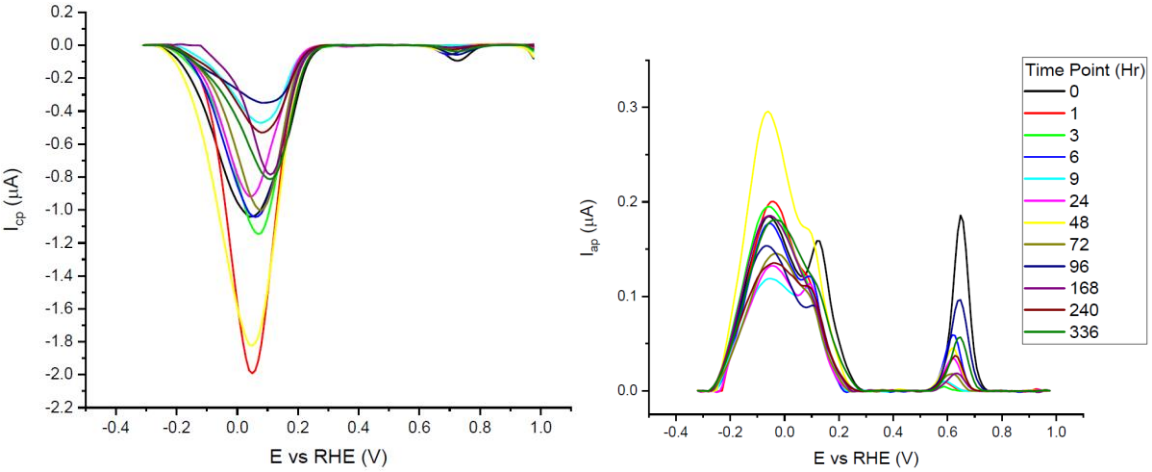

Figure C5: DPVs of reduction and oxidation sweeps of -20°C time series

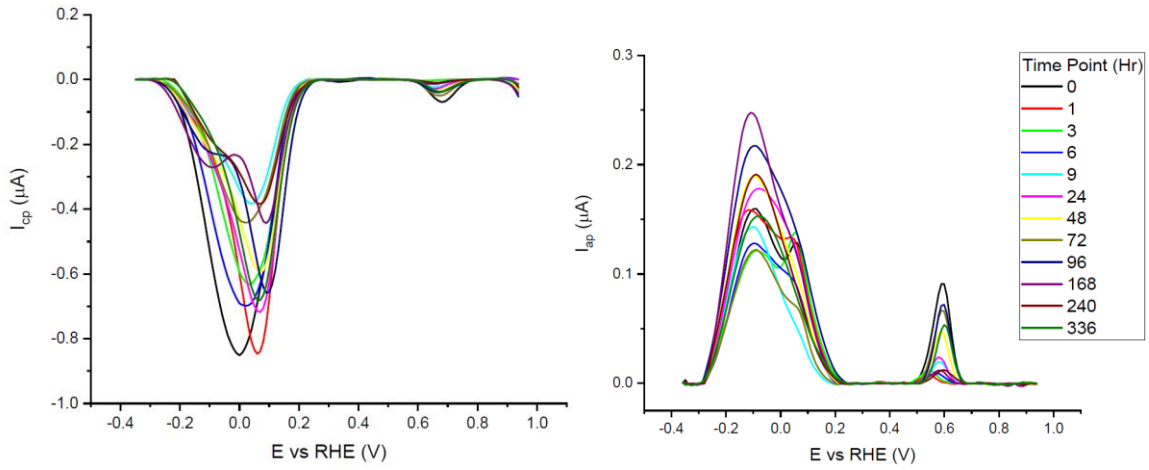

Figure C6: DPVs of reduction and oxidation sweeps of 3°C time series

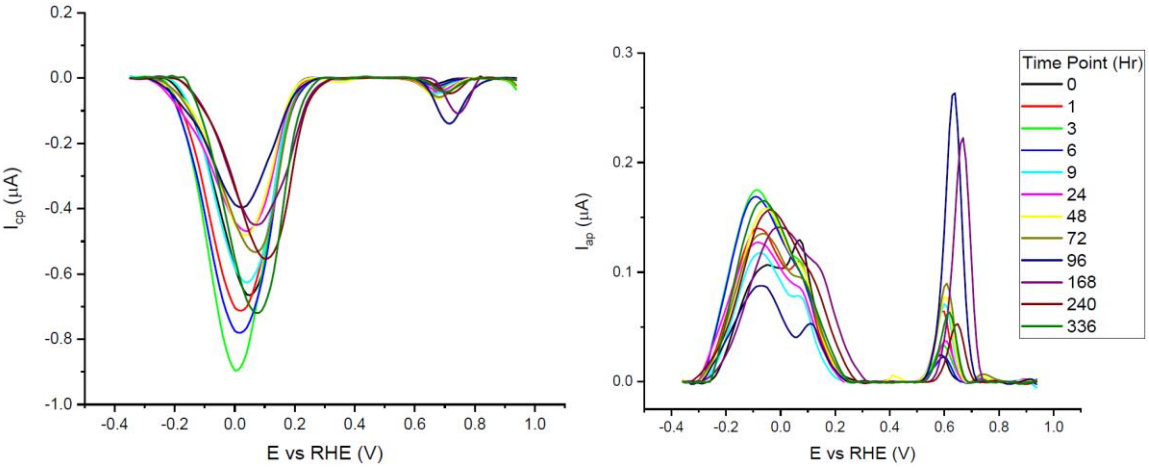

Figure C7: DPVs of reduction and oxidation sweeps of 30°C time series.

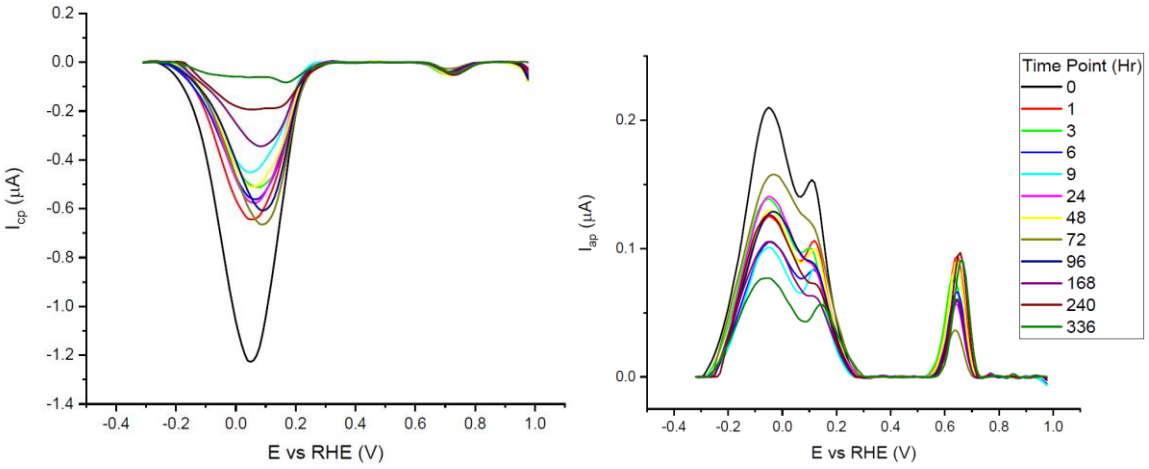

Figure C8: DPVs of reduction and oxidation sweeps of 40°C time series.

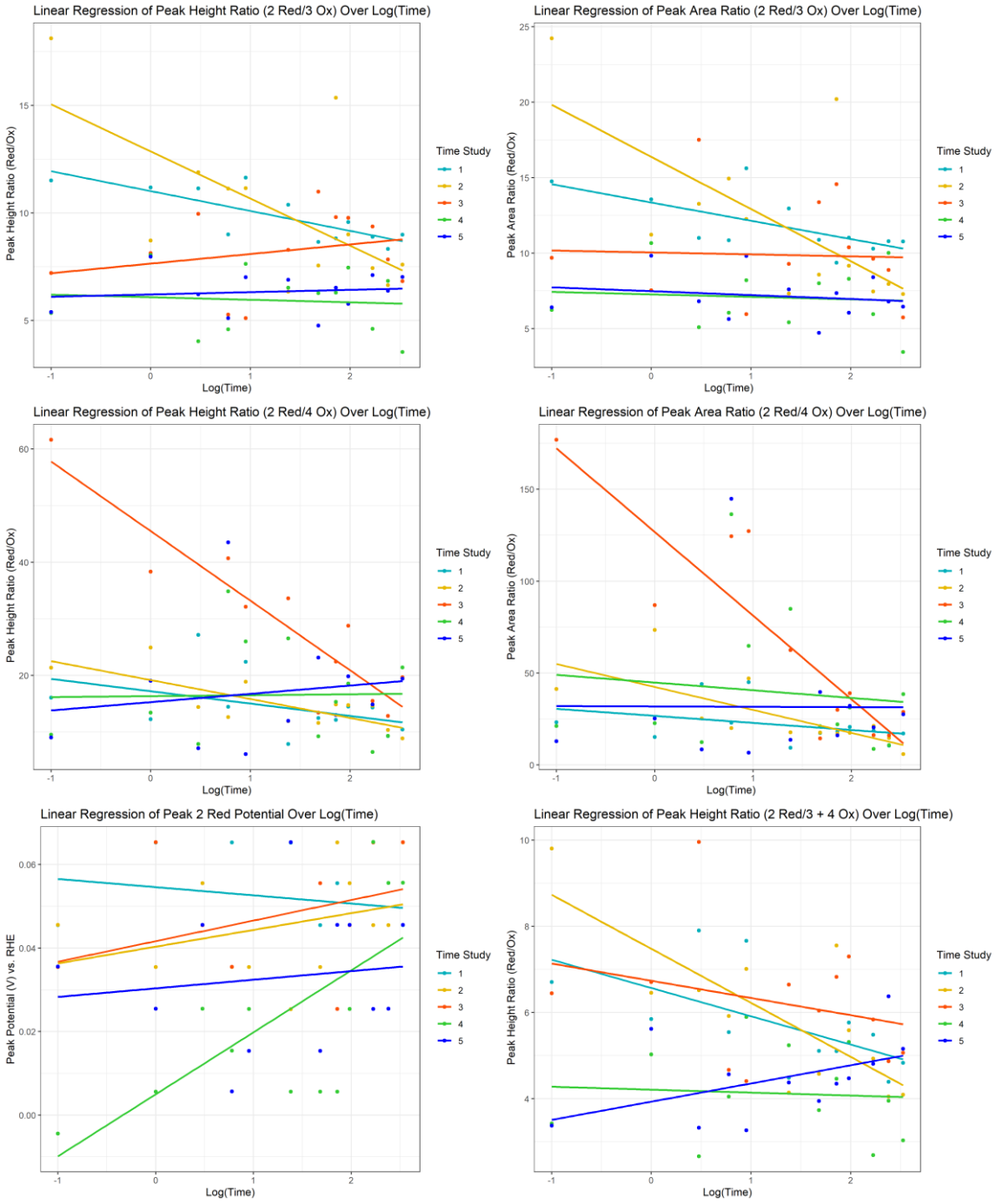

Figure C9: Linear mixed models for laboratory condition time series for significantly correlated measured responses with Log(Time).

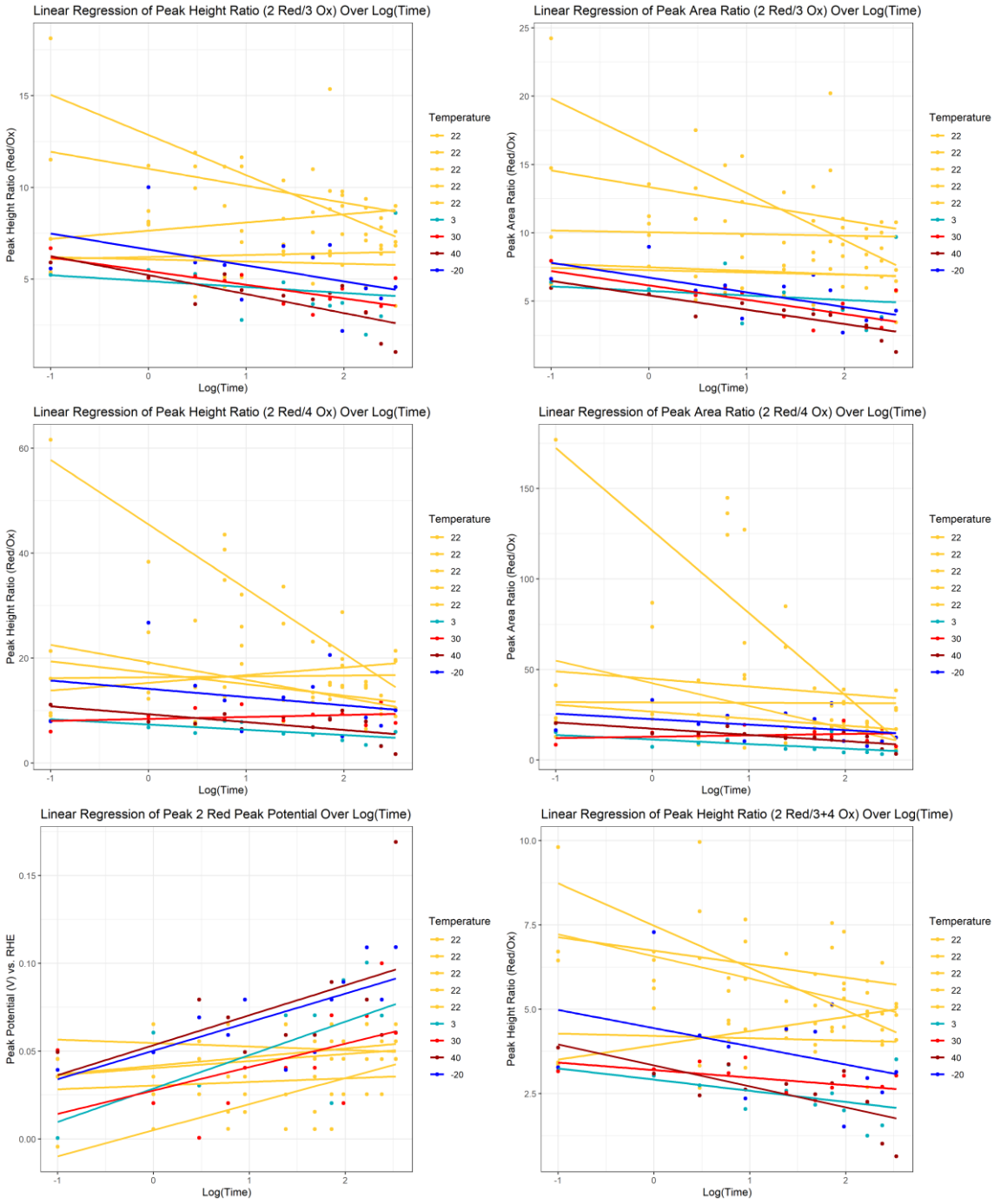

Figure C9: Linear mixed models for laboratory condition time studies (yellow) and temperature time studies (blue for colder temperatures and red for warmer temperatures) for significantly correlated measured responses with Log(Time).

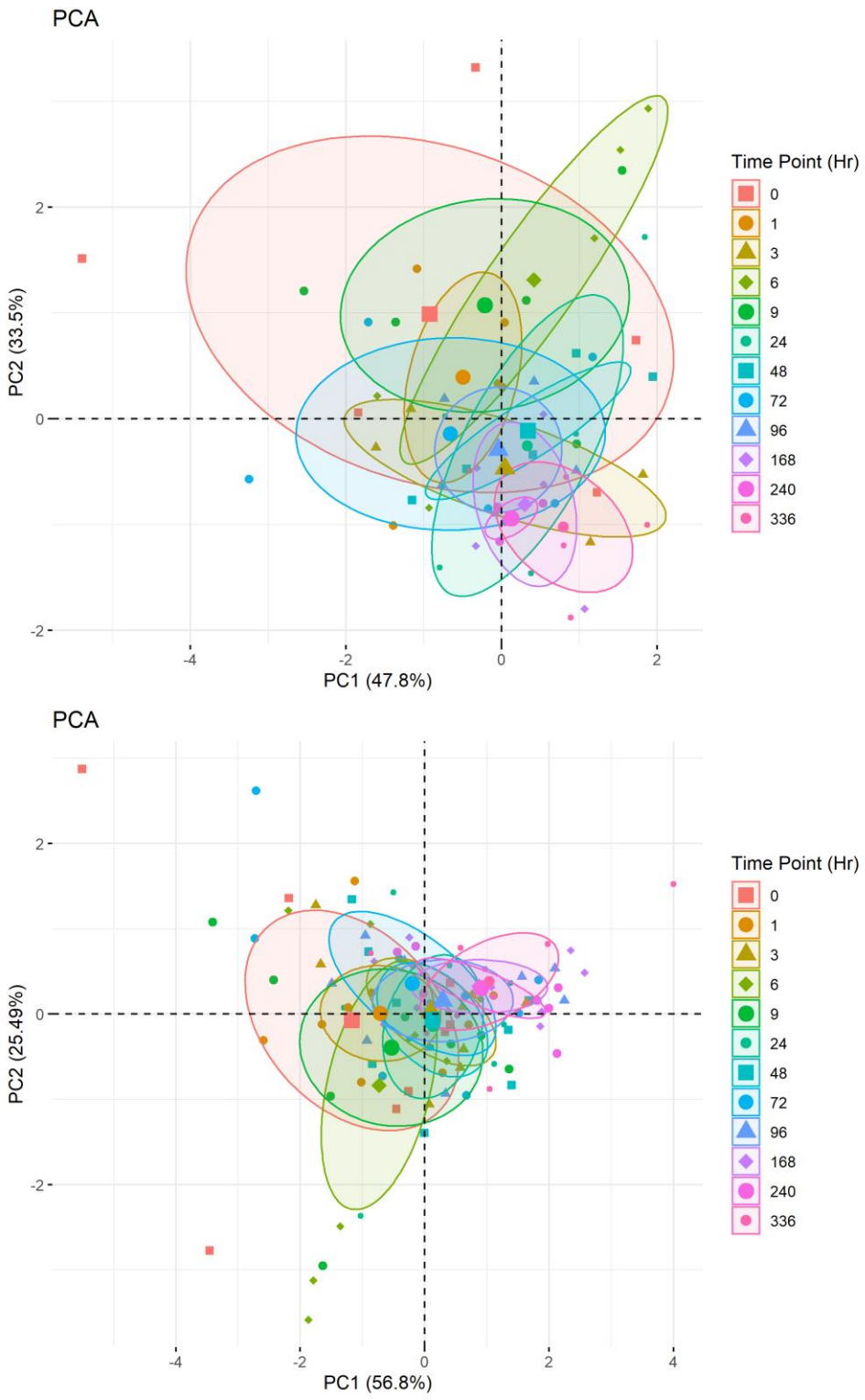

Figure C11: PCA including laboratory conditon time studies (top) and complete time series dataset (bottom)

Table C1: Linear models and Pearsons Corellations for individual tempertaure time studies with electorhcmeicla responses correlated with Log(Time) in laboratory conditon time studies.

			Log(time)			
Peak Identifier	Variable	R^2/Adjusted R^2	Estimate	Confidence Interval	p-value	Pearson's Coefficient
-20°C						
2 Red	**Potential**	0.505/0.456	0.02	0.00 – 0.03	**0.010**	0.7107456
2 Red/3 Ox	**Height**	0.221/0.143	-0.87	-2.01 – 0.28	0.123	-0.4703872
	Area	0.410/0.351	-1.08	-1.99 – -0.17	**0.025**	-0.6403454
2 Red/4 Ox	**Height**	0.070/-0.023	-1.57	-5.62 – 2.47	0.406	-0.2643495
	Area	0.137/0.051	-3.05	-8.43 – 2.34	0.236	-0.3701841
2 Red/3 Ox + 4 Ox	**Height**	0.145/0.060	-0.54	-1.46 – 0.38	0.222	-0.38118
	Area	0.339/0.273	-0.81	-1.60 – -0.01	**0.047**	-0.5824234
3°C						
2 Red	**Potential**	0.444/0.388	0.02	0.00 – 0.03	**0.018**	0.6661639
2 Red/3 Ox	**Height**	0.037/-0.059	-0.32	-1.47 – 0.83	0.547	-0.1933803
	Area	0.033/-0.064	-0.33	-1.60 – 0.94	0.573	-0.1813955
2 Red/4 Ox	**Height**	0.352/0.287	-1.01	-1.98 – -0.05	**0.042**	-0.5935065
	Area	0.390/0.329	-2.52	-4.73 – -0.30	**0.030**	-0.6245436
2 Red/3 Ox + 4 Ox	**Height**	0.246/0.170	-0.33	-0.74 – 0.08	0.101	-0.4957023
	Area	0.506/0.457	-0.62	-1.06 – -0.19	**0.009**	-0.7112913
30°C						
2 Red	**Potential**	0.264/0.191	0.01	-0.00 – 0.03	0.087	0.5141084
2 Red/3 Ox	**Height**	0.562/0.519	-0.75	-1.21 – -0.28	**0.005**	-0.7499416
	Area	0.546/0.500	-1.05	-1.73 – -0.38	**0.006**	-0.7388128
2 Red/4 Ox	**Height**	0.061/-0.033	0.38	-0.67 – 1.43	0.440	0.2465234
	Area	0.035/-0.062	0.75	-2.06 – 3.57	0.563	0.1858262
2 Red/3 Ox + 4 Ox	**Height**	0.300/0.230	-0.22	-0.46 – 0.02	0.065	-0.547536
	Area	0.455/0.400	-0.45	-0.76 – -0.10	**0.016**	-0.6744781
40°C						
2 Red	**Potential**	0.302/0.232	0.02	-0.00 – 0.04	0.064	0.549735
2 Red/3 Ox	**Height**	0.583/0.542	-1.04	-1.65 – -0.42	**0.004**	-0.7638573
	Area	0.661/0.627	-1.05	-1.58 – -0.52	**0.001**	-0.8128832
2 Red/4 Ox	**Height**	0.361/0.298	-1.51	-2.91 – -0.10	**0.039**	-0.6011769
	Area	0.607/0.567	-3.44	-5.39 – -1.49	**0.003**	-0.7789563
2 Red/3 Ox + 4 Ox	**Height**	0.524/0.476	-0.62	-1.04 – -0.20	**0.008**	-0.7237238
	Area	0.663/0.630	-0.80	-1.21 – -0.40	**0.001**	-0.8144124

Below and Above:		24 Hours	48 Hours	72 Hours	96 Hours	168 Hours
Peak Identifier	Variable	p-value	p-value	p-value	p-value	p-value
2 Red	**Potential**	0.1277	**0.0351**	**0.0211**	**0.0270**	0.0622
2 Red/3 Ox	**Height**	0.5592	0.7302	0.4376	0.2127	0.2151
	Area	0.3711	0.3604	0.1426	0.0977	0.1395
2 Red/4 Ox	**Height**	0.1355	0.3557	0.3202	0.0735	0.1220
	Area	**0.0123**	**0.0312**	0.0589	**0.0125**	0.0533
2 Red/3 Ox + 4 Ox	**Height**	0.2009	0.4444	0.2556	0.0652	0.0826
	Area	0.0635	0.0960	**0.03232**	**0.0086**	**0.0128**

Figure C12: Unpaired two-sample Wilcoxon T-test for laboratory conditon time studies with data dividied into below/above time groups. Significant vlaues are bolded ($p < 0.05$)

		Below 96 Hours		After 96 Hours	
Peak Identifier	Variable	Mean	Confidence Interval	Mean	Confidence Interval
2 Red	**Potential**	0.0372	0.0312 – 0.0432	0.0501	0.0429 – 0.0573
2 Red/4 Ox	**Area**	42.4869	29.9172 – 55.0566	18.1965	13.1147 – 23.2782
2 Red/3 Ox + 4 Ox	**Area**	7.1347	6.3064 – 7.9630	5.2568	4.6120 – 5.9016

Figure C13: Mean and confidence interval data from the below/above 96-hour groups in the laboratory conditon time studies that were significant.

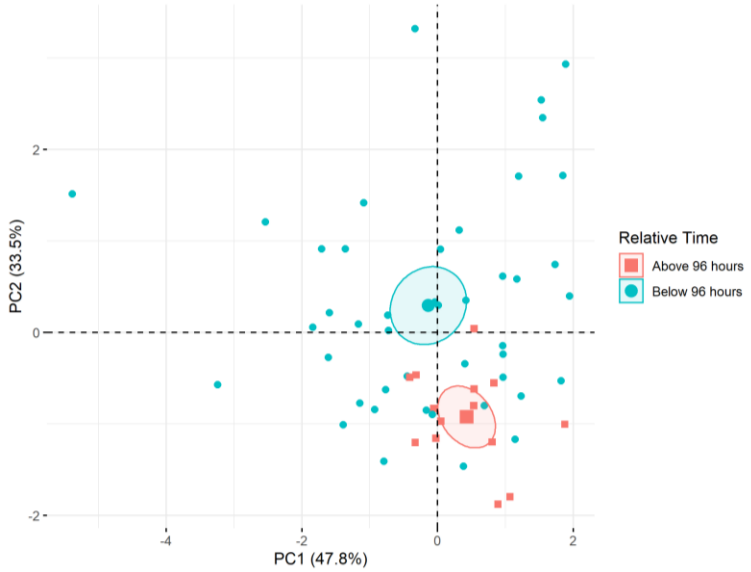

Figure C14: PCA of laboratory conditon time series data for below/above 96-hours